

MULTI-FUNCTIONAL POLYMER SCAFFOLDS AS BIOSENSORS FOR
DETECTION OF ETHANOL AND ORGANOPHOSPHOROUS PESTICIDES
AND AS A FLUORESCENT PROBE FOR CELL IMAGING PURPOSE

A THESIS SUBMITTED TO
THE GRADUATE SCHOOL OF NATURAL AND APPLIED SCIENCES
OF
MIDDLE EAST TECHNICAL UNIVERSITY

BY
MELİS KESİK MANCAR

IN PARTIAL FULFILLMENT OF THE REQUIREMENTS
FOR THE DEGREE OF DOCTOR OF PHILOSOPHY
IN
CHEMISTRY

OCTOBER 2017

Approval of the thesis:

**MULTI-FUNCTIONAL POLYMER SCAFFOLDS AS BIOSENSORS FOR
DETECTION OF ETHANOL AND ORGANOPHOSPHOROUS
PESTICIDES AND AS A FLUORESCENT PROBE FOR CELL IMAGING
PURPOSE**

submitted by **MELİS KESİK MANCAR** in partial fulfillment of the requirements
for the degree of **Doctor of Philosophy in Chemistry Department, Middle East
Technical University** by,

Prof. Dr. Gülbin Dural Ünver
Dean, Graduate School of **Natural and Applied Sciences**

Prof. Dr. Cihangir Tanyeli
Head of Department, **Chemistry**

Prof. Dr. Levent Toppare
Supervisor, **Chemistry Dept., METU**

Prof. Dr. Suna Timur
Co-Supervisor, **Biochemistry Dept., Ege University**

Examining Committee Members:

Prof. Dr. Ali Çırpan
Chemistry Dept., METU

Prof. Dr. Levent Toppare
Chemistry Dept., METU

Prof. Dr. Ertuğrul Şahmetlioğlu
Chemistry&Chem.Prog.Tech. , Erciyes University

Assoc. Prof. Dr. Yasemin Arslan Udum
Advanced Tech. Dept., Gazi University

Assoc. Prof. Dr. Görkem Günbaş
Chemistry Dept., METU

Date: 19.10.2017

I hereby declare that all information in this document has been obtained and presented in accordance with academic rules and ethical conduct. I also declare that, as required by these rules and conduct, I have fully cited and referenced all material and results that are not original to this work.

Name, Last name: Melis, KESİK MANCAR

Signature:

ABSTRACT

MULTI-FUNCTIONAL POLYMER SCAFFOLDS AS BIOSENSORS FOR DETECTION OF ETHANOL AND ORGANOPHOSPHOROUS PESTICIDES AND AS FLUORESCENT PROBES FOR CELL IMAGING PURPOSES

Kesik Mancar, Melis

Ph.D., Department of Chemistry

Supervisor: Prof. Dr. Levent Toppare

Co- Supervisor: Prof. Dr. Suna Timur

October 2017, 134 pages

Overwhelming characteristics of conducting polymers led to opening a new research field in the last decades. There are a number of application areas of CPs which attracted keen interest of scientific world. The two main concepts of this thesis are conducting polymer based biological sensors and cell imaging study. Accordingly, the use of multi-functional polymers as biosensors for detection of ethanol and organophosphorous (OPs) pesticides and as different multi-purpose fluorescent probes for cell imaging studies were discussed in three different parts. In the first study, a CP (poly(TIFc-co-BEDOA-6-poly(L-Boc)) containing polypeptide and ferrocene side chains was utilized as an immobilization matrix for AOx biosensor construction. Newly designed biosensor which combined the advantages of each component was tested as an ethanol sensing system offering fast response time, wide linear range and low detection limit with a high sensitivity. The capability of the biosensor in determining ethanol content in alcoholic beverages was also demonstrated. In the second study, a novel amperometric

biosensor based on a CP (poly(SNS-NH₂)) using MWCNT modified electrode was developed for the detection of paraoxon, parathion and chlorfenvinphos as model OPs. Inhibitory effect of OPs on AChE activity were investigated. The fabricated biosensor was tested for the detection of pesticides in fortified tap water samples. The results were found to be in good agreement with the ones determined by HPLC/DAD technique. In the third study, a fluorescent and functional monomer, PIP and an antibody labeling kit (CF555) were merged on the same scaffold to generate the proposed bioprobe offering multicolor cell images. The aim was to achieve targeted imaging of CD44 positive U87-MG cancer cells and determine specific cellular labeling via fluorescence imaging and flow cytometry experiments.

Keywords: Conducting Polymers, Alcohol Oxidase, Acetylcholinesterase, Enzyme Based Amperometric Biosensors, Fluorescent Probes, Targeted Cell Imaging

ÖZ

MULTİFONKSİYONEL POLİMER YAPILARINI BİYOSENSÖR OLARAK ETANOL VE TARIM İLACI TAYİNİNDE VE FLORESAN PROB OLARAK HÜCRE GÖRÜNTÜLEMESİNDE KULLANIMI

Kesik Mancar, Melis

Doktora, Kimya Bölümü

Tez Yöneticisi: Prof. Dr. Levent Toppare

Ortak Tez Yöneticisi: Prof. Dr. Suna Timur

Ekim 2017, 134 sayfa

İletken polimerlerin önemli özellikleri son yıllarda yeni araştırma alanlarının doğmasına sebep olmuştur. İletken polimerlerin bilimsel dünya tarafından dikkat çeken uygulama alanları vardır. Bu tezin iki ana teması iletken polimer bazlı biyolojik sensörler ve hücre görüntülemeleridir. Buna göre, multifonksiyonel polimer yapılarını biyosensör olarak etanol ve tarım ilacı tayininde ve floresan prob olarak hücre görüntülemesinde kullanımı üç ayrı bölümde tartışılmıştır. İlk çalışmada polipeptit ve ferrosen yapılarını içeren poli(TIFc-co-BEDOA-6-poli(L-Boc) iletken polimeri immobilizasyon matrisi olarak AOX sensörü yapımda kullanılmıştır. Yeni dizayn edilen ve içinde bulundurduğu her materyalin avantajlarını kullanan bu biyosensör kullanılarak hızlı cevap süresi, geniş lineer aralığı ve düşük tayin edilebilir alt limiti ile yüksek hassasiyetli etanol tayininde test edilmiştir. Ek olarak, bu biyosensör ile etanol tayininin yapabilirliği çeşitli alkol içeren içeceklerde gösterilmiştir. İkinci çalışmada, özgün bir amperometrik biyosensör geliştirilmek üzere iletken polimer ((poli(SNS-NH₂)) bazlı ve MWCNT modifiyeli elektrotu model organofosfor pestisitleri olarak seçilen paraokson, paratyon ve klorfeninfos tayini için kullanılmıştır. Bu pestisitlerin AChE

üzerindeki inhibitör etkisi araştırılmıştır. Geliştirilen bu biyosensör pestisit tayini için çeşme suyunda test edilmiştir. Elde edilen sonuçlar HPLC/DAD tekniği kullanılarak elde edilen sonuçlar ile tutarlıdır. Üçüncü çalışmada, floresan fonksiyonel bir monomer PIP ve bir antikor işaretleyicisi olan CF555 i aynı platformda çok renkli hücre görüntülemesi sunacak şekilde birleştirilmiştir. Buradaki amaç CD44 pozitif U87-MG kanser hücrelerine hedeflenmesini sağlamak ve spesifik hücre tayinini floresan görüntülemesi ve akış sitometrisi ile yapmaktır.

Anahtar kelimeler: İletken Polimerler, Alkol Oksidaz, Asetilkolinesteraz, Enzim Esaslı Amperometrik Biyosensörler, Floresan Problar, Hedeflenmiş Hücre Görüntülemesi

Dedicated to Ali Mancar....

ACKNOWLEDGMENTS

First and foremost, I would like to express my appreciation to my supervisor Prof. Dr. Levent Toppare for his deep insight, support throughout my whole graduate studies, encouragement and especially patience, Words cannot express my gratitude. I feel very lucky since he is my doctor-father.

I would like to gratefully acknowledge Prof. Dr. Suna Timur for her fruitful discussions, advices and help throughout this study.

I would like to give special thanks my Thesis Committee Members, Prof. Dr. Ali Çırpan, Assoc. Prof. Yasemin Arslan Udum for their valuable ideas and moral support. Importantly, I would like to express my sincere thanks Assist. Prof. Dr. Görkem Günbaş for his encouraging and endless support. Also, I would like to express my appreciation to Prof. Dr. Ertuğrul Şahmetlioğlu for supporting me in both important exams in my PhD life.

I wish to thank all the past and present members of Toppare, Çırpan, Günbaş and Timur Research Group for the nice research environment. I had amazing people around me. Also, special thanks must be given to Şevki Can Cevher.

In particular but not particular order, I would like to express my deepest sense of gratitude to Seza, Nehir, Esra Öz., Büke, Özge and Esra Öğ. for their great friendship and motivation. For 10 years, I am one of the luckiest person in the World for being their friend. Also, I would like to thank Berfu for being a second sister to me. She always believes in me.

Big thanks must be given to Ebru, Çağla, Saniye, Gönül, Bilal and Emine for their endless support, real friendship, surviving with me among the experiments. They make these years unforgettable for me.

No words can describe how lucky I am to have you as my parents. I would not be possible to achieve anything throughout my all life without them. It is feeling beyond words that I know they always with me.

I would like to express my profound gratitude to my husband, Ali Mancar, for his great love, continuous support, understanding, patience and encouraging me. I appreciate for being there for me every seconds I need you. I could not imagine a life journey without his warm look with a big smile and huge hug.

TABLE OF CONTENT

ABSTRACT	v
ÖZ.....	vii
ACKNOWLEDGMENTS.....	x
LIST OF TABLES	xvi
LIST OF FIGURES.....	xvii
LIST OF ABBREVIATIONS	xxi
CHAPTERS	
1. CONJUGATED POLYMERS.....	1
1.1. INTRODUCTION	1
1.1. DEFINITION OF A CONJUGATED POLYMER.....	2
1.2. SYNTHESIS STRATEGIES OF CONJUGATED POLYMERS.....	4
1.3. APPLICATION FIELDS OF CONJUGATED POLYMERS	6
1.3.1. Conjugated Polymers in Biosensor Design.....	7
1.3.2. Conjugated Structures for Bioimaging Purpose.....	8
2. CONDUCTING POLYMERS CONTAINING POLYPEPTIDE AND FERROCENE SIDE CHAINS AS ETHANOL BIOSENSORS	9
2.1. INTRODUCTION	9
2.1.1. Oxidoreductase Enzymes in Biotechnology	9
2.1.2. Biocatalysts Used for Conversion of Alcohols	10
2.1.3. Biosensors	16
2.1.4. Scope of the Study.....	22

2.2.	RESULTS and DISCUSSION.....	25
2.2.1.	Electro (co)polymerization and Electrochemical Studies	25
2.2.2.	ATR-FTIR.....	29
2.2.3.	Optimization of Experimental Parameters	30
2.2.4.	Biosensor Characterization	34
2.2.5.	Analytical Characterization.....	38
2.2.6.	Sample Application.....	41
2.3.	EXPERIMENTAL DETAILS	42
2.3.1.	Materials.....	42
2.3.2.	Measurements.....	43
2.3.3.	Synthesis of 6-(4,7-bis(2,3-dihydrothieno[3,4-b][1,4]dioxin-5-yl)-2H-benzo[d][1,2,3]triazol-2-yl)hexan-1-amine) (BEDOA-6)	43
2.3.4.	Synthesis of N6-(tert-butoxycarbonyl)-N2-(phenoxycarbonyl)-L-lysine (Urethane derivative of N-Boc-L-lysine)	45
2.3.5.	Synthesis of Electroactive BEDOA-6-poly(L-Boc).....	45
2.3.6.	Synthesis of 2-ferrocenyl-4,7-di(thiophen-2-yl)-1H-benzo[d]imidazole (TIFc)	47
2.3.7.	Electro Copolymerization of BEDOA-6-poly(L-Boc) and TIFc	47
2.3.8.	Immobilization of Enzyme, Crosslinking And Biosensing.....	48
2.4.	CONCLUSION	49
3.	AN ACETYLCHOLINESTERASE BIOSENSOR BASED ON A CONDUCTING POLYMER USING MULTIWALLED CARBON NANOTUBES FOR AMPEROMETRIC DETECTION OF ORGANOPHOSPHOROUS PESTICIDES.....	51
3.1.	INTRODUCTION	51
3.1.1.	Environmental Monitoring.....	51
3.1.2.	Strategies for Detection of OP Pesticides	53
3.1.3.	Biosensor Measurement For Pesticides.....	54

3.1.4.	Carbon Nanotubes in Biosensor Construction	58
3.1.5.	Scope of The Study	59
3.2.	RESULTS and DISCUSSION.....	60
3.2.1.	Characterization of Functionalized Multiwalled Carbon Nanotube .	60
3.2.2.	Effect of f-MWCNT and Poly(SNS-NH ₂) On Biosensor Response .	62
3.2.3.	Optimization of Experimental Parameters	63
3.2.4.	Surface Characterization	67
3.2.5.	Electrochemical Characterization of Different Electrodes.....	71
3.2.6.	Analytical Performance of The Biosensor	75
3.2.7.	Pesticide Detection.....	77
3.2.8.	Application of the Biosensor.....	82
3.3.	EXPERIMENTAL DETAILS	85
3.3.1.	Materials.....	85
3.3.2.	Instrumentation.....	85
3.3.3.	Synthesis of the Monomer.....	86
3.3.4.	Construction of the AChE Biosensor	87
3.3.5.	Electrochemical Measurement	88
3.3.6.	Evaluation of Biosenor Results with HPLC/DAD.....	89
3.4.	CONCLUSION	90
4.	MULTI-FUNCTIONAL FLUORESCENT SCAFFOLD AS A MULTICOLOR PROBE: DESIGN AND APPLICATION IN TARGETED CELL IMAGING	93
4.1.	INTRODUCTION	93
4.1.1.	Wide Spread Threat: Cancer	93
4.1.2.	Development of Fluorescent Probes	94
4.1.3.	Bioimaging Based On Synthetic Fluorescent Probes.....	95
4.1.4.	Materials Used in the Design of Fluorescent Probes	96
4.1.5.	New Designing Strategy.....	97

4.1.6.	Scope of the Study.....	98
4.2.	RESULTS and DISCUSSION.....	99
4.2.1.	Characterizations of PIP/CF555/anti-CD44 Bioconjugate	99
4.2.2.	Cytotoxicity	103
4.2.3.	Flow Cytometry.....	105
4.2.4.	Photostability.....	105
4.2.5.	Cellular Targeting	106
4.3.	EXPERIMENTAL DETAILS	109
4.3.1.	Reagents and Materials	109
4.3.2.	Measurements and Characterizations.....	109
4.3.3.	Synthesis of 3-(1H-phenanthro[9,10-d]imidazol-2-yl)phenol (PIP).....	110
4.3.4.	Synthesis of the Bioconjugate.....	110
4.3.5.	Cell Viability	111
4.3.6.	Flow Cytometry Analysis.....	112
4.3.7.	Fluorescence Microscopy - Cell Culture Experiments	112
4.4.	CONCLUSION	113
	REFERENCES.....	115
	CURRICULUM VITAE	131

LIST OF TABLES

TABLES

Table 2.1. Comparison of some parameters of various alcohol biosensors reported in literature.	39
Table 2.2. Ethanol detection in alcoholic beverages.	42

LIST OF FIGURES

FIGURES

Figure 2.1. (A) Alcohol dehydrogenase (ADH) and (B) alcohol oxidase (AOX). .	11
Figure 2.2. Classification of AOx.	13
Figure 2.3. Main components of a biosensor.	17
Figure 2.4. Schematic representation of three generations of amperometric biosensors.	18
Figure 2.5. Synthesis of poly(TIFc) and poly(BEDOA-6-poly(L-Boc)) by electropolymerization.	26
Figure 2.6. Single scan cyclic voltammograms of poly(TIFc) and poly(TIFc-co-BEDOA-6-poly(L-Boc)) in a monomer free 0.1 M ACN/DCM (95:5) solution of LiClO ₄ /NaClO ₄	27
Figure 2.7. Cyclic voltammograms of (A) poly(TIFc-co-BEDOA-6-poly(L-Boc)) film in 0.1 M NaClO ₄ /LiClO ₄ /DCM/ACN (5/95, v/v) at scan rates of 50, 100, 150, 200, 250 and 300 mV/s. (B) Correlation between scan rate and peak current of the film.	28
Figure 2.8. ATR-FTIR spectra of (a) poly(TIFc) and (b) poly(TIFc-co-BEDOA-6-poly(L-Boc)).	29
Figure 2.9. Effect of (A) polymer films as supporting matrix and (B) enzyme activity on the biosensor response. Error bars show standard deviation (SD) of three measurements.	31
Figure 2.10. Effects of (A) scan number and (B) pH on the biosensor response. Error bars show standard deviation (SD) of three measurements.	33
Figure 2.11. Typical Nyquist plots resulting from bare graphite electrode, poly(TIFc-co-BEDOA-6-poly(L-Boc)), and poly(TIFc-co-BEDOA-6-poly(L-Boc))/AOx in 5.0 mM Fe(CN) ₆ ^{3-/4-} containing 0.1 M KCl solution. (Curves in high frequency region are given as inset).	35

Figure 2.12. SEM images of (A) poly(TIFc); (B) poly(TIFc-co-BEDOA-6-poly(L-Boc)); (C) poly(TIFc-co-BEDOA-6-poly(L-Boc))/AOx under optimized conditions.	37
Figure 2.13. Calibration curve for ethanol (in 50 mM phosphate buffer, pH 7.0, 25°C, -0.7 V). Error bars show standard deviation of three measurements (A typical amperometric response to 1.7 mM ethanol in phosphate buffer, 50 mM, pH 7.0 given as inset).	38
Figure 2.14. Substrate selectivity of the biosensor (amperometric response of methanol taken as 100%).	40
Figure 2.15. Synthetic pathway of the monomer BEDOA-6 [97].	44
Figure 2.16. Synthetic pathway of N6-(tert-butoxycarbonyl)-N2-(phenoxy carbonyl)-L-lysine (urethane derivative of N-Boc-L-lysine) [97].	45
Figure 2.17. Synthesis of the electroactive electroactive polypeptide macromonomer, BEDOA-6-poly(L-Boc) [83].	46
Figure 2.18. Synthetic route of the monomer TIFc [83].	47
Figure 2.19. Preparation of the amperometric ethanol biosensor for poly(TIFc-co-BEDOA-6-poly(L-Boc)).	49
Figure 2.20. A novel ethanol biosensor based on conducting polymers containing polypeptide and ferrocene side chains [83].	50
Figure 3.1. (A) General form of pesticides, (B) Structures of the several OP compounds pesticides used in AChE biosensors.	53
Figure 3.2. Immobilization strategies used for biosensor construction.	56
Figure 3.3. FTIR spectra of MWCNT and f-MWCNT.	62
Figure 3.4. The effect of surface modification and different conditions on response current on performance of the biosensors (in 2 mmol L ⁻¹ AThCl in 50 mM PBS, pH 7, 25 °C, 0.1 V). Error bars show standard deviation (SD) of three measurements.	63
Figure 3.5. The effect of scan number (accumulated charge) (A), pH (B), applied potential (C) on performance of the biosensors (in 2 mmol L ⁻¹ AThCl in 50 mM PBS, pH 7, 25 °C, 0.1 V). Error bars show standard deviation (SD) of three measurements.	65
Figure 3.6. The effect of applied potential (A) and enzyme amount (B) on performance of the biosensors (in 2 mmol L ⁻¹ AThCl in 50 mM PBS, pH 7, 25 °C, 0.1 V). Error bars show standard deviation (SD) of three measurements.	67

Figure 3.7. SEM images of (A) MWCNT; (B) f-MWCNT; (C) f-MWCNT/poly(SNS-NH ₂); (D) f-MWCNT/poly(SNS-NH ₂)/AChE under optimized conditions.	68
Figure 3.8. XPS C1s spectra for (A) pristine MWCNT; (B) f-MWCNT; (C) f-MWCNT/poly(SNS-NH ₂); (D) AChE immobilized f-MWCNT/poly(SNS-NH ₂) and N1s spectra for (E) f-MWCNT/poly(SNS-NH ₂); (F) AChE immobilized f-MWCNT/poly(SNS-NH ₂).	71
Figure 3.9. (A) Typical Nyquist plots resulting from the bare graphite electrode (a), f-MWCNT (b), f-MWCNT/poly(SNS-NH ₂) (c), and f-MWCNT/poly(SNS-NH ₂)/AChE (d) in 5.0 mM Fe(CN) ₆ ^{3-/4-} containing 0.1 M KCl.	73
Figure 3.10. Cyclic voltammograms resulting from the bare graphite electrode (a), f-MWCNT (b), f-MWCNT/poly(SNS-NH ₂) (c), and f-MWCNT/poly(SNS-NH ₂)/AChE (d) in 5.0 mM Fe(CN) ₆ ^{3-/4-} containing 0.1 M KCl.	74
Figure 3.11. Calibration curve for AThCl (in 50 mM PBS, pH 7, 25 °C, 0.1 V). (A typical amperometric signal of the biosensor as an inset for 3 mM AThCl after (I ₁) and before (I ₀) incubation). Error bars show the standard deviation (SD) of three measurements.	76
Figure 3.12. The dependence of the inhibition curves of paraoxon, parathion, chlorfenvinphos on incubation time. Error bars show standard deviation (SD) of three measurements.	78
Figure 3.13. Calibration curves for paraoxon (A), parathion (B), chlorfenvinphos (C) detection (in 50 mM PBS, pH 7.0, 25°C, 0.1 V, 2.0 mM AThCl, 5 min incubation time). Error bars show standard deviation (SD) of three measurements.	80
Figure 3.14. Influence of reactivation time with 2-PAM on the biosensor responses at 1 mM AThCl in 50 mM PBS (pH 7.0).	82
Figure 3.15. Correlation of the quantification results for (A) paraoxon, (B) parathion, (C) chlorfenvinphos in tap water with HPLC/DAD analysis (x-axis) and the new designed biosensor (y-axis).	84
Figure 3.16. Synthetic pathway of SNS-NH ₂ [86].	86
Figure 3.17. Schematic representation of the proposed biosensor.	88
Figure 3.18. Illustration of two step procedure for pesticide detection.	88

Figure 3.19. An Acetylcholinesterase Biosensor Based On A Conducting Polymer Using Multiwalled Carbon Nanotubes For Amperometric Detection Of Organophosphorous Pesticides	91
Figure 4.1. Fluorescence spectra of PIP/anti-CD44, CF555/anti-CD44, and PIP/CF555/anti-CD44 conjugates (excited at 350 and 555 nm)	101
Figure 4.2. AFM images of PIP (A), PIP/anti-CD44 (B), PIP/CF555/anti-CD44 (C).....	102
Figure 4.3. The dose-dependent toxicity of PIP, PIP/anti-CD44 and PIP/anti-CD44 for (A) U87-MG and (B) HaCaT cells. Values are the mean \pm standard deviation of the data (n = 4).	104
Figure 4.4. CD44 expressions of U87-MG and HaCaT cell lines. Negative control staining showed no non-specific binding of secondary antibody (A); U87-MG showed higher fluorescence than HaCaT after CD44 staining (B).....	105
Figure 4.5. Imaging of HaCaT and U87-MG cells via fluorescence microscopy. Images were obtained after treatment of the cell with PIP monomer (A), PIP/anti-CD44 (B) and PIP/CF555/anti-CD44 (C1 and C2) for 2 h at 37°C and 5.0% CO ₂ atmosphere, under humidity. Photos of A, B and C1 were taken with UV filter of fluorescence set up. Photos of C2 were taken with red filter of fluorescence set up with 100X magnification. All scale bars are 10 μ m.....	108
Figure 4.6. Synthesis of 3-(1H-phenanthro[9,10-d]imidazol-2-yl) phenol (PIP) [219].	110
Figure 4.7. Preparation of the bioconjugate for PIP/CF555/anti-CD44.....	111
Figure 4.8. A multi-functional fluorescent scaffold as a multicolor probe [219].	114

LIST OF ABBREVIATIONS

2-PAM	: Pyridine 2-aldoxime methochloride
AChE	: Acetylcholinesterase
ACN	: Acetonitrile
ADH	: Alcohol Dehydrogenase
AFM	: Atomic force microscopy
AOX	: Alcohol Oxidase
AThCl	: Acetylthiocholine Chloride
BChE	: Butyryl cholinesterase
BEDO-6	: 6-(4,7-bis(2,3-dihydrothieno[3,4-b][1,4]dioxin-5-yl)- 2 <i>H</i> -benzo[d][1,2,3]triazol-2-yl)hexan-1-amine)
CDI	: Carbonyldiimidazole
CNTs	: Carbon Nanotubes
CP	: Conducting Polymer
CV	: Cyclic Voltammetry
DCM	: Dichloromethane
DMAc	: N,N-Dimethylacetamide
DMEM	: Eagle Medium
DMF	: N,N-dimethylformamide
DMSO	: Dimethyl sulfoxide
EDC	: N-(3-dimethylaminopropyl)-N'-ethylcarbodiimide hydrochloride
EIS	: Electrochemical Impedance Spectroscopy
EMEM	: Eagle's Minimum Essential Medium
FAD	: Flavin Adenine Dinucleotide
FBS	: Fetal bovine serum
f-MWCNT	: Functionalization of MWCNT

HPLC/DAD	: High Pressure Liquid Chromatography with Diode Array Detector
I_{max}	: Maximum Current
IUB	: International Union of Biochemistry
K_M^{app}	: Apparent Michaelis-Menten Constant
LOD	: Limit of detection
MFI	: Median Fluorescence Intensity
MWCNTs	: Multi-walled Carbon Nanotubes
NAD	: Nicotinamide Adenine Dinucleotide
NHS	: N-hydroxysuccinimide
nMFI	: Normalized Median Fluorescence Intensity
OPs	: Organophosphorous Pesticides
PIP	: 1H-phenanthro[9,10-d]imidazol-2-yl)phenol
RSD	: Relative Standard Deviation
SD	: Standard Deviation
SD	: Standard Deviation
SEM	: Scanning Electron Microscopy
SNS-NH₂	4-(2,5-di(thiophen-2-yl)-1H-pyrrol-1-yl)benzenamine
SPE	: Solid Phase Extraction
SWCNTs	: Single-walled Carbon Nanotubes
THF	: Tetrahydrofuran
TIFc	: 2-ferrocenyl-4,7-di(thiophen-2-yl)-1H-Benzo[d]imidazole
TMS	: Tetramethylsilane
XPS	: X-ray Photoelectron Spectroscopy

CHAPTER 1

1. CONJUGATED POLYMERS

1.1. INTRODUCTION

At the end of 1970s, accidental synthesis of poly(acetylene) which is conductive in its doped state, was counted as the beginning of a new era [1]. It exhibited metallic electrical conductivity. In 2000, Alan MacDiarmid, Alan Heeger and Hideki Shirakawa were awarded with the Nobel Prize in Chemistry [2]. This pioneer work has grounded successful developments of "plastic electronics".

Before that, a number of studies to produce polymers with the conductivity characteristic were introduced. Aniline black is one of the oldest known conductive polymer. It was generated by aniline oxidation on an electrode surface in the presence of sulfuric acid in 1862 [3]. In 1968, Natta polymerized acetylene for the first time using coordination catalyst chemistry [4]. Although the produced polyacetylene (PAC) acquired semiconductor properties, the product was in the insoluble form. That is why scientists were not interested in this polymer at that time. In 1967, Ziegler-Natta catalyst was introduced with the synthesis of polyacetylene by Shirakawa and coworkers. The proposed polyacetylene was generated as a thin silvery semiconductor film. When treated with a halogen, the conductivity of polymer was affected drastically. With this invention, it was understood that conductivity of polymer can be adjusted with a change in the dopant concentration. Then, the discovery of poly(sulfur nitride) (SN)_x established the concept of conductivity of a conjugated inorganic polymer [5].

The problem of air sensitivity in polyacetylene synthesized by Alan MacDiarmid, Alan Heeger and Hideki Shirakawa led to seeking new synthesis strategies to produce conducting polymers with better properties. In 1980s, polyheterocyclic

structures have become popular among the polymer chemists. This type of structures offers air stability as well as easy oxidation process and modification of the polymer backbone due to their electron rich character. Although heterocyclic polymers do not show electrical conductivity as much as polyacetylene has, they are preferred mostly since they allow structural modification. That is, polyheterocyclic scaffolds are more processable materials.

In modern science, conducting polymers have attracted great interests to use them as a supporting material for different application fields.

1.1. DEFINITION OF A CONJUGATED POLYMER

A polymer plastic includes alternating single and double bonds along its scaffold. In their neutral state, the electrons cannot carry electric current; however, electrons can move freely at their doped state with the help of strong electron acceptors. By this way, the polymer exhibits electrical conductivity almost as a metal. For example, MacDiarmid et al increased conductivity of polyacetylene by a factor of 10^{11} times.

Conjugated π electrons along the polymer backbone is the reason of exhibition of superior electrochemical characteristics. Conjugation provided by alternating single and double bonds results in charge mobility. Molecular orbitals are overlapped enhancing electron delocalization since each bond involves sp- or sp²- hybridized atoms [6].

Conduction mechanism of materials is explained using the band theory. Overlapping of orbitals forms delocalized energy bands. Relative population of each band determines conductivity of the material. The classification of materials as insulators, semiconductors and metals depends on the relative separation in occupied and unoccupied energy states. The band gap of a semiconductor material is between 5 and 3 eV with a filled valence band and an empty conduction band [7]. Doping procedure increases conductivity of the semiconductor creating either holes or electrons. As the electrons are taken from valence band, holes are

generated where p-type doping is achieved. On the other hand, n-type doping is performed by adding electrons to conductance band [8].

Doping is a type of redox process since it involves reduction or oxidation of electrons in the polymer chain [9]. Chemical structure of the polymer is not changed during reversible doping and dedoping mechanisms; whereas their band structure is altered upon redox processes. Doping process can be performed following either chemical or electrochemical treatment [10].

As seen in Figure 1.1, p-doping is generated during oxidation of polymer. In this process, removal of an electron from the valence band results in the formation of radical cations known as polarons. Delocalization of the created charge over the polymer segments leads to cleavage of a double bond in the scaffold. Bipolaron bands are created upon further oxidation. Removal of a second electron forms several bipolarons at high dopant concentration. Doped polymers generate partially filled bands located between valence and conduction bands. Hence, doping procedure yields electrical conductivity as metals.

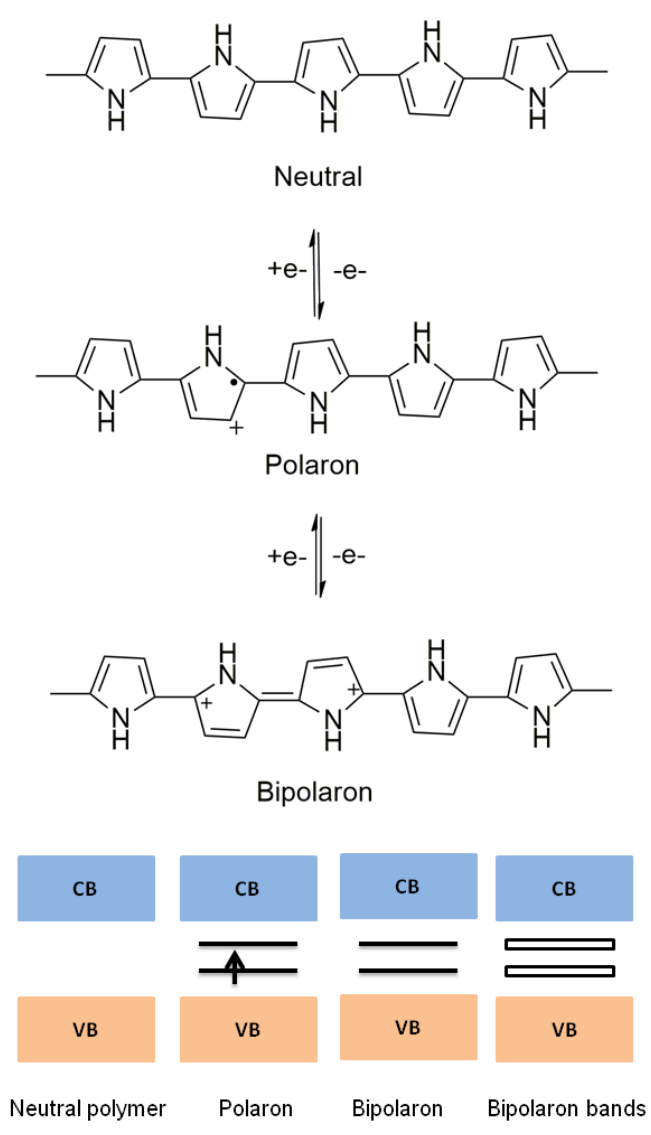


Figure 1.1. Structural representation of bipolaron formation in polypyrrole and its corresponding energy bands in the mid gap.

1.2. SYNTHESIS STRATEGIES OF CONJUGATED POLYMERS

There are two common methods employed to synthesize conjugated polymers: chemical and electrochemical polymerizations. Photochemical polymerization, solid state polymerization, pyrolysis are some examples of other strategies reported in literature [11].

Oxidation of monomers in the presence of specific agents is the basic idea behind the chemical polymerization. FeCl_3 is generally used as the oxidizing agent in the synthesis of heterocyclic polymers [12]. During such polymerization, oxidation of monomer by Fe^{3+} ions starts chain growth while Fe^{3+} ions are reduced to Fe^{2+} ions. Then, addition of strong base like ammonium hydroxide causes reduction to a neutral state. In another common employed approach of chemical polymerization is reacting a monomer with Mg in THF. Self-coupling with a metal complex catalyst like $\text{Ni}(\text{bipy})\text{Cl}_2$ is the second step for this polymerization strategy [13].

Although chemical polymerization provides the synthesis at low cost, intrinsic properties of the polymer may not be satisfied sufficiently. That is, low conductivity can be observed. Also, over-oxidation can be counted as a common consequence of chemical polymerization results in decomposition of the polymer and formation of side reaction products [14].

Furthermore, electrochemical polymerization presents many advantages over the chemical one. In this approach, the conducting polymer can be deposited on a surface by controlling the thickness of the polymer film in terms of charge passing through the cell. The reason of growing of polymer chain is the oxidation of the polymer to its doped states. This strategy offers reproducible and straightforward polymer growth. It allows controllable polymer deposition. However, characterization of the polymer is difficult using traditional methods like GPC since the product is insoluble.

There are several ways to polymerize the target monomer electrochemically: potentiostatic (constant-potential), galvanostatic (constant current) and potentiodynamic (potential scanning with cyclic voltammetry) [15]. The mechanism of electropolymerization of thiophen as an example is illustrated in Figure 1.2. The polymerization is achieved through successive electrochemical and chemical steps. That is why this procedure is also called as $\text{E}(\text{CE})_n$ mechanism (E for electrochemical, C for chemical). $\text{E}(\text{CE})_n$ mechanism continues until the oligomer product becomes insoluble in the reaction medium and is collected onto the surface which polymerization is taken place [16].

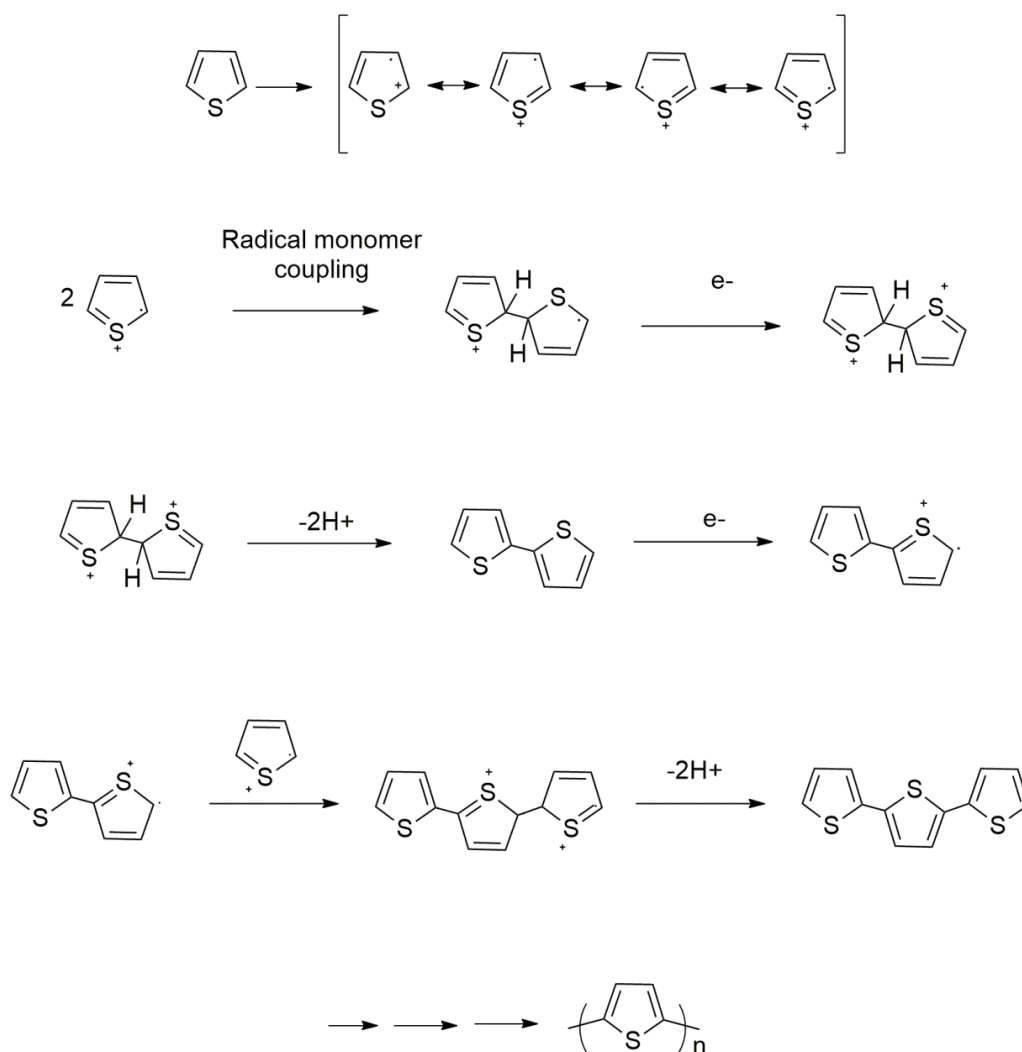


Figure 1.2. E(CE)_n mechanism of thiophen.

1.3. APPLICATION FIELDS OF CONJUGATED POLYMERS

Conjugated polymers lead opening a new research field owing to their outstanding characteristics like:

- (1) Ability to adjust their conductivity.
- (2) Having high mechanical strength.
- (3) Processability.
- (4) To be able to prepare using straightforward techniques.

Hence, their optical, mechanical and electrical properties make them fundamental materials in various fields like electrochromic devices [17], light emitting diodes [18], rechargeable materials [19], field effect transistors [20], photovoltaic devices [21], chemical and biological sensors [22], artificial muscles [23], drug delivery [24] and biomaging [25].

In this thesis, two main concepts are covered: conducting polymer based biological sensors and cell imaging studies.

1.3.1. Conjugated Polymers in Biosensor Design

Conjugated polymers have attracted keen interest throughout the world in biosensing design. They can be used as a support material of biological molecules preferring sensitive and stable sensor design [26].

Conjugated polymers offer simplicity and large scale production in the biosensor construction [27]. They can be grown over an electrode surface during electrochemical polymerization. Thickness of the polymer film can be arranged in this technique [28]. Besides, polymerization at room temperature is possible which is vital to preserve activity of the biomolecule used in sensor construction.

Moreover, they have ability to transfer electrical charge produced by enzymatic reaction. Conjugated π electron backbones provide electron mobility [29]. Such electron transfer results in direct communication between the transducer and the biomolecule [30]. Therefore, CPs in biosensor design improve the electrocatalytic properties of biological elements.

Since CPs have organized structures on transducer surfaces, three dimensional matrix onto the electrode can be created for efficient immobilization. Such matrix results in preserving the biomolecule activity for a long time [31]. In other words, CPs as a support platform offer robust enzyme activity on the transducer [32]. Also, they are known as biocompatible materials. Thus, they can mimic the naturally occurring environment of biological molecules.

One of the important advantages is that CPs allow structural and electronic modifications of the surfaces to be chosen as support matrices for biomolecule deposition [33]. They can be functionalized according to desired purpose. By this way, one can alter the structure of the polymer and thus, electronic and mechanical properties of the surface.

1.3.2. Conjugated Structures for Bioimaging Purpose

Recently, fluorescence cell imaging has attracted great interest in medical applications [34]. The materials used in imaging purposes should be stable chemically, non-toxic, have strong emission characteristics [35]. Thus, conjugated polymers are important materials preferred in this field owing to their biocompatibility and performance as imaging probes.

The interest in conjugated structures is basically attributed to their high photoluminescence and electroluminescence characteristics as well as to their color tunability achieved by molecular design [36].

π -Conjugated systems are remarkably fluorescent materials. Their fluorescent nature is the main reason for their wide use in such applications. Also, they give possibility to long term imaging without bleaching [35]. Fluorescent conjugated structures acquire extremely strong light-harvesting ability [37]. Moreover, conjugated systems offer the desired versatility by tuning structure of the polymer according to desired functionality. By this way, scientists can modify chemical structure of the polymers concerning their binding characteristics and affinity to sites of targeted agents. Furthermore, biocompatibility of the conjugated structures is the result of exhibiting low cytotoxicity against cell lines.

The detailed explanation about the requirements of materials used in cellular imaging studies is given in the chapter of 4.

CHAPTER 2

2. CONDUCTING POLYMERS CONTAINING POLYPEPTIDE AND FERROCENE SIDE CHAINS AS ETHANOL BIOSENSORS

2.1. INTRODUCTION

2.1.1. Oxidoreductase Enzymes in Biotechnology

Various chemical transformations proceed using enzymes which make these catalysts a main element in biotechnology industries. Over the last few decades, many researchers have focused on enzyme technology to operate them in practical applications. Since remarkable amount of industrial processes involve oxidation and reduction mechanism, the biggest class of enzymes, called as oxidoreductases, is a major of interest among the scientific world.

International Union of Biochemistry (IUB) has divided the enzymes into six categories: oxidoreductases, transferases, hydrolases, lyases, isomerases and synthetases (ligases) [38]. There are numerous application areas for oxidoreductases which catalyze biological oxidation/reduction reactions since a number of biochemical applications involve redox reactions.

The largest class of oxidoreductases is dehydrogenases. The most known mechanistic and substrate specificity data belongs to this class. It can be categorized according to their cofactor requirement; NAD(P) dependent and flavin coenzyme dependent. For instance alcohol dehydrogenase, malate dehydrogenases are included in NAD(P)-dependent class whereas succinate dehydrogenase is one of the flavin coenzyme dependent class.

The oxygenases are known as the second class of oxidoreductases. Incorporated molecular oxygen in their structure makes this class highly effective and selective. Oxygenases have attracted considerable interest for industrial processes thanks to their high degree of regio and stereoselectivity [39]. Dioxygenases and monooxygenases are the main class of oxygenases. The number of oxygen atoms in dioxygen molecule incorporated into the substrate is the determining factor for this classification. [40]. That is the mono- and di- terms describe only stoichiometry of the oxygen that incorporates the reaction. In industrial processes, oxygenases are not preferred since they are unstable and need expensive co-factor as NAD(P)H. Also, additional screening methods are required due to their complex educt structures and the regio- chemo- and enantiospecific reactions [41].

The last and most preferable class of oxidoreductases in biotechnology is known as oxidases. In dehydrogenases, coenzymes are used as the electron acceptors. On the other hand, oxygenases require reducing equivalents and oxygen for bioactivity. However, only molecular oxygen is needed as an electron acceptor (oxidant) for catalysis reactions of oxidases. Oxidases play a vital role in industrial applications among the other oxidoreductases [42]. They include the flavoprotein oxidases (glucose oxidase), metalloflavin oxidases (aldehyde oxidase) and heme-protein oxidases (peroxidases) [38].

2.1.2. Biocatalysts Used for Conversion of Alcohols

Two different enzymes, namely alcohol dehydrogenase (ADH) and alcohol oxidase (AOX) can be used for conversion of alcohols to their corresponding carbonyl compounds. There are several important differences between ADH and AOX. The reaction mechanisms are summarized in Figure 2.1.

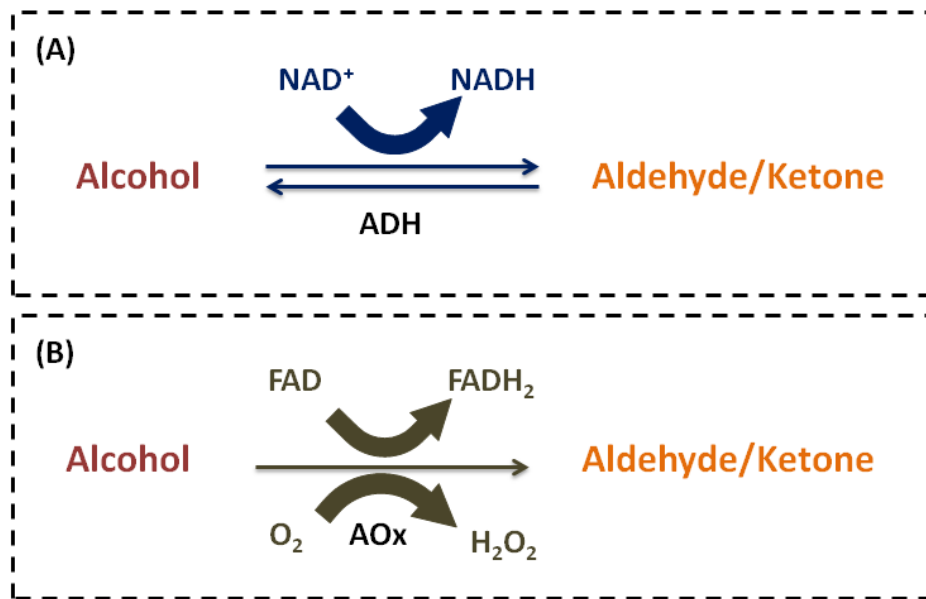
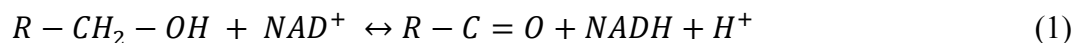


Figure 2.1. (A) Alcohol dehydrogenase (ADH) and (B) alcohol oxidase (AOX).

2.1.2.1. Alcohol dehydrogenase (ADHs)

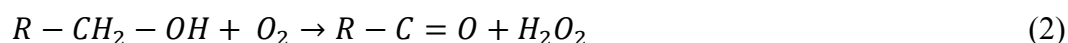
Alcohol dehydrogenase (ADH; Alcohol: NAD⁺ oxidoreductase, EC 1.1.1.1) undergoes a reversible oxidation reaction using primary aliphatic (except methanol) alcohols as the substrates, according to Eq. (1) [43];



NAD⁺/NADH is a redox pair in ADH reaction requiring the external additional NAD based cofactors. Furthermore, closeness of the co-factor to the enzyme without any irreversible entrapment is crucial. These requirements make them unfavorable in sensing technology although ADH is known to be more stable and shows high specificity to its corresponding substrates than AOx.

2.1.2.2. Alcohol Oxidase (AOx)

Alcohol Oxidase (AOX, Alcohol: O₂ oxidoreductase, EC 1.1.3.13) catalyzes the direct conversion of alcohols into corresponding aldehydes or ketones, using molecular oxygen as the electron acceptor [44]. It is included in the class of flavoprotein oxidases since AOx requires flavin-based cofactors. The redox center of the enzyme incorporates FAD which transfers the hydrate ion provided by alcohol substrates to molecular oxygen by generating H₂O₂ formation, according to Eq. (2) [43];



AOX has eight identical sub-units in a quasi-cubic arrangement. Each unit contains a strongly bound cofactor, FAD molecule [45]. Methylophilic yeast like *Hansenula*, *Pichia*, *Candida* are used as general sources to produce AOx during growth on methanol.

According to substrate specificity of AOx, short chain alcohol oxidase (SCAOx), long chain alcohol oxidase (LCAOx), aromatic alcohol oxidase (AAOx), and secondary alcohol oxidase (SAOx) are the main four categories. [46] (Figure 2.2). These enzymes are generally isolated from bacteria, yeast, fungi, plant, insect, and mollusks. SCAOx and LCAOx are intracellular in nature and described as multimeric proteins with very high holoenzyme molecular masses. On the other hand, AAOx and SAOx are known as mostly secreted to the medium.

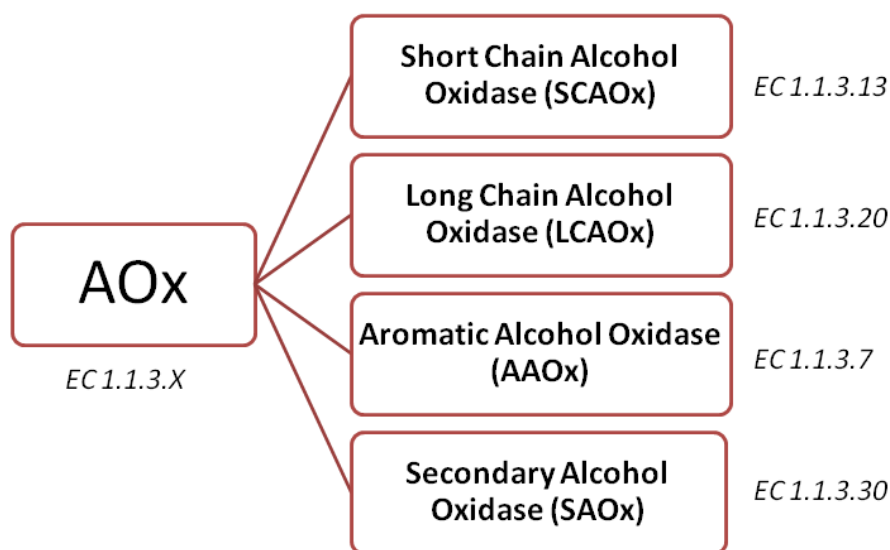


Figure 2.2. Classification of AOx.

SCAOx (EC 1.1.3.13) which is also known as methanol oxidase or ethanol oxidase is used to catalyze the oxidation of shorter chain length of alcohol substrates (C₁-C₈ carbons) [47]. Common sources of SCAOx are yeasts, fungi and limitedly mollusk. FAD as cofactor attaches to the protein non-covalently. Activity of this type of enzyme is achieved generally over a pH range of 6-9. Also, 25-30°C is widely reported optimum working temperature [48].

LCAOx (EC 1.1.3.20), also known as fatty alcohol oxidase (FAO), oxidizes alcohol analyte having carbon chain length of above C₆. General reported source of LCAOx is yeast species. Moreover, LCAOx has lower molecular mass and subunit number than SCAOx. They are very sensitive to temperature changes. LCAOx loses its activity even at 45°C [49]. The enzyme maintains its activity within the range of 4.8-10 [50].

Polyvinyl alcohol oxidase (PAO) and cholesterol oxidase (ChOx) are the examples of SAOx (EC 1.1.3.30) [46]. SAOx converts secondary alcohols to the corresponding ketones. Furthermore, aromatic alcohol oxidase or aryl alcohol oxidase (AAO; aryl-alcohol: oxygen oxidoreductase: EC 1.1.3.7) oxidizes aromatic primary alcohol to corresponding aromatic aldehyde [51].

2.1.2.2.1. Potential Application of AOx

Preferring alcohol oxidase protein in many research areas have several reasons. Firstly, the promoter including in AOx expression is one of the most effective and most tightly controlled promoter in nature. This feature makes the enzyme highly attractive host for heterologous gene expression [52]. Secondly, it has an ability to catalyze several alcohols irreversibly and selectively without needing any external co-factors. Moreover, different aerobic microorganisms play a role in producing these enzymes. Thus, production of these proteins in large scale is accessible [46].

In general, there are several difficulties in using enzymes for different application purposes. Even temperature and pH of the working environment can be controlled, inactivation and denaturation may occur. Also, organic solvents may cause to denature many enzymes whereas proper mixed solvent systems may lead to enhanced enzymatic reaction efficiency. On the other hand, enzymatic reactions have two vital advantages compared to non-enzymatic ones. Enzymatic catalysis shows high selectivity and stereospecificity and has high reaction rate under even milder conditions. Thus, the selection of proper enzymes according to the desired applications requires a big effort.

Detection and quantification of alcohols and their derivatives in various body fluids attain high interest in clinical monitoring as well as food technology. There is an increasing demand for developing sensitive, selective and accurate analytical methods which leads to improvement in biochemical sensing technology. The measurement of alcohol content is crucial in order to detect the quality of final product in alcoholic beverages, to control fermentation processes in food industry and to determine alcohol level in blood samples for clinical analysis. These industries require rapid and simple, accurate, sensitive and selective methods. This necessity leads to development of different types of biosensing systems for alcohol determination.

AOx protein is used for fabrication of alcohol sensors since [52].

- a) Primary alcohols exhibit high affinity,
- b) Its active form is very stable,
- c) It is easily available.

2.1.2.2.2. AOX-Based Alcohol Biosensor

There are numerous amperometry based alcohol biosensors revealed in literature. Detection methods differ by monitoring whether consumption of O_2 or production of H_2O_2 [53]. The most widely revealed detection technique in AOX based biosensor is O_2 monitoring in the last few decades [54]. In 1962, the first amperometric enzyme based biosensor was developed which is called as Clark type amperometric electrode [55]. The proposed sensor was designed to monitor glucose level in any test solution. The basic setup includes a Ag/AgCl reference electrode, a platinum cathode where oxygen is reduced and the designed electrode as the working electrode. Upon applied -0.68 V, a current change is detected which is proportional to the reduced oxygen level in the reaction medium. That is, application of voltage causes consumption of oxygen which is monitored as current change. By this way, consumed oxygen level is detected until the formation of new equilibrium is established in the reaction medium. Also, enzymatic reaction depends on consumption of substrate which is in direct relation with the consumed oxygen level in the reaction medium. The formation of new equilibrium is observed during the enzymatic reaction. Therefore, the rate of diffusion of oxygen in the bulk solution is the main determinant factor of the rate of electrochemical reaction [56]. However, these types of sensors, for sure, have several limitations which should be considered while designing of any enzyme electrode. Low voltage values may cause high minimum detectable concentrations. Also, low accuracy and reproducibility may count as disadvantages which should be overcome using appropriate technologies like nanostructures according to desired sensing purposes [46].

Other approach in fabrication of amperometric biosensor is following H_2O_2 production. It depends on applying $+0.68$ V potential to the cathode electrode. H_2O_2 consumption is recorded relative to the reference electrode which is also

called as the hydrogen peroxide electrode. The most important obstacle of this sensing technology is the requirement of higher potential compared to oxygen electrode. The over potential causes electrochemical interference during detection of the analyte [57]. For example, the glucose level measurement in blood samples is one of the major interests in biosensing technology. However, the blood sample includes various electroactive species like ascorbic acid, paracetamol or uric acid. Application of over potential may activate these reagents that causes change in results.

2.1.3. Biosensors

A biosensor is an analytical device combining a biological component and a transducer device that converts a biological signal into a quantifiable electric signal. Biosensors utilizing a biochemical reaction are known as a type of chemical sensors. Using selective biochemical reagent in sensor system leads to transformation of information from the chemical domain into an output signal.

The digital electrical signal generated during measurement is proportional to the concentration of analyte. The specificity is assured through the biological component integrated to the proposed biosensor since the biological materials are responsible for recognition of the substrate [58]. The biological component of biosensor is categorized into two main groups: bio-active and bio-affinitive (Figure 2.3). The bioactive group, also known as the catalytic group, consists of enzymes, microorganisms and tissues, while the non-catalytic called as bio-affinitive includes antibodies, receptors and nucleic acid etc. A biological material is incorporated with a different types of transducer to construct electrochemical (conductometric, potentiometric and amperometric), optical, colorimetric and acoustic biosensor systems [59] (Figure 2.3). The most widely used biosensing systems are the enzyme-based amperometric electrodes [60].

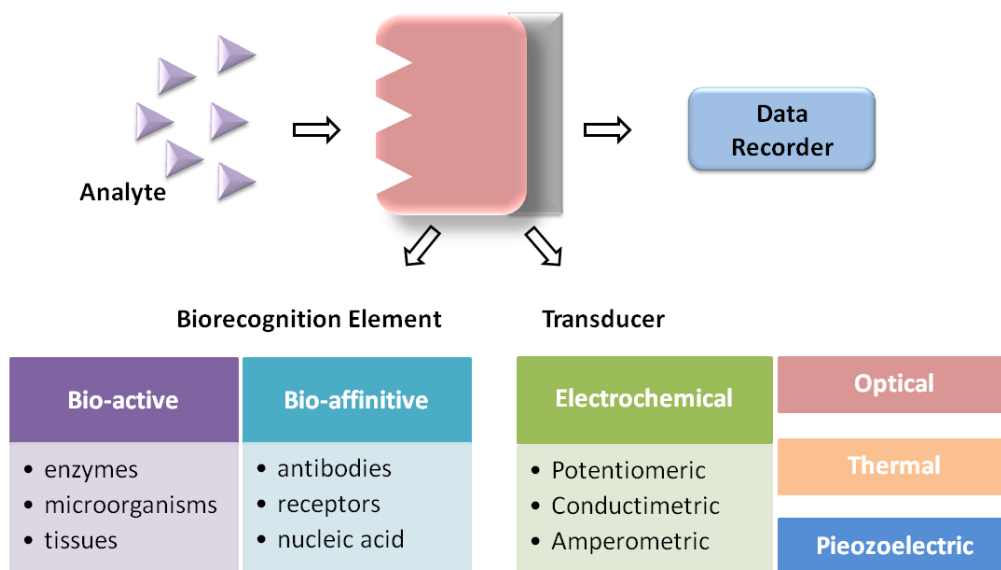


Figure 2.3. Main components of a biosensor.

The father of the biosensing technology is Prof. Clark Jr. since he defined the oxygen electrode in 1956 [61]. Then, in 1962, he proposed the first glucose electrode which included glucose oxidase as a recognition element entrapped at a Clark oxygen electrode [55]. He defined decreased oxygen level in the reaction medium which was directly related to substrate concentration. The evolution of biosensor has started with this pioneering work. Updike and Hicks in 1967 [62] described the first functional enzyme based electrode using GOx deposited directly onto the oxygen electrode. This study is counted as the beginning of a great effort in application of biosensors in terms of immobilization of biorecognition element.

2.1.3.1. Generation of Amperometric Biosensors

Amperometric biosensors monitor the current change for the reaction of an electroactive reagent upon an applied potential. Such measurement technique has several advantages over the other sensing methods since it is fast, precise and more sensitive than the others [63]. The amperometric response is a linear function of

analyte concentration in the reaction solution. During catalytic reaction, the molecular oxygen which is the natural co-substrate of oxidases is converted to hydrogen peroxide. Therefore, change in oxygen and hydrogen peroxide concentration is substrate dependent for such an oxidoreductase enzyme.

Amperometric biosensors relying on integration level in terms of the nature of mediator and the immobilization method can be categorized as *first*, *second* and *third* generations (Figure 2.4).

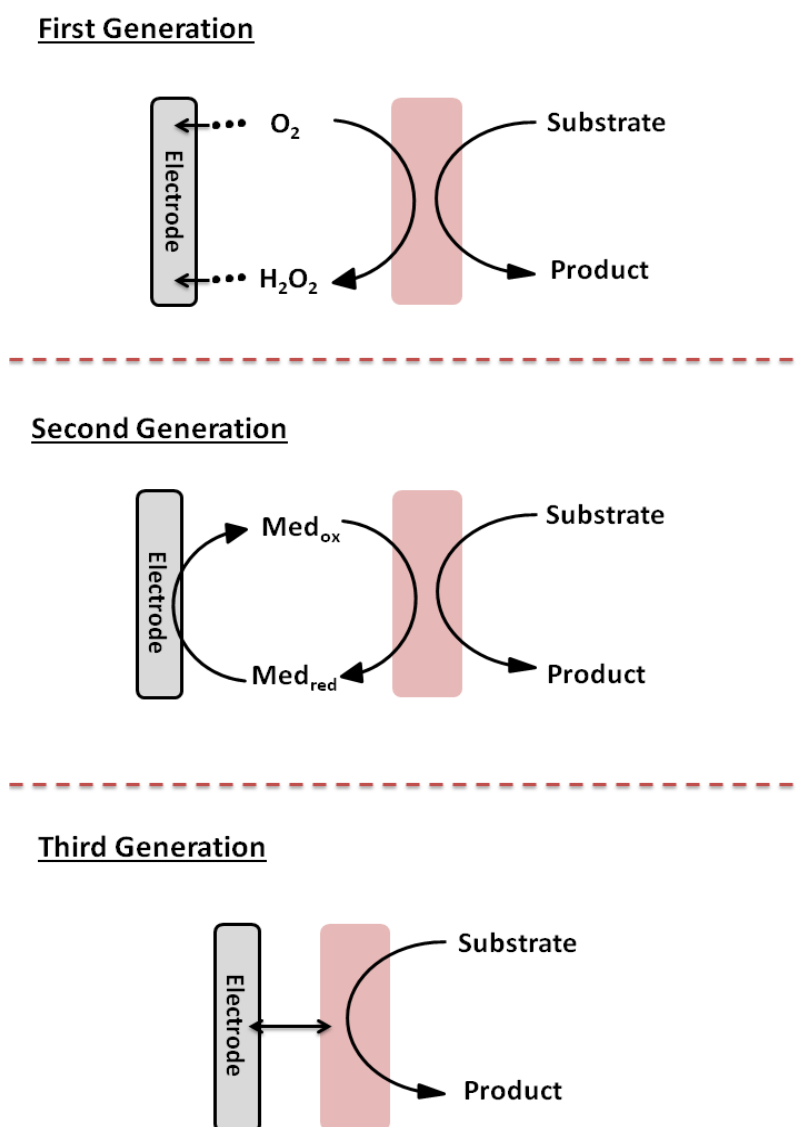


Figure 2.4. Schematic representation of three generations of amperometric biosensors.

2.1.3.1.1. *First* Generation Biosensors

First generation includes only the biological component and a transducer. The biorecognition element is attached onto the electrode surface via bounding or entrapment to either consume molecular oxygen or to produce hydrogen peroxide upon an applied appropriate potential. As a result of diffusion of the reaction product to the transducer, the electrical current is recorded. Even though the simple construction can be a good point for biosensor fabrication, selectivity is the main obstacle of this approach. The requirement of high voltage causes to interfere the sensor response negatively. Also, oxygen level in real samples may not be enough for this concept since the first generation sensors are dependent on concentration of dissolved O₂ in the bulk medium [64]. It can be a limiting factor in real time analysis.

2.1.3.1.2. *Second* Generation Biosensors

In the *second* generation, mediators are located between the receptor and the transducer in order to enhance sensor signal. Such reagents promote electron transfer between the enzyme and the electrode. Further enhancement can be achieved by replacing the oxygen with the mediator which shuttles the electrons from the redox center of the enzyme to the transducer [65]. The necessity of high applied potential in the first generation sensor design can be eliminated by using such reagents [66]. Although mediator in the sensing design may improve the selectivity of the sensor, leakage of the mediator can be appeared commonly which causes a decrease in biosensor signals [29].

2.1.3.1.3. *Third* Generation Biosensors

Integration of any reagent with the enzyme and the electrode is the main idea behind the *third* generation biosensors. In order to provide a desired electron transfer rate, immobilization method is used for both the biomolecule and the other species like mediators which can be included to improve sensor performance. Co-

immobilization of the enzyme and mediator like species on electrode surface makes the biorecognition element an integral part of the transducer [67]. The electrons behave as a second analyte for the catalytic reaction resulting in the generation of the current [63]. In general, the difference between *second* and *third* generation biosensors does not seem important. However, *third* generation sensors present both all benefits of *second* generation biosensors as well as some new ones. *Third* generation design depends on the direct immobilization of the whole sensing chemistry on the transducer that results in direct communication between the biocatalyst and the electrode [68]. This approach leads to satisfying the requirements for real time analysis. Also, the biosensors belonging to this generation can be used as an analytical tool in the fields of food industry, biomedicine or environmental monitoring effectively.

2.1.3.2. Mediators

Mediators are artificial agents which are used for transferring the electrons from the redox center of the enzyme to the electrode surface. They can take part in redox reactions and thus lead to production of rapid electron transfer [69].

A mediator should be stable under optimized working conditions of the biosensor and also should not give any side reactions during electron transfer [64]. The working potential of the designed biosensor with a mediator is expected to arrange properly. It should have a lower redox potential than the other electroactive reagents in the bulk sample. That is, the redox potential of mediator should be sufficient enough to shuttle electrons between the active side of the enzyme and transducer. Also, the potential of the mediator should be positive for oxidative reaction or negative for reductive reaction.

An ideal mediator should satisfy several requirements [64]:

- (1) Reaction between the mediator and the reduced enzyme should be rapid enough.
- (2) The working potential should be low and pH independent.

- (3) Kinetics of the mediator is expected to develop in a reversible way.
- (4) Oxidized and reduced forms of the mediator should be stable.
- (5) Molecular oxygen in the working environment should not give any reaction with the reduced form of the mediator.

Use of mediator in the biosensor fabrication results in the enhancement of selectivity and sensitivity of the biosensor [57]. There are important advantages of using mediators. Dependence of oxygen level in the reaction medium is reduced during sensor measurement. Also, the low oxidation potential can result in preventing interference of unwanted reagents in the bulk solution.

Over the last decades, organic dyes like methylene blue, phenazines, alizarin yellow, Prussian blue, thionin or inorganic redox ions such as ferricyanide have been widely used in sensor technology [70]. Nevertheless, a number of problems like pH dependency or poor stability are faced in biosensing system. For example, tuning the redox potential of inorganic mediators is severe. Solubility in the presence of other substituents included in the biosensing platform may be problematic.

2.1.3.2.1. Ferrocene and Derivatives

Recently, the use of ferrocene and its derivatives as mediators have attracted really great interest in the fabrication of high performance biosensors [71]. Ferrocene derivatives are known to be excellent electron transfer mediators due to their superior characteristics such as relatively low molecular mass, reversibility and generation of stable redox forms [72].

Development of a redox polymer modified electrode has led to a worldwide interest in biosensor construction since polymers enable the incorporation of reagents into the polymer backbone. Typical examples involving direct coordination of ferrocene to a polymer with covalent linkage demonstrates the possibility of fabrication of reagentless devices, thus preventing the leaching of the mediator [73]. The existing methodologies comprising noncovalent attachment of

ferrocene to the biosensor create problems associated with signal loss and decrease in the lifetime of the biosensor and problems with the analytical performance arising from the diffusion of ferrocene away from the surface into the bulk solution during enzymatic reaction [72]. Thus, considerable efforts have been directed towards the development of effective biosensors by incorporating ferrocene units within the polymeric chain.

2.1.3.3. Polypeptide Chain in Biosensor Applications

Polypeptides, possessing wonderful biocompatibility as well as remarkable mechanical and biological durability, are used to advance an excellent platform in biosensor fabrication [74]. Furthermore, polypeptides are assumed to exhibit a three dimensional conformation under certain conditions [75].

The elaboration of polypeptides into the polymeric structures opens new perspectives in the field of biotechnology as they are fascinating biomaterials mimicking natural proteins [76]. Therefore, combining synthetic polymers with polypeptide segments becomes a promising approach in the field of enzyme immobilization. The resulting feature reveals compelling self-assembling behavior [77] and new versatile functions are created through synergic effect of polymeric structures with polypeptide units. Hence, a novel design and syntheses of polypeptide containing conjugated polymers have attracted great interest.

2.1.4. Scope of the Study

Over the past decades, numerous studies reported in literature have been employed for the fabrication of ethanol biosensors using different support matrices. AOX from *Pichia pastoris* (EC 1.1.3.13) is the one of the most used biorecognition element owing to its high substrate specificity and availability. Low molecular weight alcohols undergo an oxidation reaction with molecular oxygen to produce the corresponding aldehydes or ketones.

Since there is an increasing demand of reliable ethanol detection in several fields like food industry, research on generation of an appropriate matrix to achieve improved sensor performance have attracted considerable interest day by day. This matrix is expected to be biocompatible, non-toxic and permanent. Also, bioactivity of the enzyme should be preserved via generating suitable attachment between transducer and the biological element. At this point, conjugated polymers have become an important material for the immobilization platform of ethanol sensing systems. Since functionality on the transducer surface can be obtained easily via modifying the polymer containing surface with desired pendant groups.

Kekec and co-workers developed a conducting polymer based ethanol biosensor [78]. For this purpose, a functional monomer, 9-methyl-9*H*-carbazole-3-carbohydrazine (MCCH) was synthesized and polymerized onto the electrode surface electrochemically. The use of CP coated transducer provides well-organized adjustable morphology and extensive stability [28,32]. Furthermore, the electrons can move freely on the conjugated π electron backbones by enhancing electrocatalytic properties of the enzyme [29]. Covalent immobilization of AOX was generated using N-(3-dimethylaminopropyl)-N'-ethylcarbodiimide hydrochloride (EDC)/N-hydroxysuccinimide (NHS) chemistry thanks to amino groups in the polymer backbone. By this way, amino groups of the polymer and carboxylic acid groups of the enzyme attach covalently resulting in wide linear range, high sensitivity and low detection limit. Also, applicability of the proposed design was proven using several commercial alcoholic beverages. In another study, the combination of a conducting polymer of 2-(4-nitrophenyl)-4,7-di(thiophen-2-yl)-1*H*-benzo[d]imidazole (BIPN) with functionalized MWCNTs (f-MWCNT) was employed as the support material for the ethanol determination. While CPs having functional groups enhance enzyme loading through the attachment between the enzyme and the polymer surface, MWCNTs provide superior electron transfer resulting in fast response time during ethanol measurement. Such strategies can improve the biosensor performance.

There are numerous structures which can be good candidates to improve biosensor signals. For example, Boujtita et al. [79] developed a support electrode doped with 5% cobalt phthalocyanine (CoPC) and casted AOX for ethanol analysis of beer. In

this study, CoPc behaved as the electrocatalyst for oxidation reaction during redox enzyme reaction [80]. By this way, low working potential can be employed during measurement. Multiwalled carbon nanotubes—Nafion® (MWCNT-Nf) matrix encapsulated with polyethylenimine (PEI) on electrode was one of the approach employed previously for ethanol detection [81]. Smutok and co-workers developed an electrode modified by Os-complex for ethanol analysis [82].

Hence, each structure can serve their own benefits on the same platform. According to desired purpose, one can create an appropriate environment through determining the suitable structure. Thus, scientists use their imagination and knowledge on material chemistry in order to develop an efficient sensing platform. This is the main delighted motivation for the development of different biosensors in the thesis.

Herein, an electrochemically simple synthetic approach, capable of yielding random conducting copolymer possessing both polypeptide side chains and ferrocene units is described. The conjugated biopolymer architecture prepared by the electroactive polypeptide macromonomer and an amino functional BEDOA-6 monomer, were copolymerized with another electroactive monomer; ferrocene imidazole derivative of dithiophene (TIFc). Such combination allows well interaction between the biomolecule and conducting layer thereby improving the stability. It was then predicted that the polymer coated on the electrode provides an excellent matrix for the immobilization of AOx through the terminal amino groups of the polypeptide side chains. In a subsequent step, the matrix was fixed by using glutaraldehyde as the cross linking agent. In this study, we demonstrate that conjugated conducting coatings based on peptide sequences in combination with ferrocene units and specific enzymes such as AOx provide a simple route to surfaces that can act as amperometric ethanol biosensor. This versatile novel coating platform is expected to be translated into a number of biosensor applications by using suitably selected enzymes.

2.2. RESULTS and DISCUSSION

A novel approach for the fabrication of a biosensor with conducting polymer bearing polypeptide segments and ferrocene moieties was reported. The approach pertains to the electrochemical copolymerization of the electroactive polypeptide macromonomer and independently prepared ferrocene imidazole derivative of dithiophene (TIFc), respectively on the electrode surface. The polypeptide macromonomer was synthesized using amino functional bis-EDOT derivative (BEDOA-6) by Yagci and co-workers [83]. Alcohol oxidase (AOx) was then covalently immobilized onto the copolymer coated electrode using glutaraldehyde as the cross linking agent.

2.2.1. Electro (co)polymerization and Electrochemical Studies

Electrochemical copolymerization is an efficient approach to obtain polymers having combined properties of the homopolymers. These copolymers are expected to embody the superiority of both of the parent polymers, display better coating and electrochemical properties. In order to combine polypeptide and ferrocene properties on a conducting polymer, electrochemical copolymerization of BEDOA-6-poly(L-Boc) macromonomer and TIFc was accomplished by cyclic voltammetry technique. For comparison, homo polymerization of TIFc in the absence of the macromonomer under identical experimental conditions was also performed (Figure 2.5).

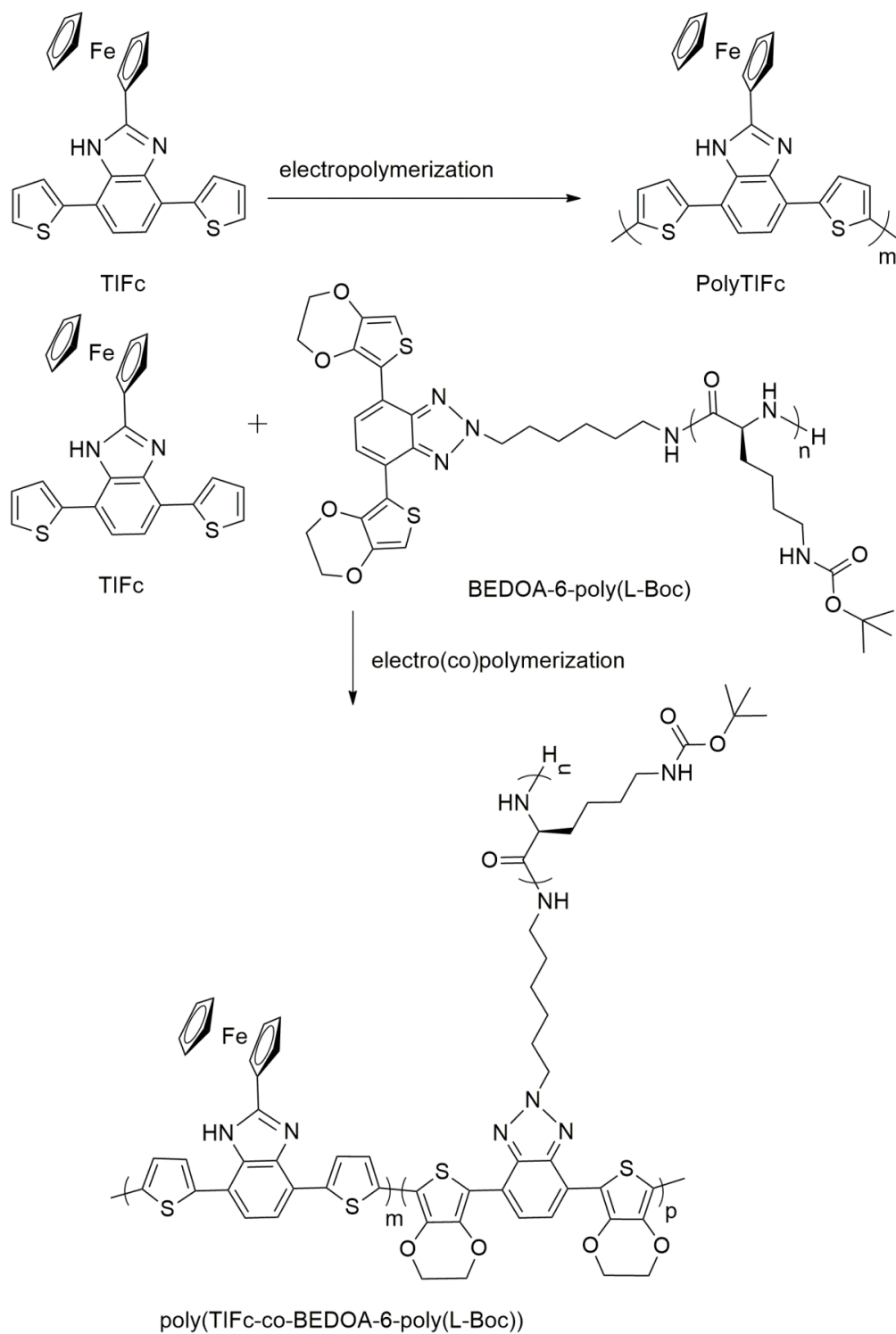


Figure 2.5. Synthesis of poly(TIFc) and poly(BEDO-6-poly(L-Boc)) by electropolymerization.

The electrochemical behaviors of deposited films of the copolymer and homopolymer were studied by cycling the potential between -0.20 V and +0.80 V vs. Ag wire in 0.1 M ACN/DCM (95:5) solution of LiClO₄/NaClO₄ (blank solution). Figure 2.6 displays the cyclic voltammogram of the poly(TIFc-co-BEDOA-6-poly(L-Boc)) copolymer and homo PolyTIFc films in blank solution at a scan rate of 100 mV/s respectively. The differences in blank solution responses can clearly be observed. While the homopolymer film shows two oxidation and two reduction peaks at 0.50 V/0.65 V and 0.55 V/0.34 V, respectively, the copolymer film presents the corresponding redox couples at different potentials at approximately 0.44 V/ 0.62 V and 0.54 V/ 0.40 V.

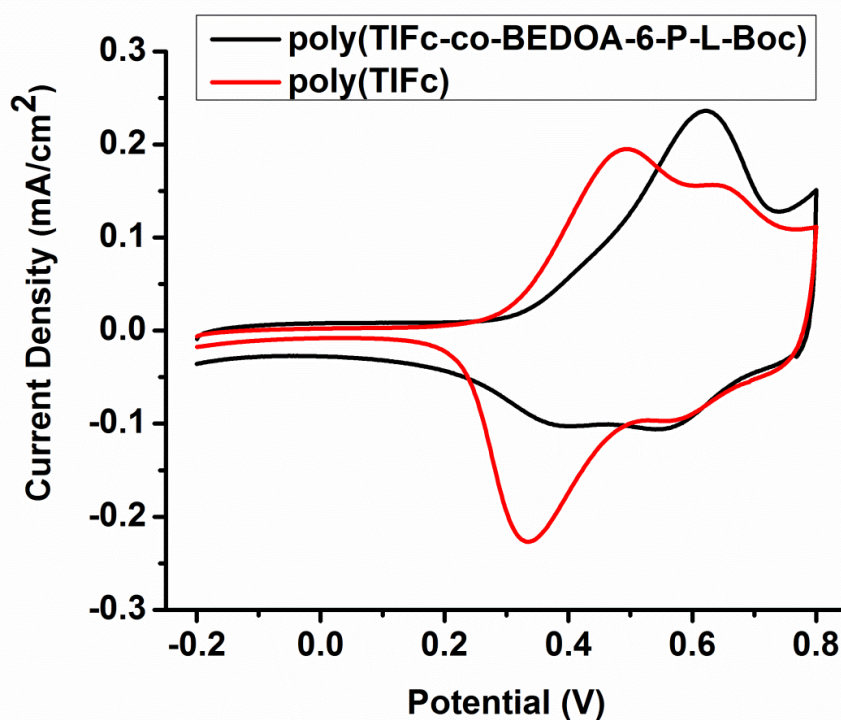


Figure 2.6. Single scan cyclic voltammograms of poly(TIFc) and poly(TIFc-co-BEDOA-6-poly(L-Boc)) in a monomer free 0.1 M ACN/DCM (95:5) solution of LiClO₄/NaClO₄.

To further confirm the electroactivity of the films thus formed on the electrode, the peak current of the copolymer was monitored in the monomer-free supporting electrolyte system as a function of scan rate during cyclic voltammetry (Figure

2.7A). The related anodic peak current density at 0.3 V responses are illustrated in Figure 2.7B. As seen, anodic current densities of the copolymer show a linear dependence with the scan rate. Such observation indicates that migration of the electroactive species is not diffusion controlled and the polymer film is well adhered.

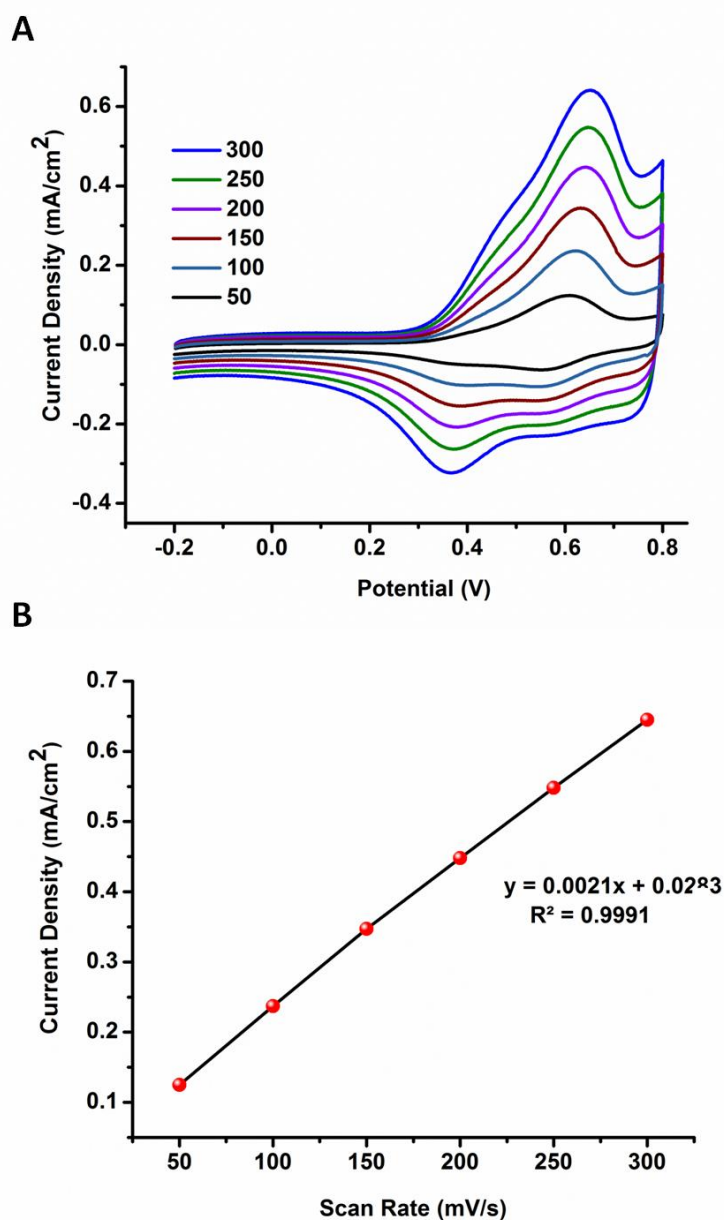


Figure 2.7. Cyclic voltammograms of (A) poly(TIFc-co-BEDOA-6-poly(L-Boc)) film in 0.1 M NaClO₄/LiClO₄/DCM/ACN (5/95, v/v) at scan rates of 50, 100, 150, 200, 250 and 300 mV/s. (B) Correlation between scan rate and peak current of the film.

2.2.2. ATR-FTIR

The structures of the polymers were confirmed by the ATR-FTIR analysis. Figure 2.8 shows the ATR-FTIR spectra of homo poly(TIFc) and poly(TIFc-co-BEDOA-6-poly(L-Boc)). In the spectrum of poly(TIFc), the characteristics ferrocene peaks appear at around 799 cm^{-1} , 1108 cm^{-1} , 1413 cm^{-1} , 3100 cm^{-1} [84]. In the copolymer spectrum, in addition to these ferrocene peaks, new bands corresponding to the polypeptide units are detected. The peak at 1168 cm^{-1} is due to C-O stretching vibration. The amide II and C=O amide stretching bands resonate at 1545 cm^{-1} and 1698 cm^{-1} , respectively [85]. The peaks at 2934 cm^{-1} and 3293 cm^{-1} are assigned to free amino acid C-H stretching and $-\text{NH}_2$ stretching vibration, respectively. The presence of conjugated backbone stemming from both monomer and macromonomer sequences was also confirmed. The signals at 1267 cm^{-1} , 1412 cm^{-1} and 1435 cm^{-1} are associated with $=\text{C}-\text{O}$ stretching, C-N stretching and C=N vibration, respectively. Aromatic conjugated C=C stretching vibration is observed at 1651 cm^{-1} [86]. The peak at 2978 cm^{-1} corresponds to C-H stretching vibration. These observations verify that both monomer and macromonomer take part in the electrochemical process and the resulting copolymer possesses their prominent features.

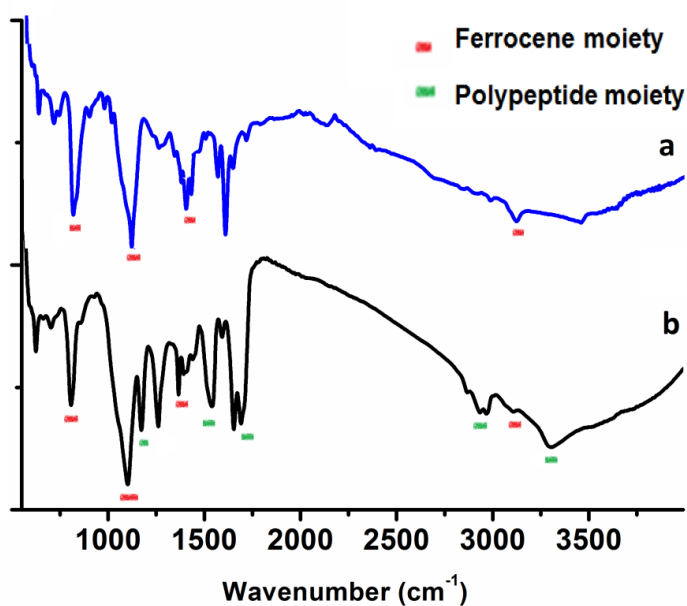


Figure 2.8. ATR-FTIR spectra of (a) poly(TIFc) and (b) poly(TIFc-co-BEDOA-6-poly(L-Boc)).

2.2.3. Optimization of Experimental Parameters

Effect of poly(TIFc) and poly(TIFc-co-BEDOA-6-poly(L-Boc)) films on biosensor performance was investigated. For this purpose, two different biosensors were prepared using different polymer films while all parameters were kept constant.

As shown in Figure 2.9A, the enzyme electrode prepared with copolymer film exhibited the highest biosensor performance. It can be easily seen that presence of only ferrocene moieties on the electrode surface do not reveal the biosensor performance as good as the one in the presence of copolymer films. Although ferrocene containing conducting polymer film facilitate the biosensor performance with mediator characteristic, it is not enough to bring about an appropriate platform for enzyme deposition. On the other hand, it was observed that when a biosensor with the incorporation of the polymeric structures bearing polypeptide segments was fabricated, biocompatible chains led to increase biosensor performance, providing three-dimensional microenvironment for biomolecules. Moreover, poly(TIFc-co-BEDOA-6-Poly(L-Boc)) copolymer film enables the formation of covalent bond during immobilization step owing to its bearing pendant amino groups which create a robust and efficient conjugation between enzyme molecules. Thus, this strong attachment enhanced retention of biocatalytic activity. Accordingly, performance of the biosensor was improved by the addition of mediators in immobilization matrix. Also, good film forming capability of poly(TIFc) makes the immobilization platform excellent for biomolecules deposition by providing appropriate morphology. Hence, the interests of each polymeric structure were combined via copolymerization and used in the same platform, achieving an excellent alcohol biosensor.

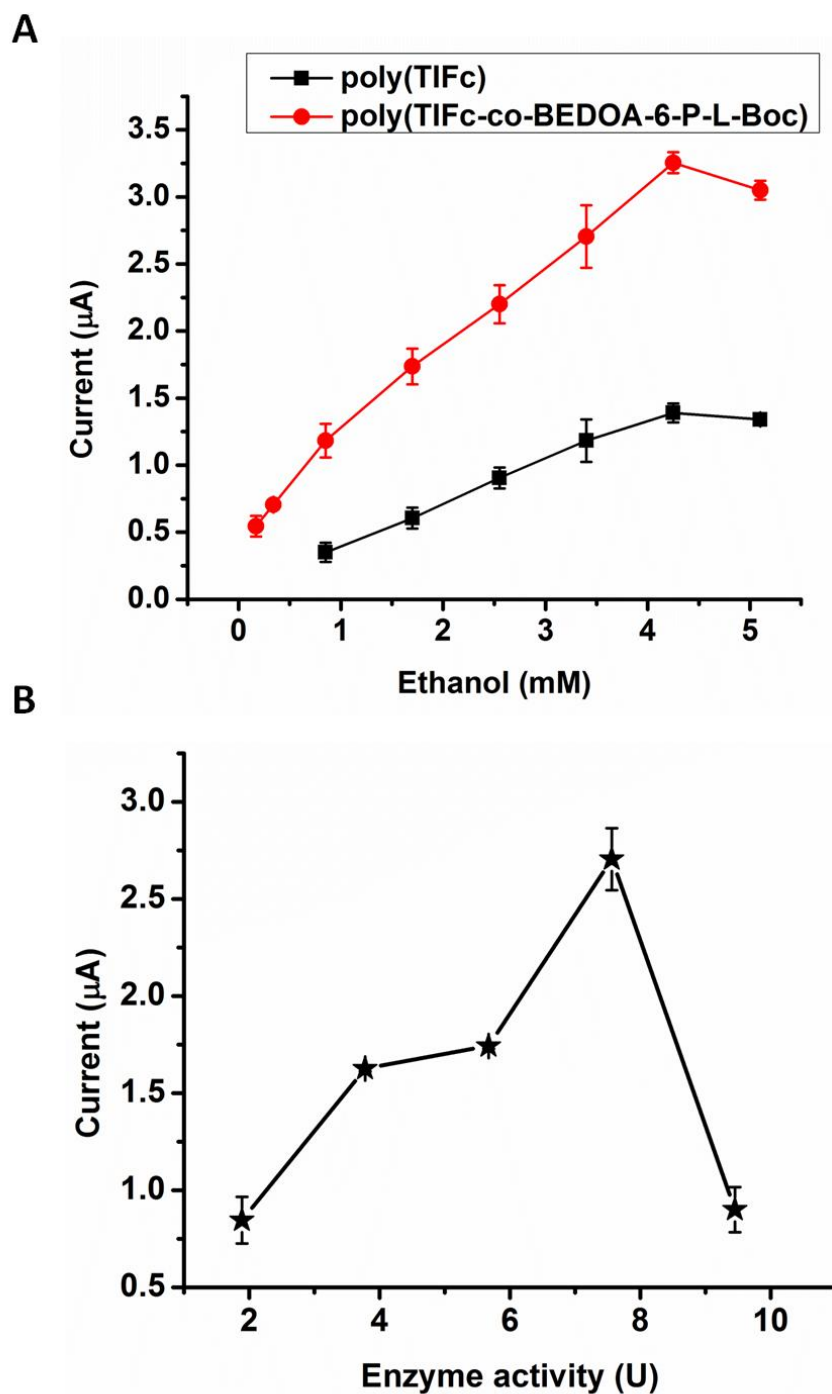


Figure 2.9. Effect of (A) polymer films as supporting matrix and (B) enzyme activity on the biosensor response. Error bars show standard deviation (SD) of three measurements.

Thickness of the copolymer film was adjusted by the duration of electro copolymerization in terms of charge passing through the cell [87]. To detect optimum thickness of the copolymer film, the bare graphite electrodes were coated

with different scan numbers. For this purpose, different biosensors with 5, 15, 25, 35 scans were prepared and their biosensor response to the substrate were compared by keeping the other parameters constant. Since the thickness of the copolymer film is crucial, it is important to choose the most satisfying immobilization matrix for stabilization of 3D structure of enzyme molecules. If the layer is not arranged properly, diffusion problems between polymer coated electrode and biomolecule or denaturation of biomolecules may arise. As seen in Figure 2.9B, the highest response was recorded with 15 cycle film deposition for biosensor application which corresponds to 27.8 nm (equivalent of 0.12 mC charge) in thickness.

Activity of biomolecules is affected seriously by the pH of the working medium, optimization of pH of the buffer solution is really important. Therefore, amperometric signals were compared in the range of pH 6.0-8.5 (50 mM sodium phosphate buffer, 25°C), using the proposed biosensor while the other preparation of biosensor parameters were kept constant. Figure 2.10A shows that the maximum signal was detected at pH 7.0. Hence, pH 7.0 sodium phosphate buffer was used for further experiments to improve the activity of enzyme.

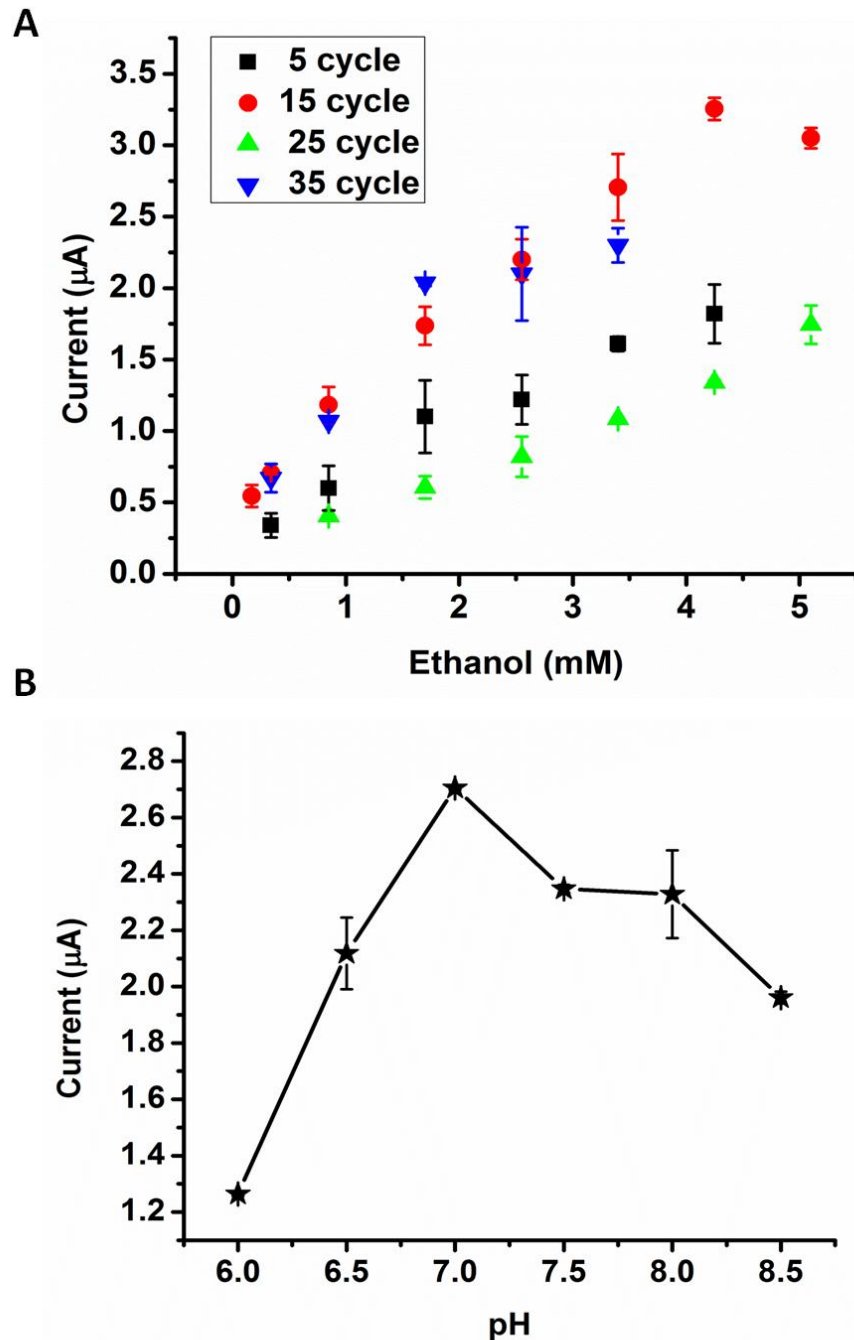


Figure 2.10. Effects of (A) scan number and (B) pH on the biosensor response.

Error bars show standard deviation (SD) of three measurements.

The effect of different amounts of AOx on biosensor performance was examined. The amounts of other components were kept constant. As seen in Figure 2.10B, the highest signal corresponds to 7.56 U AOx. Excess loading of enzyme resulted in leaching from the surface since enzyme molecules were not sufficiently stable onto

the surface area. On the other hand, inadequate enzyme loading caused low sensitivity of the biosensor due to the low yield of enzymatic reaction. Therefore, sufficient enzyme amount should be 7.56 U to achieve stable and reasonable biosensor responses.

2.2.4. Biosensor Characterization

2.2.4.1. Electrochemical Impedance Spectroscopy

Electrochemical Impedance Spectroscopy (EIS) was carried out to characterize the interface properties of the modified electrodes at the surface during the fabrication process of the biosensors [88]. Electron transfer between the species in solution and the electrode surface occurs by tunneling through the barrier. In a Nyquist plot, the semicircle portion corresponds to the electron-transfer resistance at the higher frequency range which controls the electron transfer kinetics of the redox probe at the electrode surface. The semicircle diameter equals the electron transfer resistance. Such resistance controls the electron-transfer kinetics of the redox probe at the electrode interface. Moreover, linear part of the plot at lower frequency range represents the diffusion limited process. EIS study was performed on the modified electrodes in 5.0 mM $\text{Fe}(\text{CN})_6^{3-/4-}$ containing 0.1 M KCl solution with a frequency range between 1 Hz and 200 kHz via applying a constant potential of 5 mV. Figure 2.11 illustrates typical Nyquist plots obtained from bare electrode, poly(TIFc-co-BEDOA-6-poly(L-Boc)), poly(TIFc-co-BEDOA-6-poly(L-Boc))/AOx using $\text{Fe}(\text{CN})_6^{3-/4-}$ as the redox probe. It can be seen that the bare electrode exhibited a very small interfacial resistance. After coating the electrode surface with poly(TIFc-co-BEDOA-6-poly(L-Boc)), the semicircle diameter increased slightly due to the increase in thickness of the interface. The small resistance indicated a resistance of electron flow due to the addition of a layer on the electrode surface. Furthermore, polypeptide segments cause a decrease in conductivity effectively since the units interrupt the electron flow within the conjugation pathway. Hence, this increase in semicircle diameter is justified. After AOx was immobilized onto the coated electrode surface, the semicircle diameter increased significantly since

the layer blocks the redox probe to diffuse toward the electrode. Moreover, since most biological molecules were poor electrical conductors at low frequencies, this increase in charge transfer resistance was the direct evidence of successful immobilization of enzyme on the modified transducer surface.

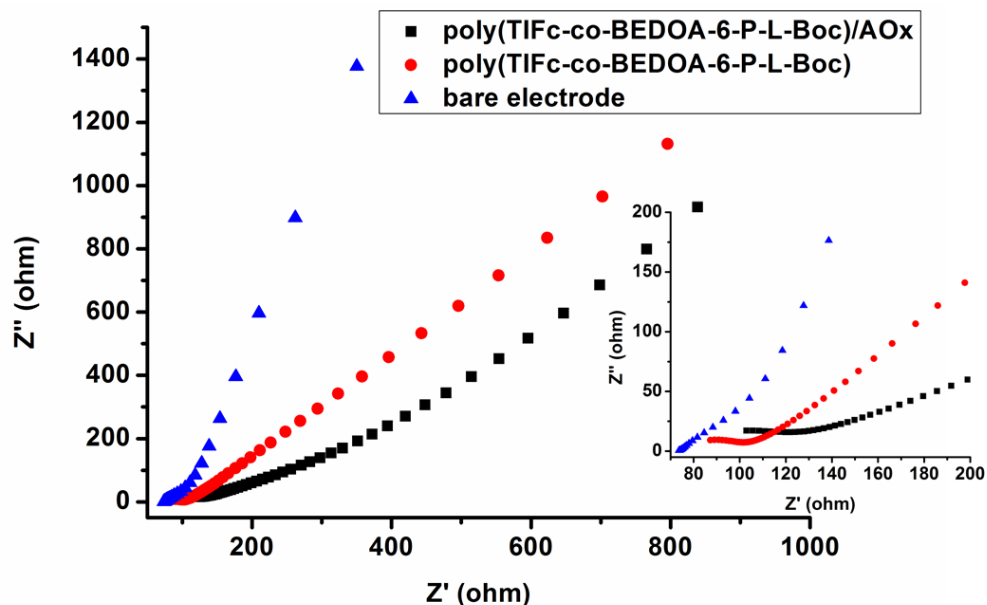


Figure 2.11. Typical Nyquist plots resulting from bare graphite electrode, poly(TIFc-co-BEDOA-6-poly(L-Boc)), and poly(TIFc-co-BEDOA-6-poly(L-Boc))/AOx in 5.0 mM $\text{Fe}(\text{CN})_6^{3-/4-}$ containing 0.1 M KCl solution. (Curves in high frequency region are given as inset).

2.2.4.2. Scanning Electron Microscopy

The surface morphology of different electrode surfaces was monitored via SEM. Figure 2.12 A-C show SEM images of the conducting polymer coated graphite electrode (poly(TIFc)), polymeric structure bearing polypeptide segments coated graphite electrode poly(TIFc-co-BEDOA-6-poly(L-Boc)) and enzyme immobilized copolymer coated graphite electrode (poly(TIFc-co-BEDOA-6-poly(L-Boc))/AOx), respectively. In case of poly(TIFc) coated electrode, granular morphology was observed. On the other hand, poly(TIFc-co-BEDOA-6-poly(L-Boc)) exhibited completely different morphology. The copolymer film has an

ability to cover the entire electrode surface homogeneously. By this way enhanced matrix properties are achieved while this serves a nice platform where enzyme molecules are freely oriented. After biomolecule deposition, enzyme exhibits its bulky characteristics. This homogeneous 3D structure leads to stabilization of the enzyme molecules, improving the biosensor performance. It can be clearly seen that the morphology of different prepared electrode alters significantly, referring copolymer formation and successful enzyme deposition.

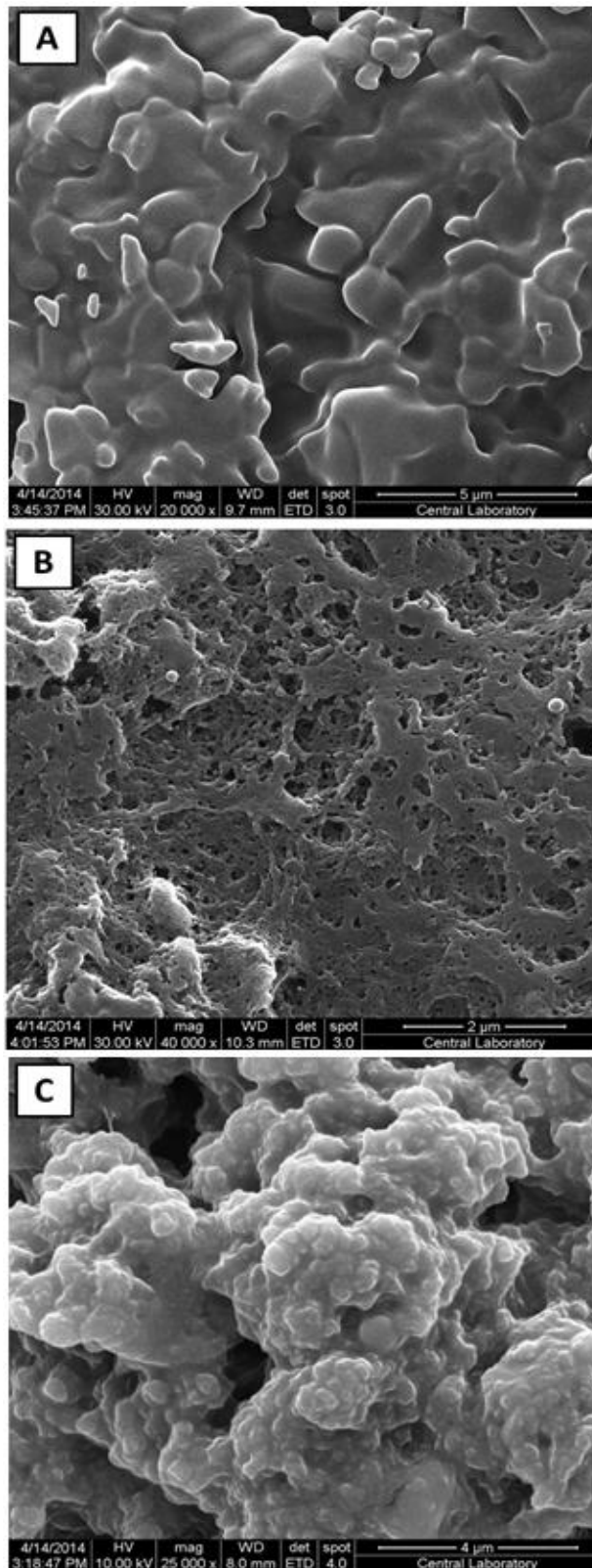


Figure 2.12. SEM images of (A) poly(TIFc); (B) poly(TIFc-co-BEDOA-6-poly(L-Boc)); (C) poly(TIFc-co-BEDOA-6-poly(L-Boc))/AOx under optimized conditions.

2.2.5. Analytical Characterization

The analytical characterization of the biosensor was examined preparing an enzyme electrode under optimum conditions. Calibration curve for ethanol was plotted with respect to substrate concentration as given in Figure 2.13. A perfect linearity was obtained between 0.17 mM and 4.25 mM ethanol as given with an equation; $y=0.6485x+0.5329$ and $R^2= 0.9945$ Limit of detection (LOD) was also calculated as 0.28 mM according to $S/N = 3$. Also, a typical amperometric response of the biosensor was given as an inset in Figure 2.13.

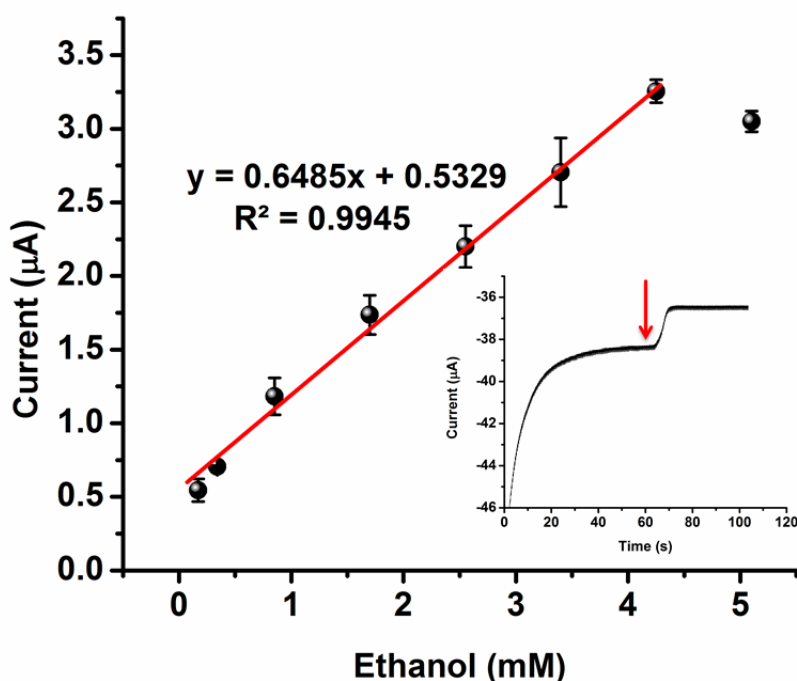


Figure 2.13. Calibration curve for ethanol (in 50 mM phosphate buffer, pH 7.0, 25°C, -0.7 V). Error bars show standard deviation of three measurements (A typical amperometric response to 1.7 mM ethanol in phosphate buffer, 50 mM, pH 7.0 given as inset).

Moreover, the biosensor signals corresponding to 1.7 mM ethanol solution were measured for ten times in order to prove repeatability of the biosensor response.

The standard deviation (SD) and the relative standard deviation (RSD) were calculated as 0.09 and 5.94 %, respectively. Also, operational stability of the biosensor was investigated under optimum conditions. During 5 h, 10 times current change was detected upon addition of 1.7 mM substrate and 16 % activity loss was found in the biosensor response.

Furthermore, kinetic parameters were characterized using Lineweaver-Burk plot [89]. The apparent Michaelis-Menten constant (K_M^{app}) and maximum current (I_{max}) were calculated as 2.67 mM and 2.98 μ A, respectively. It is known that a low K_M^{app} value corresponds to high enzyme affinity toward the substrate. In this biosensing system, such a low K_M^{app} value was observed. A comparison among the present biosensor and several others reported in literature is given in Table 2.1. Thus, it is concluded that the immobilized alcohol oxidase exhibits higher affinity toward ethanol thanks to effective immobilization matrix. Successful design of the copolymer with different specialties of each unit improves the biosensor performance by serving adequate microenvironment for the enzyme. By this way, the interaction between the substrate and active site of enzyme was increased.

Table 2.1. Comparison of some parameters of various alcohol biosensors reported in literature.

Matrices on electrodes	K_M^{app} (mM)	Linear range (mM)	Ref.
Au/PPYox/AOD-gel	5.30	Up to 0.75	[90]
Polypyrrole (PPy)/AOx	6.8	NR	[91]
f-MWCNT/poly(BIPN)/AOx	16.946	0.855 - 11.97	[92]
PNR/AOx	2.4	0-0.8	[93]
RPTP/PVI10-Os/PEG-DGE/AOx/CP5	9.5	NR	[94]
PMCCH/AOx	8.74	0.4–13.63	[78]
Poly(TIFc-co-BEDO A-6-Poly(L-Boc))/AOx	2.67	0.17– 4.25	This work

It was known that AOx contains different relative activities to several aliphatic alcohols [95]. To inquire substrate selectivity of the proposed biosensor, 1.7 mM of various alcohol substrates were tested and results were given in Figure 2.14. The response of the biosensor to methanol was higher than the one for ethanol. Since methanol has the shortest alkyl chain and the final product in the enzymatic reaction is formaldehyde acting also as a substrate for AOx [96], the biosensor signal was amplified and the highest signal was recorded upon addition of methanol as the substrate. However, the fact that the biosensor gives higher response to methanol than to ethanol may not induce any problem for the detection of alcohol content in real food samples because the only content of alcohol in food products is expected to be ethanol. Thus, the enzyme electrode is potentially useful for the determination of ethanol in real food products. Moreover, as the alkyl chain of the alcohol increases, the biosensor response decreases since the substrates with longer chain cause steric hindrance while the substrate is reaching active site of the enzyme molecules. Thus, relative biosensor response decreases as the chain length increases.

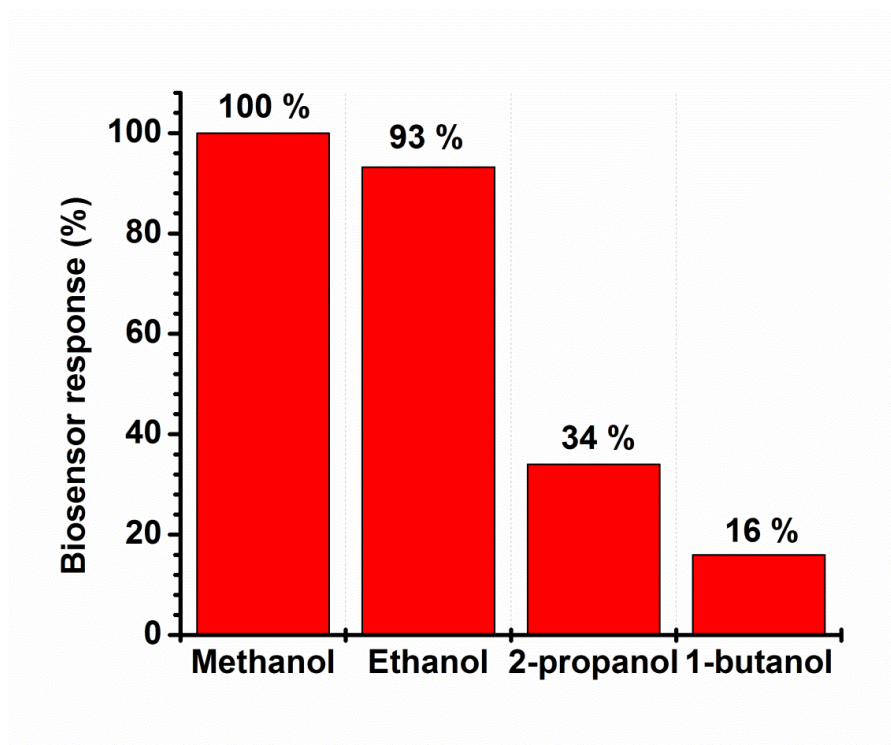


Figure 2.14. Substrate selectivity of the biosensor (amperometric response of methanol taken as 100%).

Furthermore, the effects of potential interferents such as glucose, urea, cholesterol and ascorbic acid were investigated. For this purpose, these molecules (between 1 mM and 10 mM) were injected to the reaction cell under optimum conditions instead of ethanol as the substrate and no responses were recorded for these interferents. Hence, the proposed sensing system can be used for real sample analysis even in the presence of such interferents in the sensing matrix.

2.2.6. Sample Application

The proposed sensing system was tested to analyze the alcohol content in several alcoholic beverages. The samples were injected to the cell instead of ethanol substrate without any pretreatment. The responses of biosensor for each sample were recorded and values were estimated from the calibration curve. The experiments were performed at optimum conditions. As summarized in Table 2.2, the results are in really good agreement which approves the reliability and accuracy of the biosensor. Therefore, it is a reliable strategy for alcohol determination in real samples. Since the methods which are used for routine analysis have several drawbacks, the proposed biosensor design is a favorable method for real time analysis to investigate alcohol content in real alcoholic beverages. Hence it serves several advantages over traditional methods like simple measurement procedure, short response time, easy to fabricate and sufficient sensitivity and selectivity. Hence, the constructed biosensor is an accurate way for alcohol test in real samples.

Table 2.2. Ethanol detection in alcoholic beverages.

Sample	Ethanol Content		Relative error (%)
	Product label (%)	Poly(TIFc-co-BEDOA-6-poly(L-Boc))/AOx biosensor (%)	
B® Liquor	24.0	23.7	1.28
J® Whisky	40.0	36.7	8.99
Y® Wine	14.0	14.3	2.10
Y® Raki	45.0	46.1	2.39
S® Liquor	20.0	19.4	3.09
R® Wine	12.0	12.4	3.23

2.3. EXPERIMENTAL DETAILS

2.3.1. Materials

Alcohol oxidase (AOx, E.C.1.1.3.13, 35 units/mg) from *Pichiapastoris*, methanol, NaClO₄, LiClO₄ Nε-Boc-L-lysine, tetrabutylammonium hydroxide, and diphenyl carbonate were purchased from Sigma-Aldrich and used with no further purification. Dichloromethane (DCM), acetonitrile (ACN) were purchased from Merck (Darmstadt, Germany). 2-Propanol and tert-butanol were obtained from (Merck). Ethanol (Carlo Erba) was used for the preparation of substrate solution (1.7 M) at room temperature. All chemicals for the synthesis of monomer were purchased from Aldrich except tetrahydrofuran (THF) which was obtained from Acros (Geel, Belgium, www.acros.com). THF was freshly dried over sodium and benzophenone just before the reactions. N,N-Dimethylacetamide (DMAc) and N,N-dimethylformamide (DMF) were purified by heating at 600°C for 1 h over CaH₂ followed by fractional distillation before use. All other chemicals were

analytical grade. Reactions were performed under nitrogen atmosphere unless otherwise mentioned.

2.3.2. Measurements

All amperometric measurements were performed with the potentiostat EmStat (PalmSens, Houten, The Netherlands, www.palmsens.com) in a three-electrode cell configuration consisting of a graphite electrode (Ringsdorff Werke GmbH, Bonn, Germany, type RW001, 3.05 mm diameter and 13% porosity) as the working electrode. A platinum wire as the counter electrode and a silver wire as the pseudo reference electrode were used. Amperometric measurements were performed in a three-electrode system. In amperometric analyses, the data were given as the average of three measurements and standard derivations were recorded as \pm SD. All measurements were performed at ambient conditions (25°C). For investigation of surface characteristic, scanning electron microscopy (SEM) (JEOL JSM-6400 model, Japan) was used. ATR-FTIR spectra were recorded on a Nicolet iS10 ATR-FTIR Spectrometer (Thermo Fisher Scientific Inc.). Electrochemical Impedance Spectroscopy (EIS) was performed with a GAMRY Reference 600 (GAMRY Instruments Inc., Pennsylvania, USA).

2.3.3. Synthesis of 6-(4,7-bis(2,3-dihydrothieno[3,4-b][1,4]dioxin-5-yl)-2H-benzo[d][1,2,3]triazol-2-yl)hexan-1-amine (BEDOA-6)

The monomer, BEDOA-6 was synthesized according to a previously described method (Figure 2.15) [97]. Toppare et al. synthesized the desired monomer (BEDOA-6) successfully.

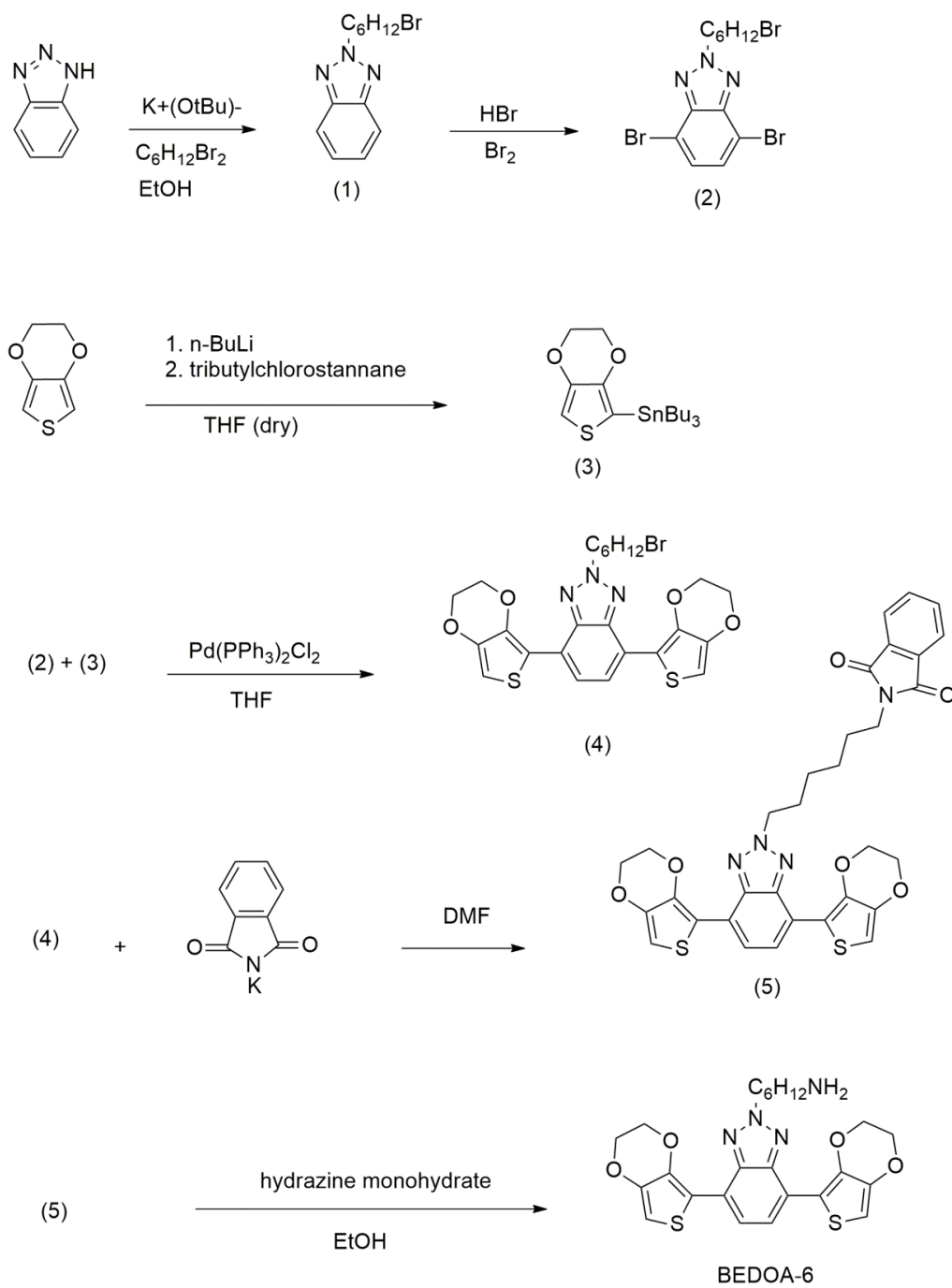


Figure 2.15. Synthetic pathway of the monomer BEDOA-6 [97].

2.3.4. Synthesis of N6-(tert-butoxycarbonyl)-N2-(phenoxy carbonyl)-L-lysine (Urethane derivative of N-Boc-L-lysine)

Synthetic route for urethane derivative of N-Boc-L-lysine is based on successive protection of the acid group of N-Boc-L-lysine with diphenyl carbonate by an ionic exchange reaction with the corresponding ammonium salt and N-carbamylation reaction. The detailed description of the synthetic route is described in an earlier study [83] (Figure 2.16). Yagci and co-workers performed the synthesis of urethane derivative of N-Boc-L-lysine.

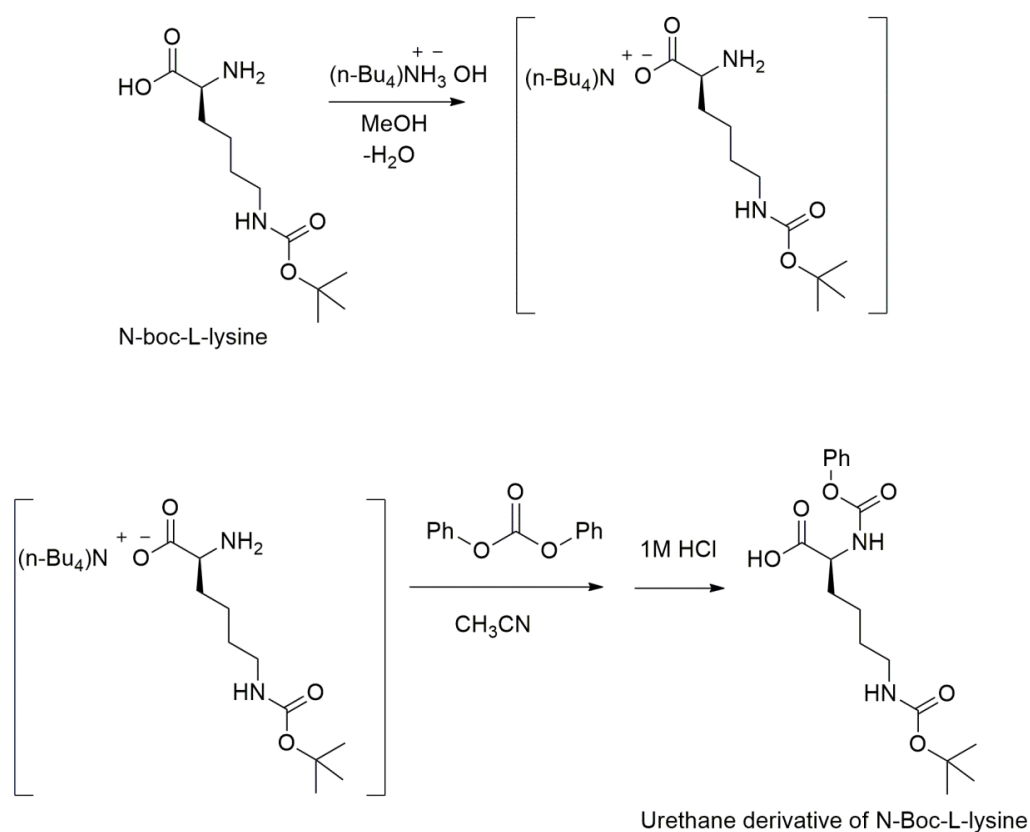


Figure 2.16. Synthetic pathway of N6-(tert-butoxycarbonyl)-N2-(phenoxy carbonyl)-L-lysine (urethane derivative of N-Boc-L-lysine) [97].

2.3.5. Synthesis of Electroactive BEDOA-6-poly(L-Boc)

Polymerization of the urethane derivative of N-Boc-L-lysine proceeded in the presence of BEDOA-6 and an initiator in DMAc in a one-pot reaction through in

situ intramolecular cyclization followed by a ring-opening reaction with CO₂ elimination [83]. Yagci et al. performed the synthesis of BEDOA-6-poly(L-Boc) (Figure 2.17).

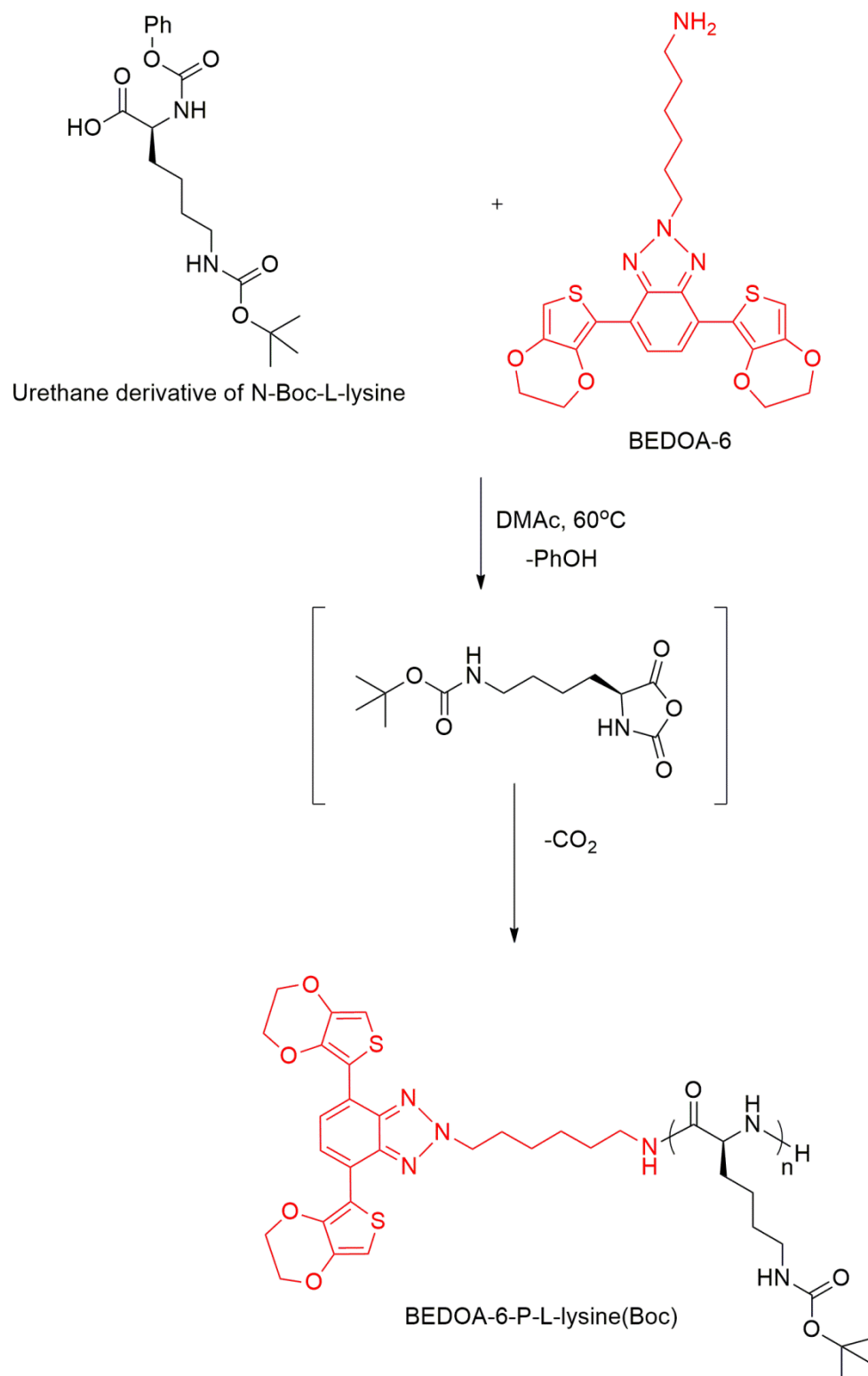


Figure 2.17. Synthesis of the electroactive electroactive polypeptide macromonomer, BEDOA-6-poly(L-Boc) [83].

2.3.6. Synthesis of 2-ferrocenyl-4,7-di(thiophen-2-yl)-1H-benzo[d]imidazole (TIFc)

4,7-Dibromobenzothiadiazole [98], 6-dibromobenzene-1,2-diamine [99], tributyl(thiophen-2-yl)stannane [100] were synthesized according to the literature procedures. The desired monomer 2-ferrocenyl-4,7-di(thiophen-2-yl)-1H-benzo[d]imidazole (TIFc) was synthesized by Cirpan and co-workers [83] as described in literature [101] (Figure 2.18).

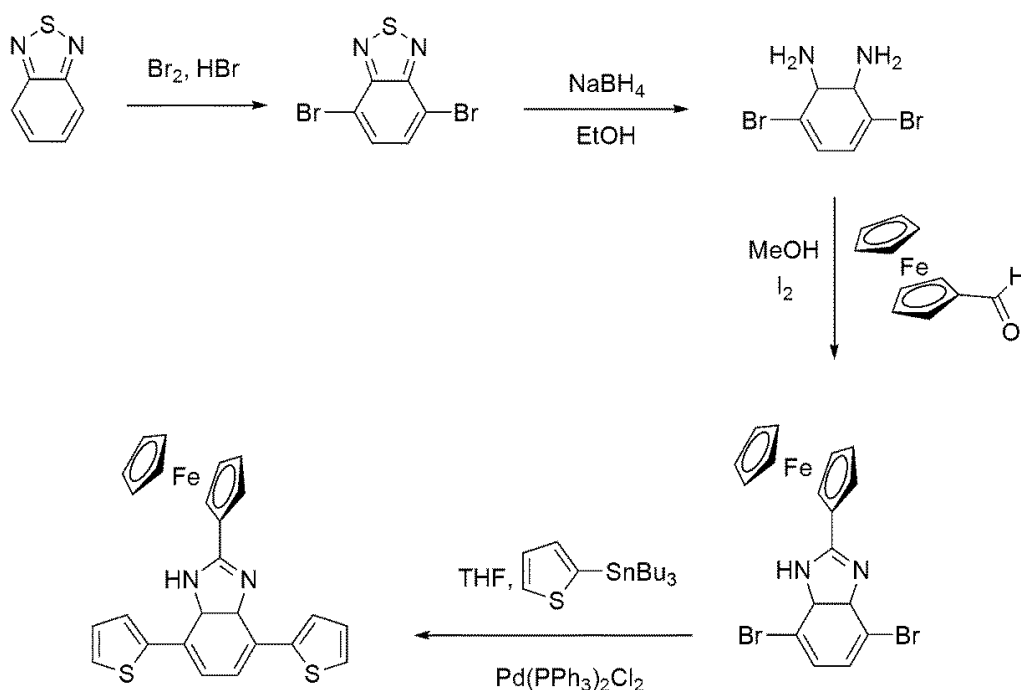


Figure 2.18. Synthetic route of the monomer TIFc [83].

2.3.7. Electro Copolymerization of BEDOA-6-poly(L-Boc) and TIFc

Prior to polymerization, spectroscopic grade graphite rods were polished on an emery paper and washed thoroughly with distilled water. After the cleaning procedure, electrochemical copolymerization and film deposition was carried out on the graphite electrode via cyclic voltammetry. A mixture of TIFc and BEDOA-

6-poly(L-Boc) solution was subjected to cyclic voltammetry (CV) for 15 cycles in 0.1 M NaClO₄/LiClO₄/ACN electrolyte/solvent system by scanning the potential between -0.2 V and 0.8 V. Polymer coated electrode was rinsed with distilled water to remove possible impurities. Similar experimental procedure was applied for the polymerization of TIFc in the absence of BEDOA-6-poly(L-Boc).

2.3.8. Immobilization of Enzyme, Crosslinking And Biosensing

To immobilize the enzyme, 3 μL of AOX solution (50 mM pH 7.0 sodium buffer solution containing AOX) was spread over the polymer coated electrode surface. Then, glutaraldehyde solution (5 μL, 1%, in 50 mM phosphate buffer, pH 7.0) was casted on the electrode as the cross linker agent and the electrode was allowed to dry for 2 h at room temperature. Before use, the electrode was rinsed with pH 7.0 phosphate buffer solution to remove loosely bound enzymes from the electrode. It was stored at 4°C when not in use.

Amperometric biosensor measurements were performed at ambient conditions in a cell containing 5 ml buffer solution under a mild stirring. After the electrodes were initially placed in the cell, the signal baseline reached a steady state and certain amount of substrate was injected to the reaction cell. At this point the response of the biosensor was measured by detecting the current change when equilibrium was established. The electrode was washed with distilled water and buffer was refreshed after each measurement. Figure 2.19 depicts the construction procedure of the amperometric ethanol biosensor for poly(TIFc-co-BEDOA-6-poly(L-Boc)).

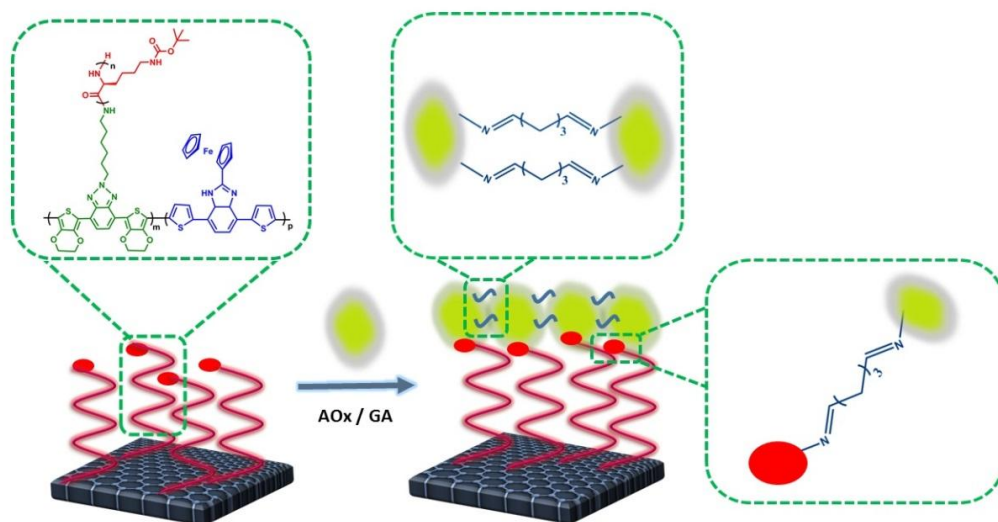


Figure 2.19. Preparation of the amperometric ethanol biosensor for poly(TIFc-co-BEDO-6-poly(L-Boc)).

2.4. CONCLUSION

In this study, a complex macromolecular architecture based on a conjugated copolymer to construct a novel biosensor was successfully achieved. Conducting copolymers possessing both polypeptide and ferrocene units were prepared by electrochemical copolymerization and used as an immobilization platform of AOx. While polypeptide segments created an excellent biocompatible environment for biomolecule deposition as well as enabling covalent attachment of the enzyme, the ferrocene units provided enhanced biosensor performance without any leaching. The constructed biosensor reflecting the advantage of each component was characterized in detail by FTIR, SEM, and EIS analyses. The biosensor was used to analyze ethanol content in real sample and proposed as an alternative sensing system for ethanol analysis in alcoholic beverages. We anticipate the described approach will be applicable to numerous other types of enzymes with different sensing abilities. The combination of polypeptides with conjugated polymers by means of electro copolymerization has potential use in the construction of new biological macromolecular architectures.

This work was described in the following publication [83]:

M. Kesik, H. Akbulut, S. Söylemez, Ş.C. Cevher, G. Hızalan, Y. Arslan Udum, T. Endo, S. Yamada, A. Çırpan, Y. Yağci and L. Toppare, Polym. Chem., 2014, 5, 6295.

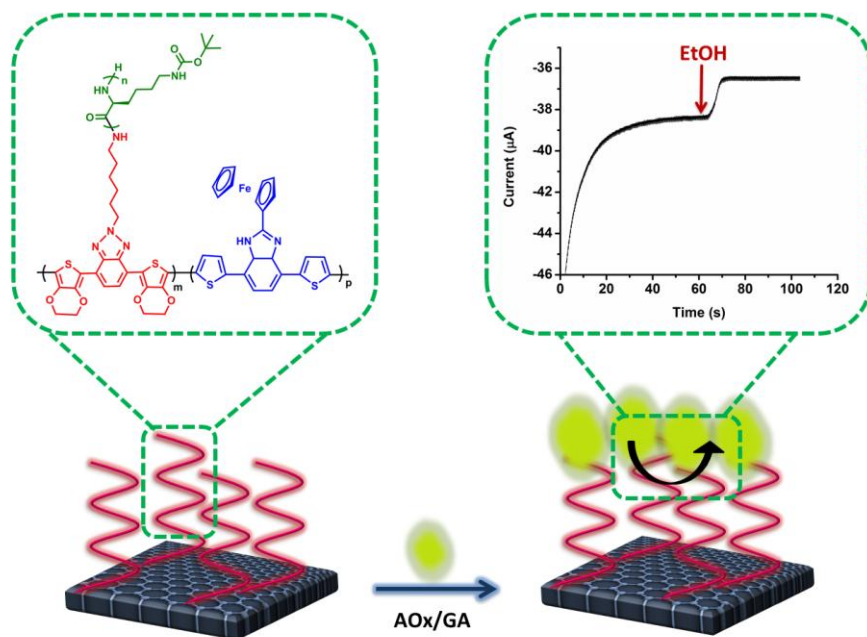


Figure 2.20. A novel ethanol biosensor based on conducting polymers containing polypeptide and ferrocene side chains [83].

CHAPTER 3

3. AN ACETYLCHOLINESTERASE BIOSENSOR BASED ON A CONDUCTING POLYMER USING MULTIWALLED CARBON NANOTUBES FOR AMPEROMETRIC DETECTION OF ORGANOPHOSPHOROUS PESTICIDES

3.1. INTRODUCTION

3.1.1. Environmental Monitoring

In order to prevent fungi, bacteria or nematodes, farmers commonly prefer using several organic substances like insecticides, herbicides or pesticides in agriculture [102]. Using such organic substances leads to high product yield. However, uncontrolled use causes serious health problems to whole ecosystem since pesticide residues may diffuse into the food products through air, water and soil.

The meaning of the term pesticides is a reagent used for plant-growth regulators, defoliant or desiccants [103]. Pesticides, also known as Chemical Warfare Agents (CWAs) [104], are natural or synthetic substances or mixtures which can be carcinogenic or citogenic. That is why they can produce several diseases related to bone marrow, infertility, nerve disorders and immunological and respiratory diseases [102]. USA and European governments with the help of internal organizations (e.g. Food and Agriculture Organization) introduce a new regulation on the residue level of pesticides on agricultural products to prevent such problems. This legislation relies on the enforcement of monitoring of the levels of such compounds in the environment. For example, the highest acceptable level of pesticides in water is between 0.3 to 400 $\mu\text{g/L}$ in water [105]. This policy intends to induce contamination of pesticides to ground and surface waters.

Even though organochlorine insecticides like DDT, aldrin and lindane have been replaced by organophosphorus and carbamate insecticides exhibiting low endurance in the environment; their high toxicity level causes a severe risk. The toxicity of organophosphorous (OPs) and carbamic acid insecticides affects functioning of acetylcholinesterase (AChE) in the body which has essential role in central nerve system of living beings. Cholinesterase enzymes hydrolyze the acetylcholine, known as a neurotransmitter, in the nervous system. In vertebrates and insects, ChE transmits nerve impulses to the cholinergic synapses connected with memory and Alzheimer's diseases.

In the active site of AChE, a serine residue catalyzes the hydrolysis of neurotransmitter acetylcholine and terminates the impulse transmission at cholinergic synapses [106]. OPs, known as cholinesterase inhibitors, are widely used in agriculture, medicine, industry and chemical warfare. OPs exhibit high toxicity and their presence in the environment can be fatal for human health as they inhibit the catalytic activity of AChE irreversibly by forming a stable complex in the active site of AChE [107]. During the inhibition mechanism, the serine residue is blocked. The resulting high production of acetylcholine interferes with brain response since acetylcholine level depends on availability of active AChE [108,109]. For this reason, the need of monitoring devices for detection of OPs (Figure 3.1A) in the environment is vital and subjected to keen interest for several decades. There are numerous organophosphate and carbamate pesticides showing different toxicity level which depends on chemical structure of the pesticide (Figure 3.1B) [110].

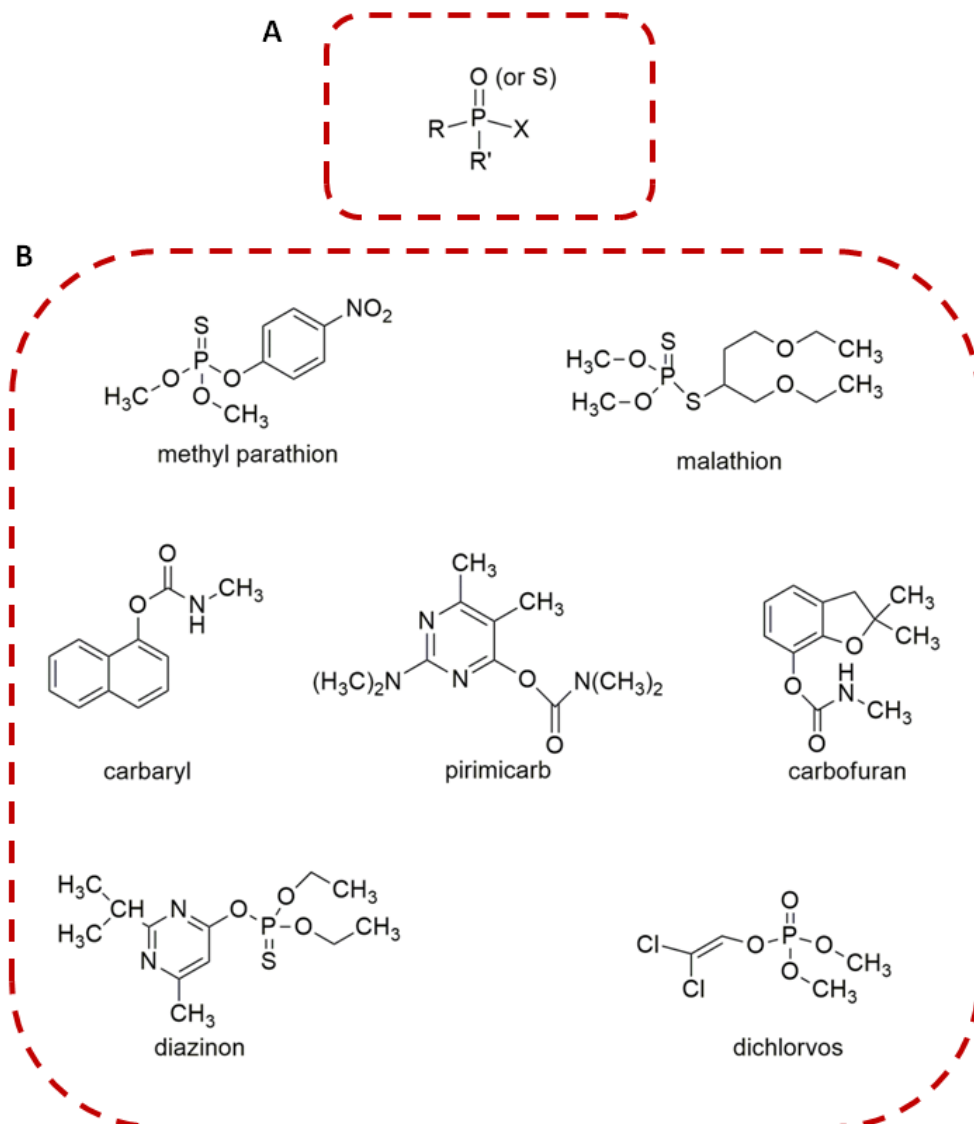


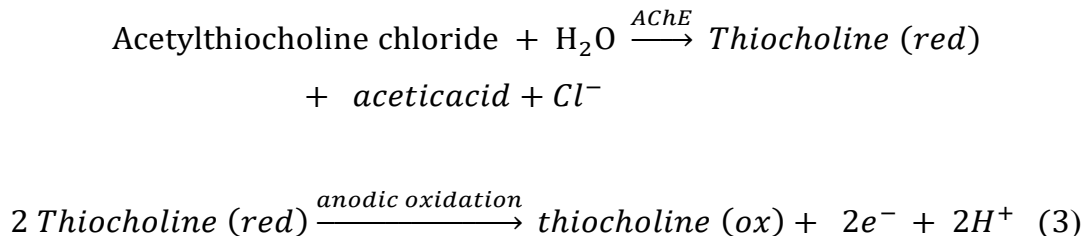
Figure 3.1. (A) General form of pesticides, (B) Structures of the several OP compounds pesticides used in AChE biosensors.

3.1.2. Strategies for Detection of OP Pesticides

Global attention is given in developing analytical systems to monitor OPs in the environmental surveillance and protection [111,112]. However, the complexity of analyte and low concentration level of pesticides in the samples like fruits make the analysis difficult. The common methods for pesticide detection are based on calorimetry, capillary electrophoresis (CE), mass spectrometry (MS),

chromatographic separation such as gas (GC) and liquid chromatography (LC) using several detectors. Despite of their sensitivity and reliability, they are time consuming, require expensive equipments, highly qualified personnel and are not adapted for in situ detection [102].

The development of enzyme-based electrochemical biosensors appears as a promising alternative to the classical methods owing to their simple measurement procedure, short response time, sufficient sensitivity and selectivity. Biosensors can satisfy benefits of traditional methods mentioned above by simplifying sample preparation and eliminating sample pretreatment which reduces analysis time and cost. Therefore, biosensors based on the inhibition of acetylcholinesterase are attractive for the detection of acetylcholine or organophosphorous pesticides. The inhibition of enzyme activity is monitored by measuring the oxidation current of acetylthiocholine upon a certain applied potential. The reaction mechanism is as follows [113] (eq 3):



3.1.3. Biosensor Measurement For Pesticides

3.1.3.1. The Choice of Enzyme

Selectivity and sensitivity of a biosensor are achieved by the biorecognition element used in the sensor construction. Common biocatalysts used in pesticide biosensors are enzymes. Inhibition property of the enzymes is the basic idea behind the fabrication of pesticide sensors. Inhibitors affect the functioning of the enzyme resulting in decrease in enzyme activity. This inhibition is proportional to the amount of inhibitors in the analyte. AChE and butyryl cholinesterase (BChE) are

the most preferable enzymes in pesticide biosensors [114]. In vertebrates, AChE (EC 3.1.1.7) has a function of termination of acetylcholine action at synaptic membrane in the neuromuscular joint. It is found in whole neutral and blood systems. BChE (EC 3.1.1.8) is found in nerves but the main production is in liver. Its activity can be used as a liver function test [114]. BChE role in human body is not well understood since the rate of BChE production does not have individual effect in human health. It is used to detoxify cocaine and succinylcholine [115]. Both biocatalysts are good contamination markers for neurotoxic reagents. Acetyl esters such as acetylcholine butyrylthiocholine, propionylthiocholine, indophenylacetate can be used as the substrates of AChE whereas BChE hydrolyzes butyrylcholine [116]. Furthermore, AChE and BChE have similar molecular structures; 65% of their amino acid sequence are the same [117]. However, some reagents can inhibit only AChE or the reverse case can be observed for some compounds [118,119].

3.1.3.2. Immobilization Techniques

Contrary to the advantages of AChE biosensors for the detection of OPs, they suffer from a major drawback; loss of enzyme activity. In order to keep fragile enzyme activity during the electrochemical measurements, the adopted immobilization method should be strong enough to maintain mechanical stability of the biosensor and sufficiently soft to arrange optimal conformation of the enzyme [120]. There are several requirements that should be taken into consideration while choosing the electrode material [118]:

1. Biocompatibility,
2. Stability,
3. Being functionalized easily to have strong attachment with the enzyme,
4. Sensitivity,
5. Selectivity,
6. Low cost,
7. Easy fabrication,
8. Immobilization chemistry should not involve any toxic reagent resulting in denaturation of the biocatalyst.

Several immobilization strategies (Figure 3.2) and materials were developed such as physical adsorption [121], entrapment [122], covalent binding [123] and intermolecular cross linking [124].

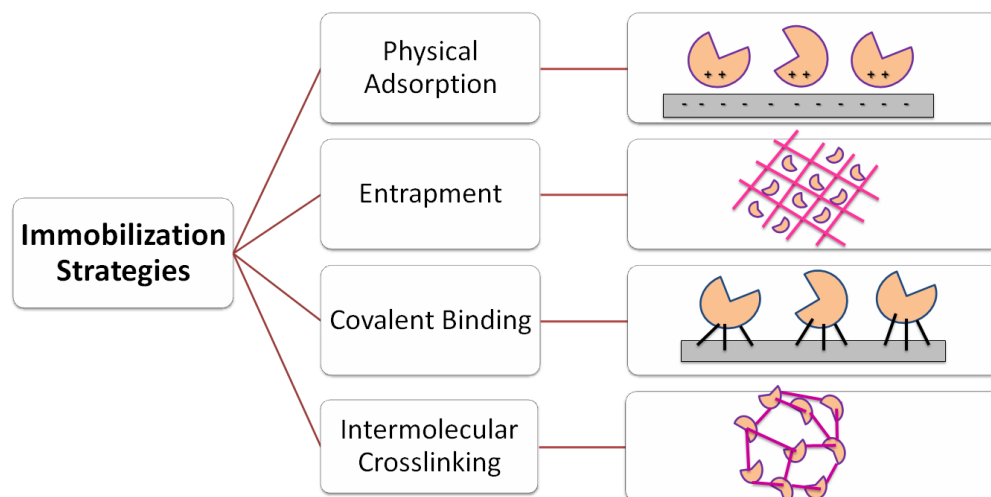


Figure 3.2. Immobilization strategies used for biosensor construction

Physical adsorption, known as the simplest immobilization method, relies on reversible surface interaction between the biorecognition element and the transducer. Van der Waals forces, ionic and hydrogen bonding interactions are the main forces which can be used in the strategy. By this method, biological component does not have any chemical attachment to the electrode; thus, there is a little or no damage to enzyme. Also, this strategy is very simple and cheap. However, any change in matrix conditions affects the interaction strongly between the enzyme and electrode. Moreover, the enzyme is casted onto the outer layer of the transducer. Therefore, leaching out of the enzyme during the measurement can be observed. Hence, the lifetime of the biosensor fabricated by physical adsorption may not sufficient enough.

Entrapment depends on the fixing of biological material into 3D network on the electrode surface. This technique is quite easy: The biomolecule is dissolved in a

solution with other reagents which are necessary for biosensor fabrication. In order to form the desired phase, it is caged into a network [125]. This network is enhanced using polymer [126], dialysis membrane [127] etc. One of the biggest advantages of the method is the entrapment of reagents like enzyme, additives or mediators simultaneously. That is, fabrication of the biosensor can be achieved via simple one-step procedure [128]. However, the network created in this approach may restrict the diffusion of analyte to the biorecognition element that results in long response time. Accessibility of substrate to the biomolecules is restricted due to an additional layer like membrane [66,125].

The most preferable immobilization strategy is covalent immobilization owing to its several advantages [129]. Formation of covalent binding using functional groups on the transducer and the enzyme is the basic idea. Such attachment results in long life time and high operational stability of the biomolecule. This method involves all the benefits of the other strategies mentioned above and besides generates higher enzyme stability [29]. The only drawback is that covalent bond formation may result in excess attachment causing bioactivity loss of enzyme [130]. However, it can be handled by optimizing the amount of enzyme and bonding agents used in biosensor fabrication.

Intermolecular cross linking involves formation of cross linked or covalent bond between the support electrode and the biomolecule or within the enzyme itself. There are numerous reagents used in this strategy like bovine serum albumin (BSA), glutaraldehyde (GA) or carbodiimide [131]. Thanks to this strategy, compact protein structure can be achieved. Since leaching out of the enzyme is limited, operational and storage stability can be improved. Generally, covalent immobilization and cross linking strategy are employed together. By this way, the biosensor performance is improved serving all necessity for an ideal electrode after applying several optimization studies.

3.1.4. Carbon Nanotubes in Biosensor Construction

Carbon nanotubes (CNTs) are fascinating materials for sensing applications due to several properties like small dimensions, functional surface, good conductivity, excellent biocompatibility, modifiable side walls and high reactivity [132,133]. In addition to enhanced electrochemical reactivity, CNT-modified electrodes are widely used for the immobilization of biomolecules [134,135]. π - π electronic and hydrophobic interactions allow them to interact with some aromatic compounds [136]. To take advantage of such superior properties in electrochemical sensing applications, the CNT should be properly functionalized. With their unique electron transfer property and desirable shapes for surface design, CNTs are valuable candidates for surface modifications especially in the case of electrochemical processes.

There are two main classes of carbon nanotubes: multi-walled (MWCNTs) and single walled carbon nanotubes (SWCNTs) [135]. SWCNTs having a cylindrical nano sized structure are produced by rolling up a single graphite sheet. On the other hand, MWCNTs are composed of several cylinders which are nested concentrically.

There are different types of defects on the surface of CNTs upon applied different fields of chemistry. During CNT growth, formation of defects generally started to form 5 and 7 membered rings in the carbon lattice. Heat treatment of acid washing or generated oxidative harsh conditions result in the opening and breaking of tubes [137]. This leads to the formation of carboxylic and hydroxyl groups at the tips of the nanotubes. Also, such harsh conditions create also defects on the side wall of nanotubes resulting in the carboxylic acid groups generations. These defects serve as binding sites for covalent attachment via a bonding chemistry. However, it is noteworthy to mention that increasing number of defects on nanotubes may cause decrease in their electronic and mechanical properties [138].

Functionalization of CNTs has several advantages in terms of ease of application. Functional groups of CNTs provide better dispersion by stabilizing CNTs in the solvent matrix. By this way, nanotube aggregation can be prevented.

There are several ways to create harsh oxidative conditions in order to functionalize CNTs with hydroxyl or carboxylic acid groups. One of the most known way is the use of strong oxidants (HNO_3 and H_2SO_4) which leads to oxidation of defects on the surface of CNTs by producing hydrophilic groups [139]. However, excess acids should be removed from the CNT solution. In the reverse case, enzyme denaturation can be easily observed due to the presence of acids in the CNT solution. It means that purification of the functionalized CNTs is the most crucial part of this approach. Also, the control of such chemical reaction is not possible. The more defects nanotubes have, the more probability to lose electronic properties. Another approach to functionalize CNTs, known as electrochemical etching, is very simple and rapid. The electrode is immersed in 1.0 M NaOH and etched at 1.5 V for 150 seconds [140]. By this way, carboxylic acid functional groups were formed at the CNT tips during the etching without any need of additional purification.

As a result, the presence of functional groups generated in CNTs surface helps to better dispersion as well as to create sites for covalent attachment. The introduction of functionalized CNTs in the biosensing design improves sensing performance by serving both electronic and mechanical properties of CNTs. Functional groups lead to covalent immobilization of the enzyme onto the electrode surface via cross linking chemistry which resulted in improved operational and storage stability.

3.1.5. Scope of The Study

The combination of carbon nanotubes with conducting polymers has attracted great attention due to their biomolecule anchorage tools. Synergistic effect leads to a significant enhancement in the electronic and mechanical properties of each single component. Also, electrical wiring effect of MWCNT incorporated with the polymer film diminishes the diffusion problems [141]. In the nanoscale interface of CNTs and conducting polymer, the electron transfer can be easily achieved due to the high affinity of both groups.

Herein a conducting polymer; poly(4-(2,5-di(thiophen-2-yl)-1*H*-pyrrol-1-yl)benzenamine), poly(SNS-NH₂), was used as the immobilization matrix for acetylcholinesterase. Pendant amino groups in the structure of the polymer serve as a host matrix for immobilization of AChE via covalent immobilization. Functionalization of MWCNT (f-MWCNT) was achieved via electrochemical etching method [140] to possess free carboxylic acid moieties. By this way, both pendant amino groups of poly(SNS-NH₂) and free carboxylic acid groups of f-MWCNT were linked with AChE through covalent binding using a two step carbodiimide coupling method simultaneously. This method involves the formation of amide bonds between modified transducer with poly(SNS-NH₂) and f-MWCNT and the enzyme molecules. In order to increase lifetime stability of the enzyme electrode, covalent immobilization procedure was chosen since there exists a strong and efficient bonding between the enzyme molecules and the support. The aim of this work is to develop sensitive amperometric biosensor based on AChE for indirect measurements of OPs on the basis of their inhibitory effect on AChE activity. After investigation of the experimental conditions related to the performance of the fabricated biosensor, paraoxon, parathion and chlorfenvinphos in tap water samples were analyzed with the proposed sensor. The results were compared with those determined by high pressure liquid chromatography with diode array detector (HPLC/DAD) as the reference method with solid phase extraction (SPE) technique in order to validate the accuracy of the biosensor. To the best of our knowledge, there are no reports presenting such a single biosensor detecting paraoxon, parathion and chlorfenvinphos.

3.2. RESULTS and DISCUSSION

3.2.1. Characterization of Functionalized Multiwalled Carbon Nanotube

In the sensor construction, considerable efforts have been demonstrated to functionalize CNTs. There are several specific methods for this purpose. In order to functionalize MWCNT, an electrochemical treatment was performed. The multi

walled carbon nanotube coated graphite electrode was treated by electrochemical etching at 1.5 V vs Ag wire in 1.0 M NaOH for 150 seconds. By this technique, most of the end groups on MWCNTs were converted to carboxylic acid groups [140]. These ends can be etched electrochemically to enable the modification and perfect transfer. Since MWCNT ends are dominated by carboxylic groups, the attained functional end groups gave opportunity to attach both enzymes and immobilization matrix covalently with the help of cross linking agents. Amino groups of enzyme and free amino ends of conducting polymers formed covalent attachment with f-MWCNT through an amide bond. This linkage leads to increase in shelf life stability of the proposed biosensor excessively.

FTIR spectroscopy was used to investigate the end groups of MWCNT after electrochemical treatment. The FTIR spectra of MWCNT and f-MWCNT were shown in Figure 3.3. These characteristic bands confirmed the functionalization of MWCNT with carboxylic acid groups. The peaks at 1213 cm^{-1} and 1694 cm^{-1} were attributed to C-O and C=O stretchings, respectively. Moreover, the bands observed at 3447 cm^{-1} correspond to O-H groups of carboxylic acids. The results demonstrated successful modification of the MWCNT composite onto the electrode surface. This proves that carboxylic groups on the external surface of MWCNT are free to bond with amino groups of both the biomolecule and the polymer on the surface of proposed electrode. Immobilization of enzyme without losing its bioactivity was achieved through covalent bond formation.

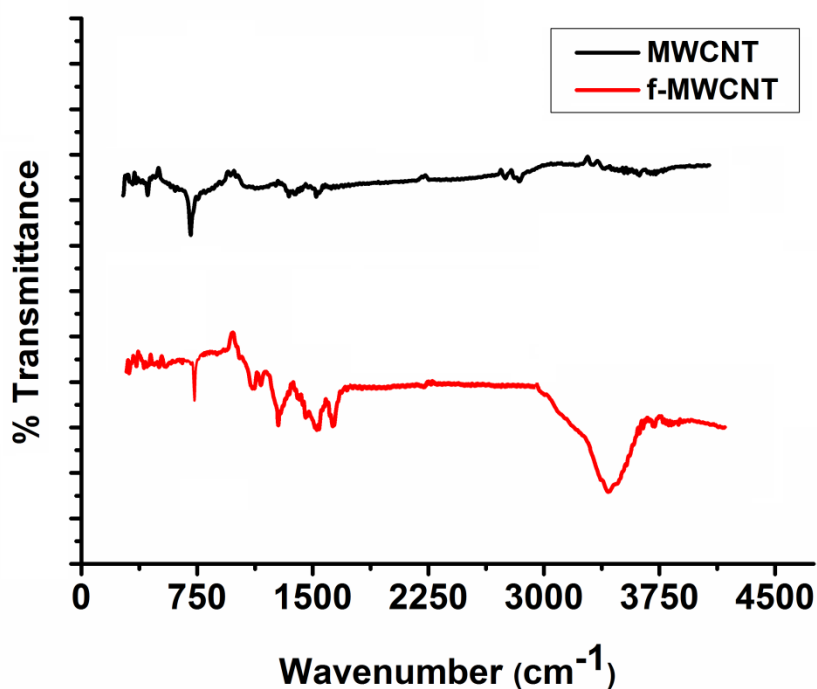


Figure 3.3. FTIR spectra of MWCNT and f-MWCNT.

3.2.2. Effect of f-MWCNT and Poly(SNS-NH₂) On Biosensor Response

Combining unique properties of individual structures and their synergistic effect, the proposed immobilization platform leads to a significant enhancement in the electronic and mechanical properties. To investigate the effect of f-MWCNT and poly(SNS-NH₂) on the performance of acetylthiocholine biosensor, three different electrodes were prepared. As seen in Figure 3.4, combination of poly(SNS-NH₂) and f-MWCNT revealed the highest biosensor performance among the three studied. In addition, effect of conducting polymer on biosensor response was examined. The presence of conducting polymer on the electrode surface enhanced the biosensor performance and enzyme stability. The biomolecule was immobilized successfully onto the electrode satisfying immobilization matrix. The linkage resulted in effective conjugation and enhanced enzyme stability. Thus, the amperometric studies proved that f-MWCNT/poly(SNS-NH₂) possesses a synergistic effect of f-MWCNT and poly(SNS-NH₂) showing better biosensor

performance with higher analytical parameters than those of each individual component.

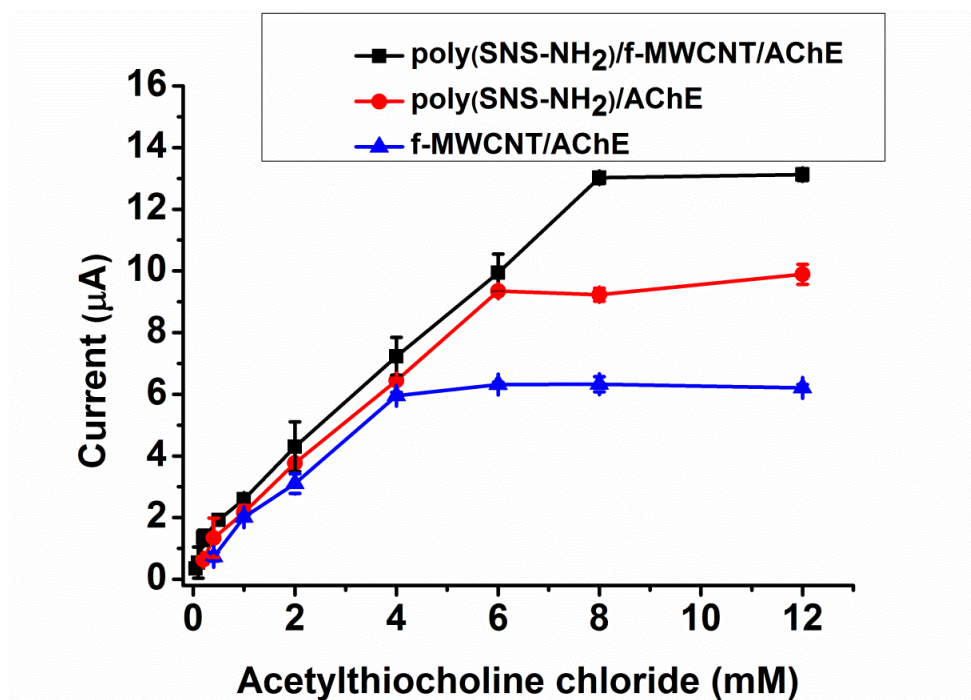


Figure 3.4. The effect of surface modification and different conditions on response current on performance of the biosensors (in 2 mmol L⁻¹ AThCl in 50 mM PBS, pH 7, 25 °C, 0.1 V). Error bars show standard deviation (SD) of three measurements.

3.2.3. Optimization of Experimental Parameters

Thickness of the polymer film was adjusted by the duration of electropolymerization in terms of charge passing through the cell [87]. The optimum polymer thickness on the electrode was determined using cyclic voltammetry. In doing so, different scan numbers were used which satisfies to prepare proper immobilization matrix for the maintenance of 3D structure of biomolecule. Different matrices with 15, 25, 35, 45 scans during electropolymerization were prepared and their biosensor responses to the substrate were compared by keeping the other parameters constant. As seen in Figure 3.5A,

the highest response was recorded with 25-cycle deposition. The charges and film thicknesses for 15, 25, 35 and 45-cycle polymer films were calculated as 1.07 mC (23.8 nm), 1.23 mC (27.2 nm), 1.31 mC (10.2 nm) and 1.39 mC (30.1 nm), respectively. If the layer was too thick, diffusion problems between polymer coated transducer and biomolecules may arise causing a lower charge transfer rate. On the contrary, if the layer is too thin, 3D structure of biomolecules may not be satisfied causing denaturation. Therefore, the biosensor coated with 25-cycle showed high amplified signal arranging excellent immobilization structure and used for subsequent experiments.

Since the activity of biomolecules is affected by the pH of the medium, working buffer pH was optimized while the other parameters were kept constant. In the range of pH 6.0-8.5 (50 mM sodium phosphate buffer, 25°C), amperometric signals were recorded. Figure 3.5B shows that the maximum peak current was obtained at pH 7.0. Therefore, pH 7.0 sodium phosphate buffer was used as the buffer solution improving the enzyme activity.

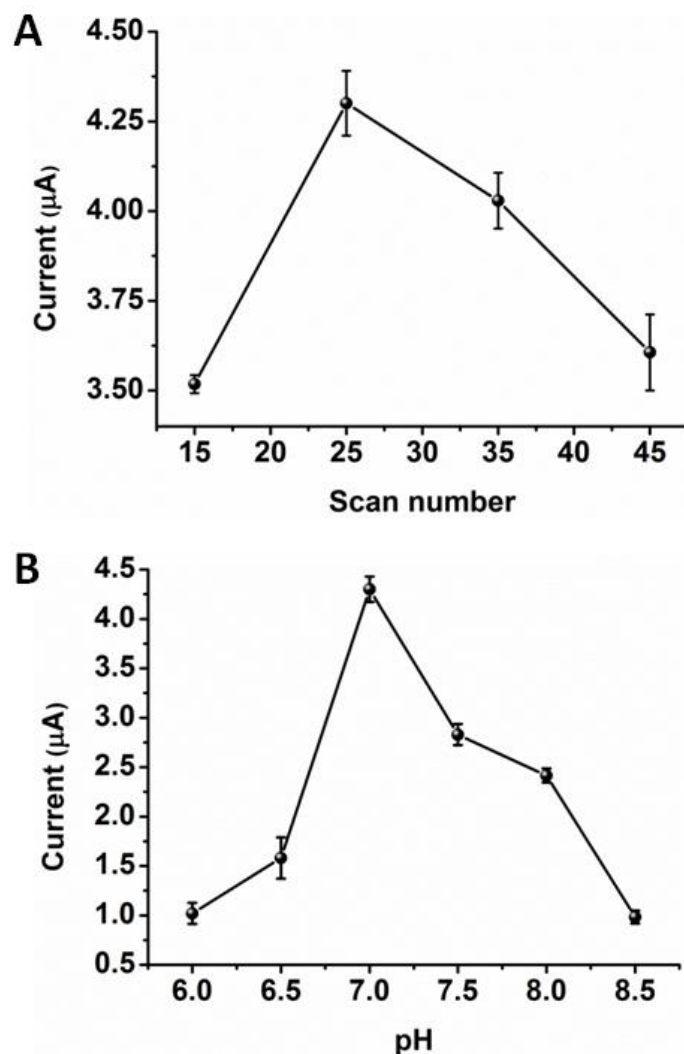


Figure 3.5. The effect of scan number (accumulated charge) (A), pH (B), applied potential (C) on performance of the biosensors (in 2 mmol L^{-1} AThCl in 50 mM PBS, pH 7, $25 \text{ }^\circ\text{C}$, 0.1 V). Error bars show standard deviation (SD) of three measurements.

The major drawback in AChE biosensors is that the oxidation of enzymatic product, thiocholine, requires a high potential at the transducer [102]. According to literature, most of the sensor designed for detection of pesticides works in the range of $600\text{-}800 \text{ mV}$ [142-145]. This over potential may affect the activity of enzyme resulting in poor biosensing performance and instability of the biosensor. Moreover, high working potential can cause oxidation of other species present in the media. Thus, possible lower potentials are preferred in amperometric systems. To overcome the problem, acetylthiocholine detection could be achieved using

electrochemical mediators onto the transducers. In this system, combination of nanostructures and the conducting polymer eases the electrooxidation of thiocholine, hence amplifying the sensitivity and amperometric response of the biosensor. The constructed biosensor was tested at different working potentials for the same amount of substrate to investigate optimum working potential. As illustrated in Figure 3.6A, the highest amperometric response was recorded at 100 mV applied potential versus Ag wire reference electrode [146-151].

To examine the relationship between enzyme amount and biosensor response, different biosensors were prepared with different AChE amounts between 0.5 U and 3.0 U where other components were kept constant. As seen in Figure 3.6B, the highest signal was recorded with 1.5 U AChE. In case of excess loading of enzyme, the enzyme molecules leached from the surface since adsorbed enzyme was not sufficiently stable on the limited electrode area. On the other hand, if substantial amount of biomolecule could not be immobilized onto the electrode, biosensor responses were decreased due to inadequate enzymatic reaction which leads to low sensitivity. In addition, since the inhibition of AChE by OPs is an irreversible process, the enzyme amount should be as low as possible for practical purposes [152]. The use of a small amount of enzyme enables to reach a low detection limit as well as to perform repeated measurements. Sufficient working stability and reasonable signals were achieved with 1.5 U AChE.

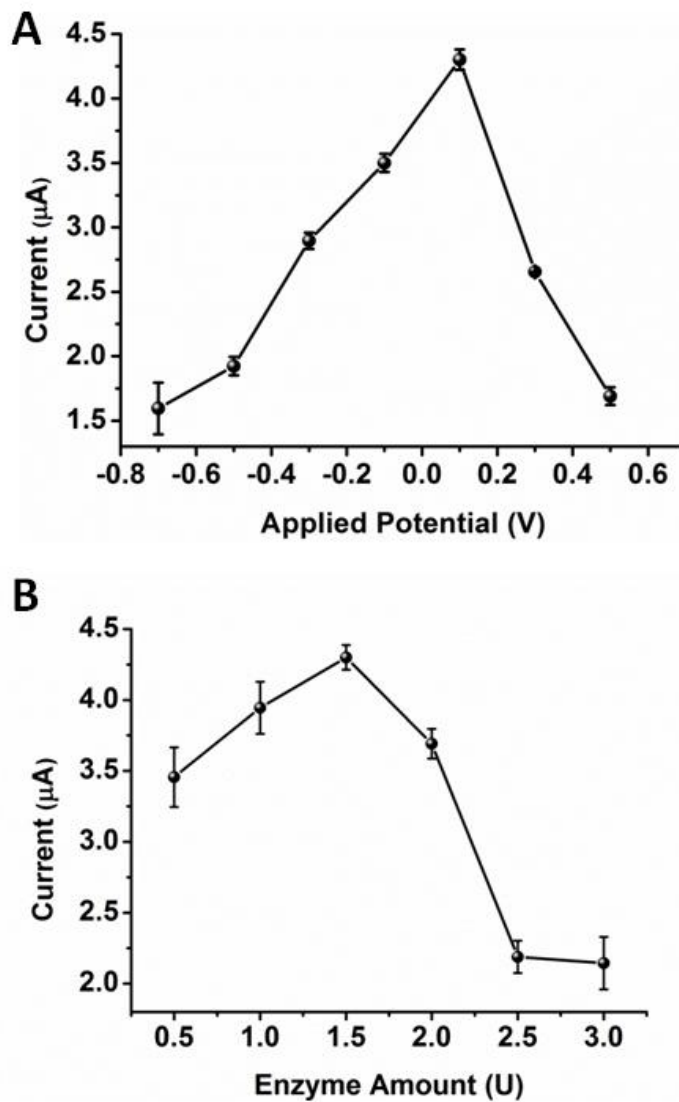


Figure 3.6. The effect of applied potential (A) and enzyme amount (B) on performance of the biosensors (in 2 mmol L^{-1} AThCl in 50 mM PBS, pH 7, $25 \text{ }^\circ\text{C}$, 0.1 V). Error bars show standard deviation (SD) of three measurements.

3.2.4. Surface Characterization

The change in surface morphology during deposition process was investigated by Scanning Electron Microscope (SEM) as shown in Figure 3.7. Figure 3.7A and B refer to the SEM images of MWCNT and f-MWCNT composites, respectively. MWCNT and f-MWCNT were coated nicely onto the bare electrode showing

typical fibrous structure. f-MWCNT are dispersed more uniformly than pristine MWCNT. When conducting polymer film was coated onto the f-MWCNT surface (Figure 3.7C), the typical homogeneous, cauliflower-like structure of the conducting polymer was revealed with uniform MWCNT distribution. It can be clearly seen that the f-MWCNT/poly(SNS-NH₂) film presents homogeneous morphology, which may be attributed to the incorporation of f-MWCNT into the polymer film. Moreover, the wiring effect of MWCNT via tiny bridges towards polymer film serves excellent immobilization platform for biomolecules. When AChE was immobilized onto the modified electrode (Figure 3.7D), a morphology change in the electrode surface can be easily observed. Moreover, homogeneous coating of the enzyme proved that the proposed electrode before immobilization serves as an excellent host-guest platform for biomolecule immobilization.

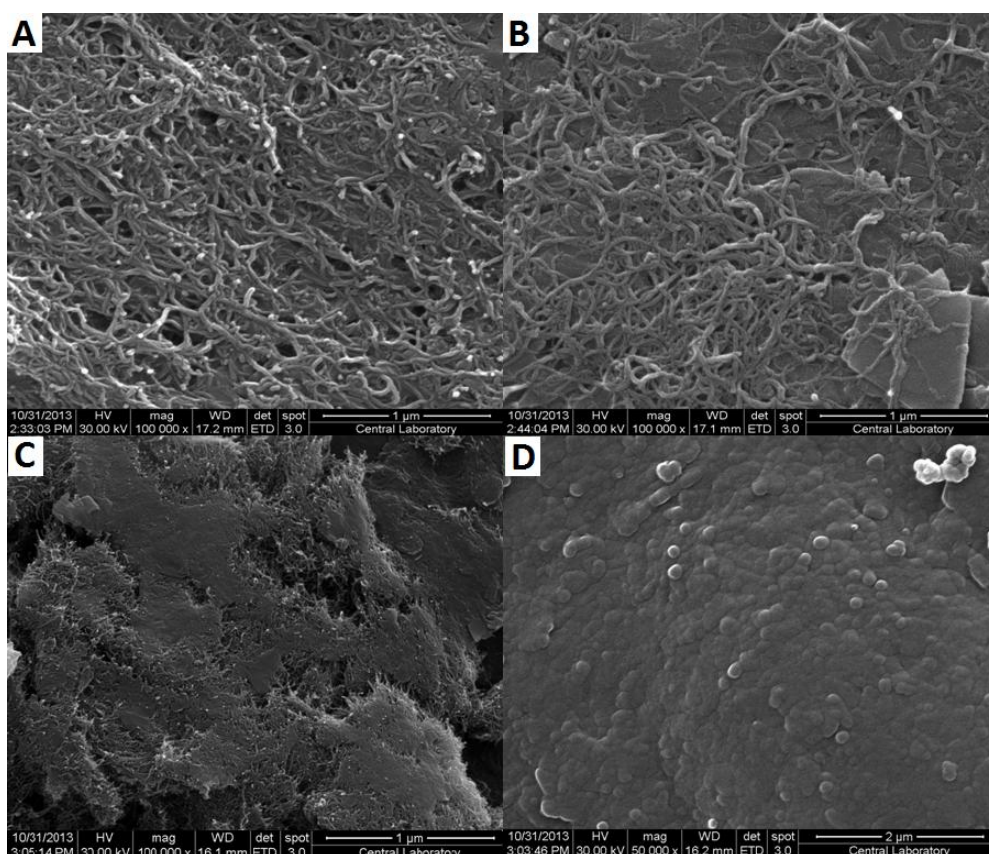


Figure 3.7. SEM images of (A) MWCNT; (B) f-MWCNT; (C) f-MWCNT/poly(SNS-NH₂); (D) f-MWCNT/poly(SNS-NH₂)/AChE under optimized conditions.

Contact angle measurement is a simple and alternative tool to examine the surface property after each modification. Therefore, it is possible to investigate the deposition processes by following the changes in surface hydrophilicity. Also, the biocompatibility of an interface can be characterized by its hydrophilicity, which can be qualitative by measuring the contact angle of the substrate [153]. For this purpose, electrodes with MWCNT, f-MWCNT, f-MWCNT/poly(SNS-NH₂) and f-MWCNT/poly(SNS-NH₂)/AChE were prepared. Ability of a drop of water to spread over the surface was studied by averaging the left and right angles of drops with the same volume. The electrode with MWCNT was highly hydrophobic with a contact angle of $103.9 \pm 2.8^\circ$. This value decreases dramatically to $37.1 \pm 2.2^\circ$ when MWCNT was etched electrochemically to obtain carboxylic acid to form f-MWCNT. This result serves for yet another proof of successful functionalization of MWCNT. Poly(SNS-NH₂) coating on this electrode reveals an increase in the contact angle ($41.3 \pm 4.1^\circ$) owing to more hydrophobic character of the conducting polymer film. Hence the hydrophilicity of f-MWCNT/poly(SNS-NH₂) was dominant, indicating excellent biocompatibility for the immobilization of biomolecules. This platform improved the loading capacity of enzymes and retain activity of enzyme onto the electrode; thus providing a fascinating platform for biosensing application. Finally, immobilization of AChE led to a decrease in the contact angle ($28.4 \pm 1.4^\circ$) illustrating successful immobilization on the transducer.

X-ray Photoelectron Spectroscopy was performed to prove the success of functionalization and immobilization processes (Figure 3.8). XPS data were recorded after each biosensor preparation step and the specific peaks for characterization were fitted using binding energies via a fitting program. In Figure 3.8A, C1s spectra for MWCNT and f-MWCNT were represented. The peaks around 284.3 eV represent the unmodified carbon (C-C/C=C) in Figure 3.8A and B, simultaneously, the peaks at 287.1 and 288.9 eV in Figure 3.8B belong to C-O/C=O and O=C-OH which approves the carboxylic acid functionalization of the carbon nanotubes on the electrode surface [154]. Propitiously, these data for MWCNT functionalization are comprehensible with the FTIR determinations. Moreover, after the polymerization the XPS spectrum for this surface also confirms the surface modification with both f-MWCNT and the conducting polymer (Figure 3.8C). The peaks at 284.1 and 284.8 eV can be attributed to C_α, C_β, C-S in the

structure of the conducting polymer. Also, the peak at 286.1 eV represents C-N, C=N groups in the polymeric structure due to the benzamine and pyrrole units. Additionally, the peak at 287.9 eV affirms the presence of f-MWCNT in the polymeric network which is attributed to C=O, O=C-OH groups [92,155]. After AChE immobilization, in Figure 3.8D, the increase in the peak intensity of C-N peak (at around 286.0 eV) and appearance of the peak at 287.0 eV confirm the noteworthy covalent binding via amide bond between amino and carboxylic acid groups of enzyme molecules, the polymer and f-MWCNT [92,156]. Also, the peak at 288.1 eV is due to the carboxylic acid groups of both f-MWCNT and enzyme molecules.

Furthermore, N1s spectra of modified surfaces also confirm the efficacious immobilization. In Figure 3.8E nitrogen spectrum refers to poly(SNS-NH₂) and f-MWCNT coated surface where the peaks at 398.9, 399.8 and 401.4 eV arise from tertiary benzamine substituted amine in pyrrole units, free amino groups of poly(SNS-NH₂) and protonated amino groups in the structure of free amino containing polymeric network, respectively [157]. When biomolecule immobilized modified surface is considered, the covalent immobilization was reiteratively confirmed in nitrogen spectrum with the disappearance of the bands for free amino groups and newly appearance of amide nitrogen at 400.8 eV in Figure 3.8F [158].

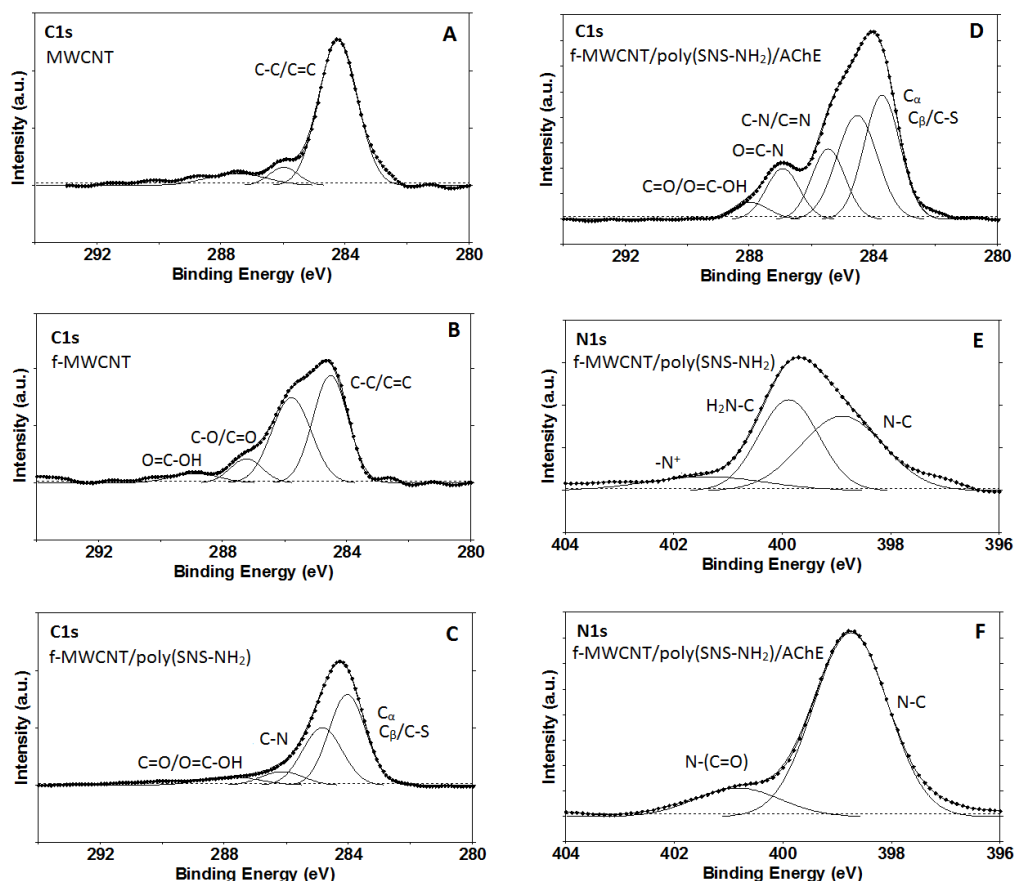


Figure 3.8. XPS C1s spectra for (A) pristine MWCNT; (B) f-MWCNT; (C) f-MWCNT/poly(SNS-NH₂); (D) AChE immobilized f-MWCNT/poly(SNS-NH₂) and N1s spectra for (E) f-MWCNT/poly(SNS-NH₂); (F) AChE immobilized f-MWCNT/poly(SNS-NH₂).

3.2.5. Electrochemical Characterization of Different Electrodes

Electrochemical Impedance Spectroscopy (EIS) was carried out to characterize the interface properties of the modified electrodes during the fabrication process of the biosensors [88]. Electron transfer between the solution species and the electrode surface occurs by tunneling through the barrier. In a Nyquist plot, the semicircle portion corresponds to the electron-transfer resistance at the higher frequency range which controls the electron transfer kinetics of the redox probe at the electrode surface. The semicircle diameter represents the electron transfer resistance.

Moreover, linear part of the plot at lower frequency range represents the diffusion limited process. Figure 3.9 illustrates typical Nyquist plots obtained for bare graphite electrode (a), f-MWCNT (b), f-MWCNT/poly(SNS-NH₂) (c) and f-MWCNT/poly(SNS-NH₂)/AChE (d) using Fe(CN)₆^{3-/4-} as the redox probe. It is easily seen that the electron transfer resistance of the bare graphite electrode and f-MWCNT were almost straight line which is a characteristic of a diffusion limiting step for the electrochemical process. The adsorbed f-MWCNT provided a conductive pathway for the electron transfer. After coating the electrode surface, the EIS of the f-MWCNT/poly(SNS-NH₂) showed that the semicircle diameter increased slightly due to the increase in the thickness of the interface. The small resistance indicated a resistance of electron flow due to the addition of a layer on the electrode surface. However, it is known that the combination of layers promoted electron transfer to the electrode surface owing to the conductivity of polymer film and MWCNT matrix. After AChE was immobilized onto the modified transducer, there was a great increase in the diameter of semicircle, indicating that this layer formed an additional barrier and blocked the redox probe to diffuse towards the electrode. It is also known that most biological molecules were poor electrical conductors at low frequencies. Increase in semicircle diameter proved the hindrance of the electron flow. On the basis of the EIS results, immobilization of AChE was achieved successfully onto the carbon nanotube modified polymer matrix. Hence the matrix in concern is a well-established candidate for immobilization and biosensor preparation.

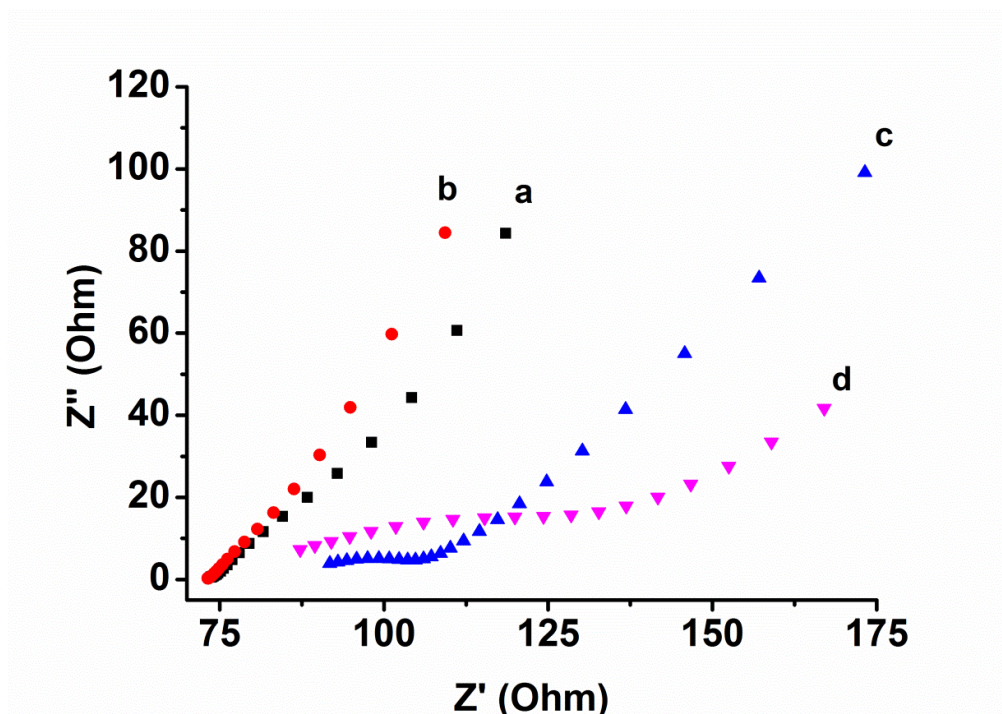


Figure 3.9. (A) Typical Nyquist plots resulting from the bare graphite electrode (a), f-MWCNT (b), f-MWCNT/poly(SNS-NH₂) (c), and f-MWCNT/poly(SNS-NH₂)/AChE (d) in 5.0 mM Fe(CN)₆^{3-/4-} containing 0.1 M KCl.

Cyclic voltammetry (CV) studies were carried out in 5 mM Fe(CN)₆^{3-/4-} containing 0.1 M KCl (100 mVs⁻¹ as scan rate) to characterize the electrode surface after each layer construction (Figure 3.10). Successive formation of layers onto the electrode surface resulted in a large different interfacial structures. In case of the bare graphite electrode a well-defined oxidation peak (current 86 μA) was observed (Figure 3.10, curve a). After modification with f-MWCNT, there was an increase in oxidation peak current to 121 μA which exhibits a higher electroactive surface area than the one for bare electrode. f-MWCNT adsorption onto the graphite electrode improved the conductivity of the surface. When poly(SNS-NH₂) was coated onto the modified electrode, excessive increase in peak current to 294 μA resulted since introduction of conducting polymer film played an important role in electronic transport with the help of f-MWCNT. It is clearly seen that electron transfer rate was accelerated and obviously the oxidation current was increased. On

such a surface, AChE was immobilized and the decrease of oxidation current (245 μA) confirmed the effective attachment of the biomolecule on the electrode. This occurs owing to the insulating character of the biological molecules. However, electroactive surface area was sufficient enough for effective electron transfer between the enzyme molecules and the coated electrode surface.

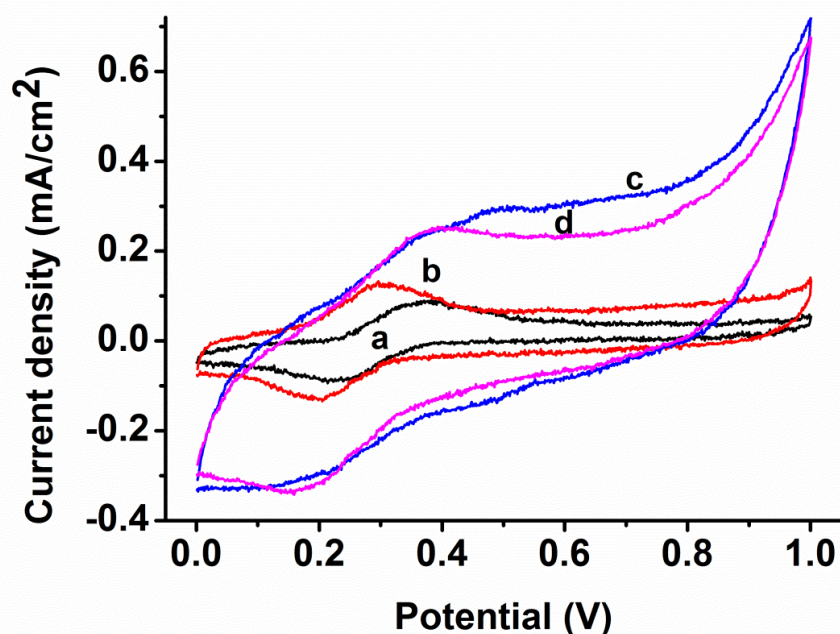


Figure 3.10. Cyclic voltammograms resulting from the bare graphite electrode (a), f-MWCNT (b), f-MWCNT/poly(SNS-NH₂) (c), and f-MWCNT/poly(SNS-NH₂)/AChE (d) in 5.0 mM Fe(CN)₆^{3-/4-} containing 0.1 M KCl.

The average value of the electroactive surface area was calculated according to the Randles–Sevcik equation (4) [159]:

$$I_p = 2.69 \times 10^5 AD^{1/2} n^{3/2} \nu^{1/2} C \quad (4)$$

where n is the number of electrons participating in the redox reaction, A is the area of the electrode (cm^2), D is the diffusion coefficient of the molecule in solution

(cm^2s^{-1}), C is the concentration of the probe molecule in the bulk solution (molcm^{-3}), and v is the scan rate (Vs^{-1}).

According to the equation, the increase in the peak currents can be attributed to an increase in the effective surface area. The electroactive surface area for bare graphite electrode, f-MWCNT, f-MWCNT/poly(SNS-NH₂) and f-MWCNT/poly(SNS-NH₂)/AChE modified electrodes were 0.076 cm^2 , 0.108 cm^2 , 0.261 cm^2 and 0.218 cm^2 respectively. The electroactive surface area for f-MWCNT/poly(SNS-NH₂) was 1.42 times higher than that of f-MWCNT and 3.43 times higher than the one for bare graphite electrode. Also, immobilization of AChE onto the polymer coated electrode caused a decrease in the surface area. Therefore, f-MWCNT/poly(SNS-NH₂) electrode exhibited the highest electroactive surface area.

3.2.6. Analytical Performance of The Biosensor

The analytical characteristics of the biosensor were examined under optimized conditions using acetylthiocholine chloride as the substrate. Figure 3.11 shows a typical current-time plot of optimum f-MWCNT/poly(SNS-NH₂)/AChE biosensor. Using selected applied voltage (+100 mV), a calibration curve was plotted. A good linearity was obtained between 0.05 mM and 8.00 mM acetylthiocholine chloride in 50 mM PBS pH 7.0 as given with the equation; $y=1.539x+0.843$ with $R^2=0.994$. In order to calculate the limit of detection (LOD), the intercept of the linear range of the calibration curve was set to zero using S/N (signal-to-noise ratio) = 3 criterion and found as 0.09 mM for the biosensor. Sensitivity of the biosensor is found to be 24.16 $\mu\text{A mM}^{-1}\text{cm}^{-2}$. Also, a typical amperometric response of the biosensor was given as an inset in Figure 3.11. It is clearly seen that the response time is about 6 s. The response of the enzymatic substrate depends on the enzymatic activity and on the electrochemical behavior of thiocholine. Hence, the time interval was attributed to the efficient immobilization matrix; conducting polymer film incorporated with MWCNT.

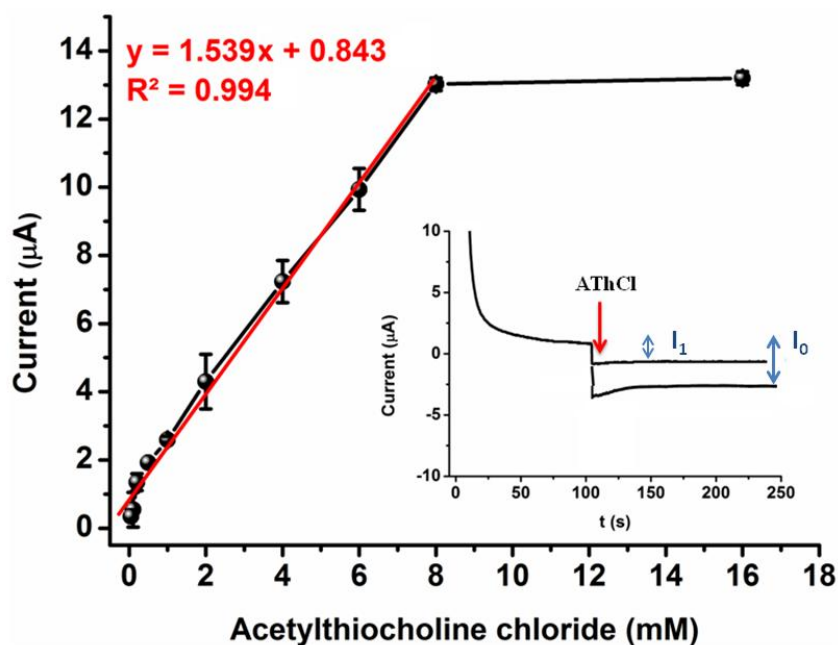


Figure 3.11. Calibration curve for AThCl (in 50 mM PBS, pH 7, 25 °C, 0.1 V). (A typical amperometric signal of the biosensor as an inset for 3 mM AThCl after (I_1) and before (I_0) incubation). Error bars show the standard deviation (SD) of three measurements.

Furthermore, kinetic parameters were obtained from Lineweaver-Burk plots using Solver application [89]. The apparent Michaelis-Menten constant (K_M^{app}) and maximum current (I_{max}) in the present were calculated as 1.038 mmol L⁻¹ and 14.61 μA, respectively. It was highlighted that the estimated K_M^{app} value for the proposed system was lower than that for immobilized AChE on polyethyleneimine-modified electrode (1.5 mmol L⁻¹) [160], AChE biosensor modified by PbO₂/TiO₂/Ti (1.34 mmol L⁻¹) [161] or entrapped AChE on carbon paste electrode (1.12 mmol L⁻¹) [104]. According to these results, the biosensor design showed greater affinity for AChE onto the electrode surface to the substrate. Thus, the biosensor performance was improved as the interaction between the substrate and active site of the enzyme was increased.

Shelf life of the biosensor was also investigated. Amperometric response to the same amount of substrate of the sensor was recorded every day for the same sensor. No activity loss was observed for 15 days. After 45 days of storage, the sensor retained 72 % of its initial current response. Presence of covalent binding between enzyme and immobilization matrix resulted in a stable and long life biosensor with a high sensitivity. Moreover, this high shelf life stability indicated that there was no enzyme leakage from the surface. Hence, the immobilization platform provided a biocompatible microenvironment around the enzyme by retaining its biological activity. Furthermore, to test the selectivity behavior of the proposed biodetector, interfering compounds such as ascorbic acid, cholesterol, glucose (in 1.0 mM - 0.1 M concentration range) were tested and no response to these solutions was recorded for any sample.

3.2.7. Pesticide Detection

After the construction of f-MWCNT/poly(SNS-NH₂)/AChE biosensor, three different pesticides (paraoxon, parathion, chlorfenvinphos) were used as the model inhibitors to investigate pesticide sensitivity to AChE. One of the most important parameters in pesticide analysis is the incubation time. Preincubation method was chosen to eliminate the competition between substrate and inhibitors and to get the maximum inhibition. The proposed biosensor was immersed in the standard solution of pesticides at a certain concentration for several minutes and biosensor responses were explored. Following exposure, pesticides bind to the serine active site of AChE covalently. Blocking of serine hydroxyl group by phosphate group results in a decrease in the biosensor response. Therefore, this inhibition causes a decrease in the activity of the enzyme. In other words, the incubation time was the time required for the reaction between the enzyme and the inhibitor. For all the pesticides, as the incubation time increased, degree of enzyme inhibition increased as seen in Figure 3.12. It is possible to achieve lower detection limits by longer incubation times. However, a longer incubation time makes the analysis quite slow. The most suitable analysis should be a compromise between good detection limit and appreciable measurement period [162]. In order to investigate the optimum time interval for enzyme inhibition, the optimized biosensor was immersed in 0.4

$\mu\text{g/L}$ pesticide solution separately for a given time. After rinsing the sensor with the buffer solution and distilled water, the biosensor response was recorded upon addition of 2 mM acetylthiocholine into the reaction cell. Although the level of inhibition increased with the increase of the immersing period until 15-20 min, the incubation time was selected as 5 min for all three pesticides, since the decrease in the enzyme activity could be detected after 5 min.

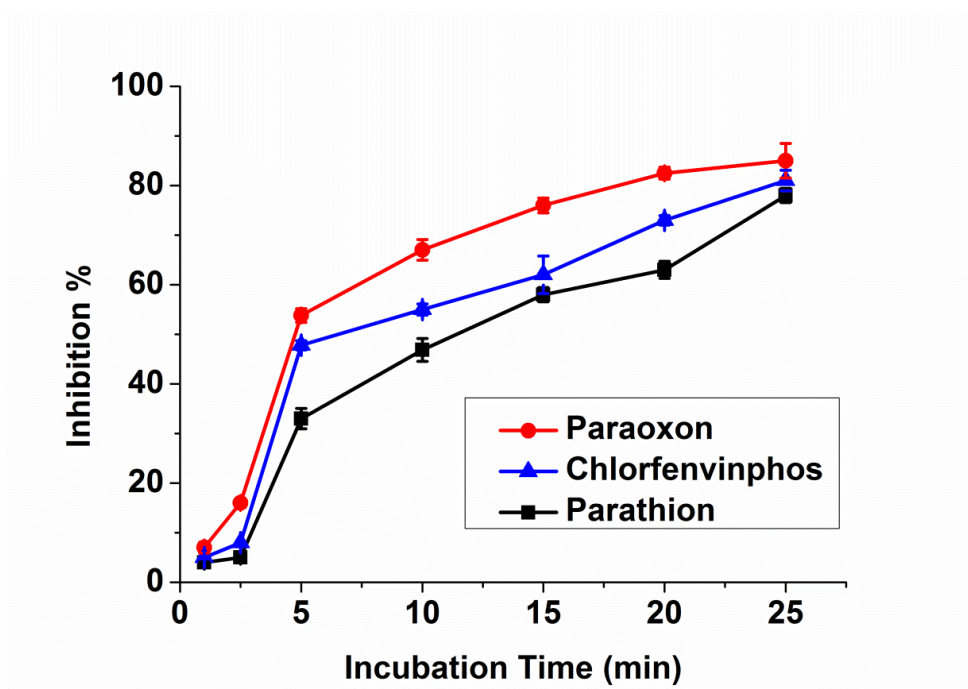


Figure 3.12. The dependence of the inhibition curves of paraoxon, parathion, chlorfenvinphos on incubation time. Error bars show standard deviation (SD) of three measurements.

The detection limit and the linear working range of the biosensor were examined for three different pesticides. For this purpose, percent inhibition was calculated after immersing the sensor in pesticide solution with different concentration for 5 min and analytical curves were plotted for each pesticide (Figure 3.13). Since activity of enzyme was reduced by inhibitors, increasing concentration of pesticide solutions led to a decrease in detected signals. Under the optimal experimental conditions, two linear ranges with different sensitivities were observed for each pesticide. The inhibition of paraoxon was proportional to its concentration in the

ranges between 0.005 $\mu\text{g/L}$ and 0.1 $\mu\text{g/L}$ and 0.1 $\mu\text{g/L}$ - 10 $\mu\text{g/L}$, with the linearization coefficient of 0.996 and 0.995, respectively. For parathion, the relationships were from 0.001 $\mu\text{g/L}$ to 0.01 $\mu\text{g/L}$ and from 0.01 $\mu\text{g/L}$ to 7 $\mu\text{g/L}$, with the regression coefficients of 0.995 and 0.994, respectively. There was a linear relationship between inhibition of chlorfenvinphos on the proposed biosensor in the ranges 0.005 – 0.1 $\mu\text{g/L}$ and 0.1 – 12.5 $\mu\text{g/L}$ with the R^2 values of 0.996 and 0.995, respectively. The maximum inhibition was not 100 % due to the equilibrium established between pesticide and active sites of the enzyme [163]. Moreover, the detection limits of the present biosensor were found to be 2.46 ng/L for paraoxon, 0.542 ng/L for parathion, 4.90 ng/L for chlorfenvinphos, which are lower than those reported in previous studies. For example, LOD of immobilized AChE via glutaraldehyde on a cysteamine self-assembled monolayer on gold screen electrodes was calculated as 2 $\mu\text{g/L}$ for paraoxon [164]. and captured AChE in a gelatin membrane onto the carbon screen printed electrode was calculated as 2.5 $\mu\text{g/L}$ for paraoxon [165]. For the detection limit of parathion, AChE immobilized onto SAM gold electrode was found as 9.3 $\mu\text{g/L}$ [166] and AChE immobilized by adsorption into the $\text{PbO}_2/\text{TiO}_2/\text{Ti}$ was detected as 29.1 ng/L [104]. Detection limit of entrapped AChE in a polyvinylalcohol-based matrix for chlorfenvinphos was calculated as 46.7 $\mu\text{g/L}$ [167].

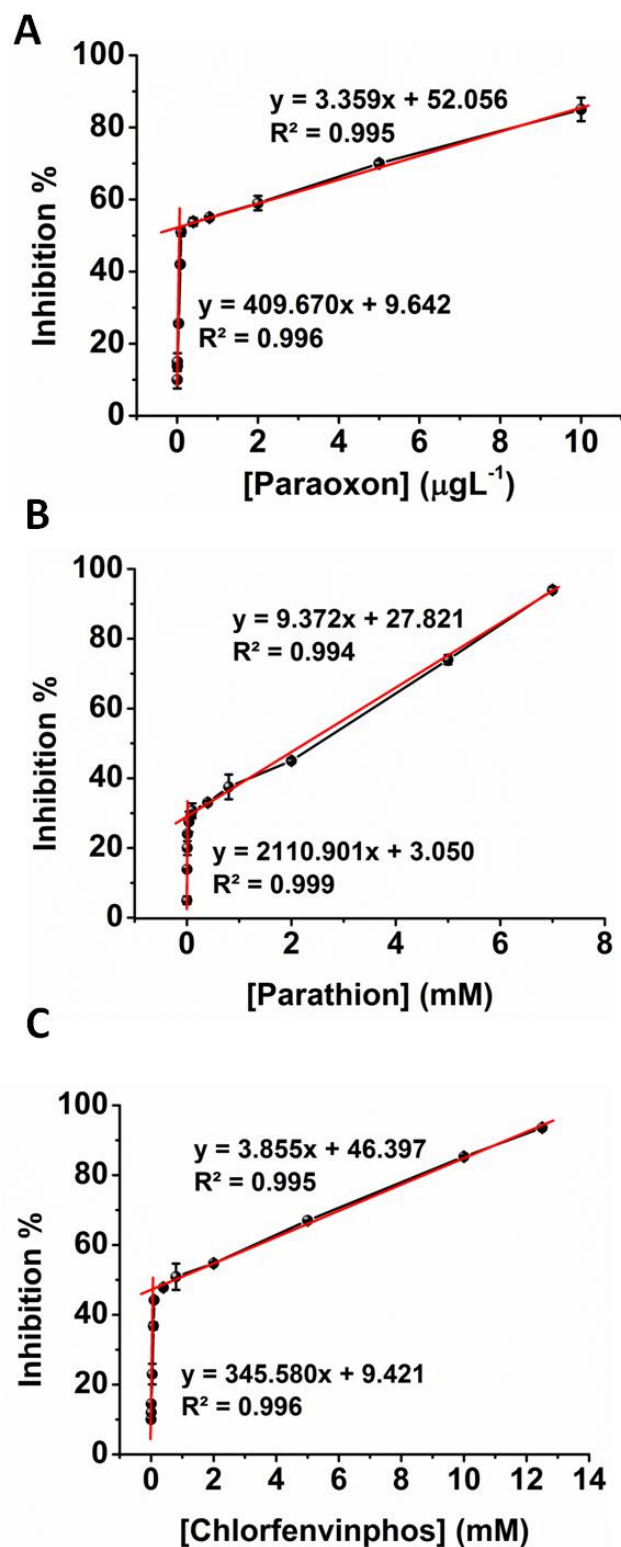


Figure 3.13. Calibration curves for paraoxon (A), parathion (B), chlorfenvinphos (C) detection (in 50 mM PBS, pH 7.0, 25°C, 0.1 V, 2.0 mM AThCl, 5 min incubation time). Error bars show standard deviation (SD) of three measurements.

Hence, the f-MWCNT/poly(SNS-NH₂)/AChE biosensor shows good analytical performance with high sensitivity. It can be used for detection of various pesticides (paraoxon, parathion, chlorfenvinphos) effectively. Owing to the overwhelming characteristics of immobilization matrix for the AChE biomolecule, the proposed sensing system is a novel method for the detection of three pesticides with the same sensor. Moreover, to the best of our knowledge, there is no report on the use of a same biosensor for detection of paraoxon, parathion and chlorfenvinphos.

A crucial problem for practical applications is caused by irreversible inhibition mechanism forming a covalent link between AChE and pesticide. However, it is possible to reactivate the enzyme completely using nucleophilic oximes. Nucleophilic attack of the agents at the phosphorylated enzyme enables the release of pesticides from AChE. Pyridine 2-aldoxime methochloride (2-PAM) was used as the chemical reactivator of AChE to recover the activity of inhibited AChE [168]. With increasing reactivation time, the reactivation efficiency (R%) increased and reached a constant value after 10 min (Figure 3.14). It was observed that treatment of inhibited working electrode with 4 mM 2-PAM for 10 min, original enzymatic activity of AChE could resume 92.8%. Thus, 10 min incubation time in 4 mM 2-PAM solution was chosen as the optimum reactivation time for the constructed biosensing system. This reactivation allowed using the sensing system repeatedly for the detection of pesticides.

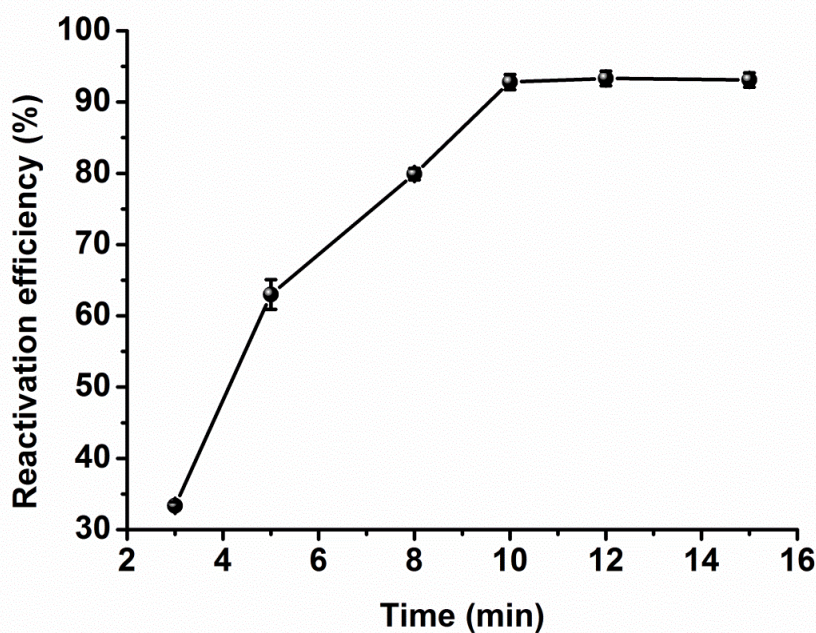


Figure 3.14. Influence of reactivation time with 2-PAM on the biosensor responses at 1 mM AThCl in 50 mM PBS (pH 7.0).

3.2.8. Application of the Biosensor

In order to test the practicality of the present biosensor in real water samples, several of them were fortified with the pesticides in several concentrations between 10.0 and 100 $\mu\text{g/L}$. In parallel, the samples were also studied with HPLC/DAD. As illustrated in Figure 3.15, a well defined linear relationship was observed in the range of 10.0 - 100 $\mu\text{g/L}$ for the pesticides, indicating a good agreement with the ones detected by a conventional method. Thus, the proposed biosensor was applied satisfactorily for determination of paraoxon, parathion and chlorfenvinphos in real water samples. In comparison to HPLC/DAD method (combined with SPE) which had a detection limits of about 1 $\mu\text{g/L}$ water using 500 mL water sample, the present biosensor is much more sensitive (DL 0.5 – 5 ng/L) and needs just a few milliliters of water sample. However, it is not possible to distinguish between the different pesticides with the biosensor. Determining the concentration of a specific OPs or carbamic pesticide in a water sample, the use of this kind of sensors

(enzyme inhibition based biosensors) permits to measure the total anticholinesterase charge in the sample defined as the amount of compounds which cause a percentage of cholinesterase inhibition equivalent to that caused by a known amount of a pesticide (e. g. Parathion or Paraoxon) taken as a reference compound [169,170].

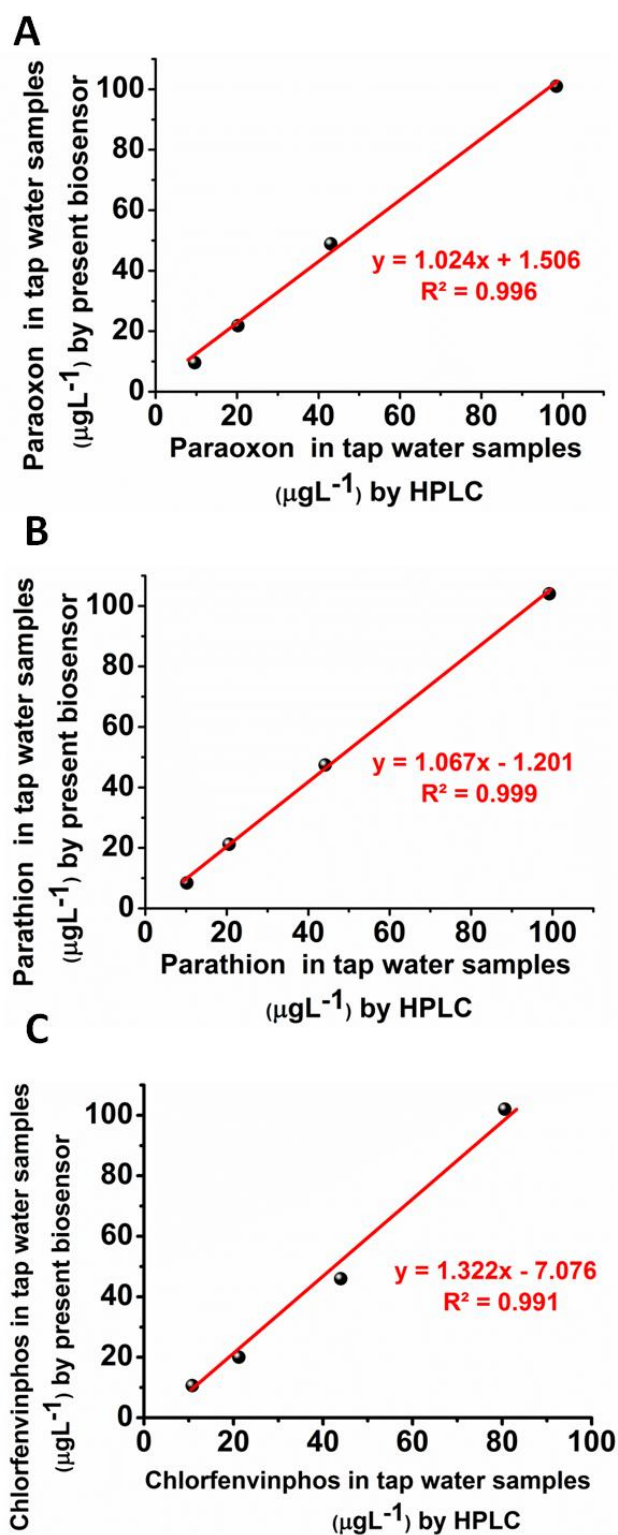


Figure 3.15. Correlation of the quantification results for (A) paraoxon, (B) parathion, (C) chlorfenvinphos in tap water with HPLC/DAD analysis (x-axis) and the new designed biosensor (y-axis).

Based on these results, this biosensor design becomes a promising complementary method to conventional chromatographic techniques for acetylcholinesterase inhibiting pesticide detection and quantification. The biosensor allows a very sensitive and quick screening of water samples for the presence of inhibitors, delivering data in form of a sum or toxicity parameter.

3.3. EXPERIMENTAL DETAILS

3.3.1. Materials

Acetylcholinesterase (AChE, EC 3.1.1.7, 518 U mg⁻¹ from Electrophorus Electricus (electric eel)), acetylthiocholine chloride, paraoxon, parathion, chlorfenvinphos, multi walled carbon nanotube, N-hydroxysuccinimide (NHS) and pyridine 2-aldoxime methochloride (2-PAM) and chemicals used for the synthesis of the monomer and electropolymerization were purchased from Sigma–Aldrich Co. LCC. (St. Louis, USA). N-(3-dimethylaminopropyl)-N'-ethylcarbodiimide hydrochloride (EDC) was purchased from Fluka (Buchs, Switzerland). Acetonitrile (ACN), sodium hydroxide were purchased from Merck (Darmstadt, Germany) and tetrahydrofuran (THF) from Acros (Geel, Belgium). All chemicals were analytical grade.

3.3.2. Instrumentation

All amperometric measurements were performed with the potentiostat CompactStat (Ivium Technologies B.V., Eindhoven, Netherlands) in a three-electrode cell configuration consisting of a graphite electrode (Ringsdorff Werke GmbH, Bonn, Germany, type RW001, 3.05 mm diameter and 13% porosity) as the working electrode. A platinum wire as the counter electrode and a silver wire as the pseudo reference electrode (vs. Ag/AgCl (0.05 V)) were used. Amperometric measurements were performed in a three-electrode system. In amperometric analyses, the data were given as the average of three measurements and standard

deviations were recorded as \pm SD. All measurements were performed at ambient conditions (25 °C). For the investigation of surface characteristics, scanning electron microscopy (SEM) (JEOL JSM-6400 model, Japan) and X-ray photoelectron spectroscopy (XPS) (PHI 5000 Versa Probe (FULVACPHI, Inc., Japan/USA) with monochromatized Al K α radiation (1486.6 eV) 10 as the X-ray anode at 24.9 W were used. Contact angle measurements (2.0 μ L water) on the polymer surfaces were carried out using the sessile drop method with a CAM 100 KSV (KSV, Finland). Recording the drop profile with a CCD camera allowed monitoring the changes in contact angle. All reported data were given as the average of three measurements \pm SD. FTIR spectra were recorded on a Varian 1000 FTIR spectrometer. Electrochemical Impedance Spectroscopy (EIS) was performed with a GAMRY Reference 600 (GAMRY Instruments Inc., Pennsylvania, USA). HPLC (Agilent 1100 Series, Waldbronn, Germany) equipped with a diode array detector (DAD) and a LiChrospher 100 RP-18 (250 mm \times 4.0 mm, 5 μ m) column (Merck, Darmstadt, Germany) was used for the chromatographic analyses of pesticides. SPE was carried out using C18 polar plus cartridges (J.T. Baker, Mallinckrodt Baker Inc., Deventer, Netherlands).

3.3.3. Synthesis of the Monomer

The monomer, SNS-NH₂, was synthesized and characterized according to a previously described method (Figure 3.16) [86,171]. The monomer (SNS-NH₂) which is one of catalog polymers was synthesized in Toppare Research Group.

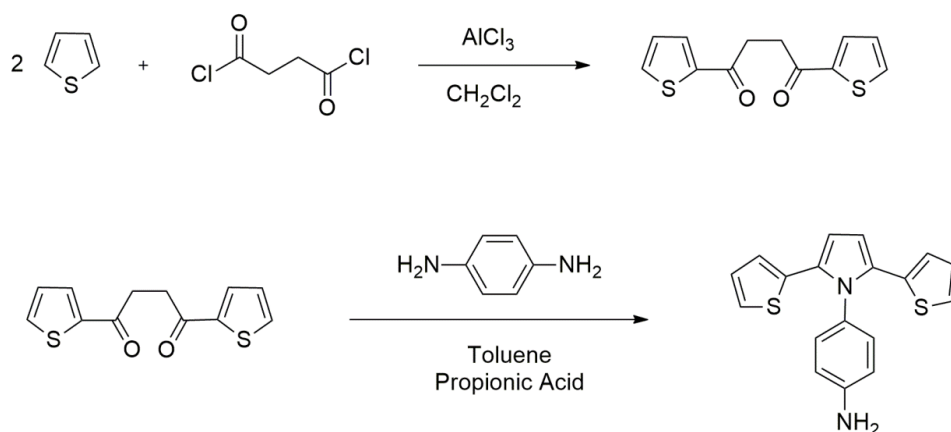


Figure 3.16. Synthetic pathway of SNS-NH₂ [86].

3.3.4. Construction of the AChE Biosensor

Prior to modification, spectroscopic grade graphite rods were polished on an emery paper and washed thoroughly with distilled water. After the cleaning procedure, 1 mg MWCNT was dispersed in 10 mL DMF and ultrasonicated for 15 min to obtain a black suspension. A 10 μ L aliquot of this solution was casted on the graphite electrode, followed by drying at room temperature.

An electrochemical treatment was used to functionalize MWCNT with carboxylic acid groups. For this purpose, the coated electrode was etched in 1.0 M NaOH at 1.5 V for 150 seconds [140]. Carboxylic acid functional groups were formed at the CNT tips during the etching. Then, activated carbon nanotube electrode was rinsed with distilled water. The conducting polymer was synthesized electrochemically. Poly(SNS-NH₂) were coated onto the electrode via 25 cycle voltammogram (CV) in 0.1 M NaClO₄/LiClO₄/ACN electrolyte/solvent system while scanning the potential between -0.5 V and +1.2 V. Polymer coated electrode was rinsed with distilled water to remove possible impurities.

To immobilize the enzyme, 3 μ L AChE solution (dissolved in 50 mM PBS pH 7) (1.5 U) was casted onto the modified graphite electrode with the help of EDC/NHS (0.1 M/0.4M) as the cross linking agents. Then, the enzyme electrode was stored overnight. Before use, the dried electrode was rinsed with phosphate buffer (pH 7.0) to remove loosely bound enzymes from the electrode. The prepared electrode was stored at 4°C when not in use. Figure 3.17 displays the procedure for the construction of the proposed amperometric AChE biosensor.

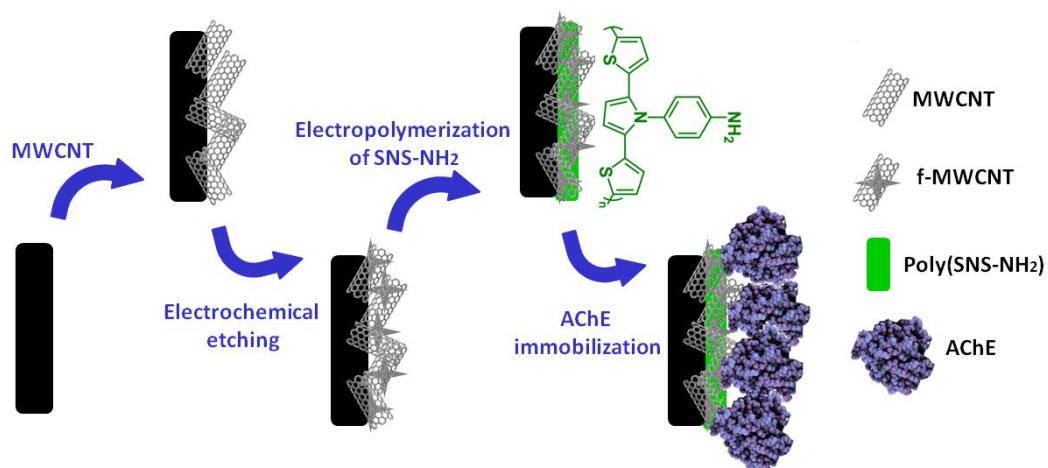


Figure 3.17. Schematic representation of the proposed biosensor.

3.3.5. Electrochemical Measurement

The biosensor was immersed in a cell containing 5 mL 50 mM PBS pH 7 under mild magnetic stirring. A potential of 100 mV vs. Ag reference electrode was applied to the working electrode. After the current reached equilibrium, acetylthiocholine chloride (AThCl) solution was injected into the reaction cell as the substrate. The response of the sensor was measured when the current reached a steady state. The cell and the electrodes were washed with distilled water between the measurements.

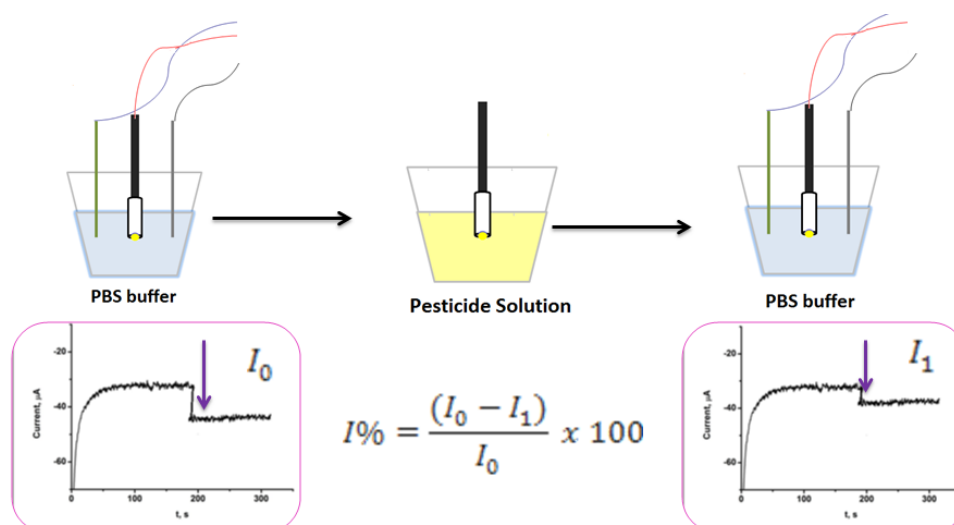


Figure 3.18. Illustration of two step procedure for pesticide detection.

The pesticide detection was carried out with a two-step procedure, illustrated in Figure 3.18. The initial response of the biosensor for AThCl was recorded as I_0 , then, the biosensor was incubated for 5 min in 5 mL of standard solution of pesticides. After the incubation, the biosensor was washed with PBS and distilled water many times. The biosensor was transferred to the cell containing 5 mL PBS pH 7 under mild magnetic stirring and AThCl was injected during the amperometric measurement. The peak current was recorded as I_1 . The inhibition rate of pesticides was calculated as follows (Eq.5) [172]:

$$\%I = \frac{(I_0 - I_1)}{I_0} \times 100 \quad (5)$$

Based on these data calibration curves were plotted for each pesticide. Moreover, tap water samples from Braunschweig, Germany were fortified with the stock solution of each pesticide to obtain different concentrations. The concentrations were determined with the biosensor.

After the biosensor was exposed to pesticides, it was washed with PBS and distilled water and reactivated with 4.0 mM pyridine 2-aldoxime methochloride (2-PAM) for several minutes, then transferred to the electrochemical cell of 5 mL PBS pH 7 under mild magnetic stirring. AThCl was added and the peak current was recorded as I_r . The reactivation efficiency (R%) was estimated as follows (Eq. 6) [172]:

$$\%R = \frac{(I_r - I_1)}{(I_0 - I_1)} \times 100 \quad (6)$$

3.3.6. Evaluation of Biosenor Results with HPLC/DAD

Tap water samples obtained from Braunschweig, Germany fortified with stock solutions of each pesticide in different concentrations were analyzed with the constructed biosensor and also with HPLC/DAD in order to test the applicability of

the biosensor. Mobile phase A was acetonitrile:water (1 : 1 v/v) and mobile B was acetonitrile. Experiments were run with a gradient at a flow rate of 1 mL/min. The injection volume of the samples was 10 μL . The paraoxon and parathion detections were performed at 270 nm. The chlorfenvinphos detection was performed at 245 nm. Fortification of tap water and calibrations of stock solutions of pesticides (1 $\mu\text{g}/\mu\text{L}$) were done in methanol. Calibration standards in methanol for 1.0, 5.0, 10, 25 and 50 $\text{ng } \mu\text{L}^{-1}$ were prepared from the stock solution. 500 mL tap water samples were fortified with stock solutions of each pesticide in a range of 10 – 100 $\mu\text{g}/\text{L}$. Solid-phase extraction (SPE) was used for the enrichment of the pesticides before HPLC/DAD analysis. After conditioning with 5 mL methanol and 10 mL deionized water, tap water samples were loaded. SPE procedure was performed under low pressure at a flow rate of 2-3 mL/min. After running the sample, the flask was rinsed with 5 mL deionized water for three times. Then the cartridges were dried by passing air under low pressure. Then, the pesticides were eluted with 15 mL methanol, respectively. The methanol eluates were concentrated at 40 $^{\circ}\text{C}$ with a rotary evaporator and finally concentrated to 1 mL under nitrogen stream. The concentrated eluates were used for HPLC/DAD analysis.

3.4. CONCLUSION

In this work, a novel acetylcholinesterase biosensor based on a conducting polymer and multi walled carbon nanotubes was developed for amperometric detection of organophosphorous pesticides. The f-MWCNT/poly(SNS-NH₂)/AChE biosensor was demonstrated to be useful for the analysis of organophosphorus pesticides, presenting long term stability, excellent kinetic parameters and high sensitivity. The biosensor exhibited low detection limit in a good linear range with a good operational stability since combination of f-MWCNT and conducting polymer film serves as an excellent immobilization platform, promoting charge transfer between the active site of enzyme and coated polymer electrode. Presence of functional amino groups of the polymer backbone enabled covalent attachment with enzyme molecules forming amide bond. The linkage resulted in effective conjugation and enhanced enzyme stability. HPLC coupled with SPE was also used to analyze the pesticides in tap water samples. The results obtained by the proposed methodology

were quite similar to those obtained by a conventional method. Thus, validity of the proposed biosensing system was proven. The novel acetylthiocholine biosensor working at a low potential (+100 mV) was developed as an alternative method for chromatographic techniques for the detection of paraoxon, parathion and chlorfenvinphos.

The work was supported by the German Federal Ministry of Education and Research (BMBF WTZ project TUR 10-003). Also, this work was described in the following publication [172]:

M. Kesik, F. Ekiz Kanik, J. Turan, M. Kolb, S. Timur, M. Bahadir, L. Toppare,
Sens. Actuat. B-Chem., 2014, 205, 39.

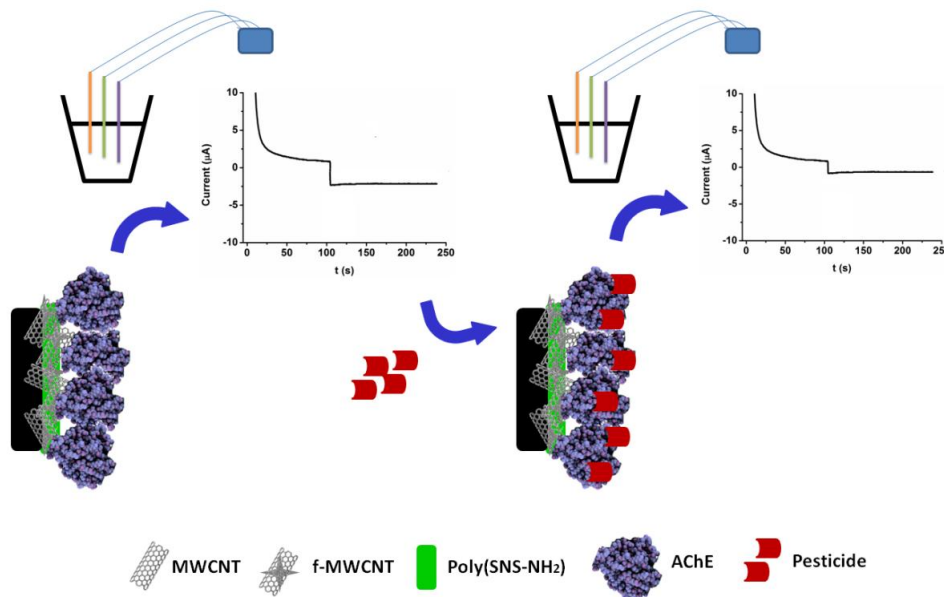


Figure 3.19. An Acetylcholinesterase Biosensor Based On A Conducting Polymer Using Multiwalled Carbon Nanotubes For Amperometric Detection Of Organophosphorous Pesticides

CHAPTER 4

4. MULTI-FUNCTIONAL FLUORESCENT SCAFFOLD AS A MULTICOLOR PROBE: DESIGN AND APPLICATION IN TARGETED CELL IMAGING

4.1. INTRODUCTION

4.1.1. Wide Spread Threat: Cancer

The leading causes of death in today's world is cancer [173]. Although there is an increasing number of developing technologies to understand the molecular basis of the disease, success in fighting cancer has been limited. Modern clinical cancer treatments ask basic questions which should be answered to cure such diseases [174]:

- What is the precise location of tumor?
- How large is it?
- What does the shape of tumor look like?

Detection of cancer at its earliest stages plays a vital role since stage 1 cancers associated with >90% exhibit 5-year survival rate in most cases [175]. Lesions at the premalignant stage can be treated effectively. That is why, development of new molecular imaging techniques is very important.

Moreover, conventional anatomic imaging techniques can detect cancer cell groups when their size is in centimeter or greater in diameter. At this stage, it has already at least 10^9 cells [175]. At this point, molecular imaging plays an important role in these sizes. It allows specific imaging of the target point and specific responses associated early events in carcinogenesis.

Molecular imaging is developed for in-vivo characterizations and measurement of processes at the cellular and molecular level [176]. It is used to monitor spatiotemporal distribution of molecular or cellular processes for several biochemical applications [177]. It is expected to be a next step after anatomic imaging (e.g., X-rays) and functional imaging (e.g., MRI) [178]. Furthermore, radionuclide imaging techniques like positron emission tomography (PET) are widely used for diagnosis purpose. They are known to be highly sensitive and quantitative. They also have ability to scan the whole body at the same time. However, these methods exhibit poor spatial and temporal resolution [179]. Also, the necessity of using radioactive compounds in this type of techniques is the biggest disadvantage. Since the radioactive compounds have intrinsically limited half life and expose the human body to ionizing radiation. Thus, stringent safety rules limit their repeated use [180].

4.1.2. Development of Fluorescent Probes

Great attention has been paid to the design and development of novel optical molecular probes due to their potential applications in the field of biomedicine since fluorescence based strategies are of great interest in understanding cellular and physiological processes and probing biomolecular interactions [181-183].

The use of fluorescent probes has become a promising approach for more efficient diagnosis of wide spread threat; cancer. This type of materials should be highly fluorescent, photostable, available for bioconjugation, have good biocompatibility, maximum spatial resolution, and minimal perturbation to biological systems [184]. In the design of a successful probe for medical imaging purpose, there are several parameters which should be taken into consideration: wavelength, brightness, bio- and photostability. In order to emit light, fluorophores require excitation light. While excitation in the ultraviolet range may cause direct damage on tissues, excitation in the near-infrared range may lead to heating tissues. In probe design, Stokes shift is an important parameter which should be considered. It is defined as asymmetry between excitation and emission wavelength [178].

Secondly, brightness is an important parameter in the design of probe. It is known that the brighter the probe, the more penetration is expected. Thus, the higher quantum yield leads to requiring less excitation light for fluorescence. Generally, brightness increases as the size increases that is the point counting as an obstacle during applications. For example, quantum dots are preferred due to especially their enormous brightness [185]; however, the probe prepared using quantum dots is hard to target due to their large size.

In vivo stability is the another approach taken into consideration. After intracellular internalization, the proposed probe is needed to keep their fluorescence in a certain level. For instance, BODIPY derivatives may lose their fluorescence properties within several days, whereas rhodamine derivatives preserve their fluorescence over a week. Moreover, organic fluorescent probes can be injected repeatedly since organic fluorophore can suffer from photobleaching. This way makes longitudinal observation possible [178].

To date, various organic and inorganic molecules like fluorescent organic dyes, nanomaterials and conjugated polymers were used for cancer cell targeting and imaging purposes [186]. Most of the existing fluorescent materials exhibit superior characteristics yet together with important disadvantages. Thus, several scientists as well as our group have developed new fluorescent materials with improved properties to enhance targeting and imaging ability [187-189]

4.1.3. Bioimaging Based On Synthetic Fluorescent Probes

When one focus on bioimaging using fluorescent probes, three different techniques are observed [190].

(1) A strong fluorescent agent can be internalized into the cells to be imaged. The biggest purpose is to make the cells or tissues fluorescent. They do not have any binding sites to exhibit affinity.

(2) This second technique, known as targeted bioimaging, presents specific domains or species. The proposed probe is functionalized with receptors, ligands, antibodies etc. Such functionalization results in recognizing their specific counterparts serving specific domains to be detected.

(3) The third approach includes sensing ability. The chemical species can be imaged which is not intrinsically fluorescent. Distribution of several chemical species like pH values or oxygen in the living cell can be imaged. This type of species attaches to the molecular probes which affects their binding constants or acts as quenchers.

4.1.4. Materials Used in the Design of Fluorescent Probes

There are numerous studies reported in literature about materials used in the design of the fluorescent probes for the purpose of bioimaging. These materials can be NPs [191], polymers [192], semiconducting organic polymers [193], quantum dots [194], carbon nanoclusters and nanotubes [195], metal particles [196] and metal oxides [197]. In this thesis, the main point is not to cover all materials used in bioimaging purpose so far.

Yagcı et al [189] developed a fluorescent probe combining single walled carbon nano tubes (SWCNT) with a copolymer; (PPP-g-PSt-PCL) which contains poly(para-phenylene) (PPP), polystyrene (PSt) and poly(ϵ -caprolactone) (PCL) side chains. In that study the polymer was non-covalently bound to carboxyl functional SWCNTs. Folic acid conjugation of the probe was achieved for targeted imaging of folate receptor (FR) overexpressing cancer cells. In vitro studies show that this conjugate can specifically bind to HeLa cells.

Liu and coworkers [198] developed anti-HER2-conjugated multifunctional nanoparticles (MFNPs) with a core-shell structure of UCNP@Fe₃O₄@Au using the layer-by layer assembling system. It was presented that these bioconjugated MFNPs can detect breast cancer BT474 cells (HER2+).

Jana et al [199] synthesized europium incorporated ZnO-chemically converted graphene nanocomposites. Fluorescence images of MCF7 cancer cells with the nanocomposite indicate the internalization of the nanomaterials within the cells.

4.1.5. New Designing Strategy

These studies are just few examples in this field. When one focused on the studies of developing fluorescent probes for cancer cell targeting and imaging, we figured out that regardless of the material type, a number of particular drawbacks were observed [36,200]. This has motivated us to search for a totally new strategy for the development of fluorescent probes for effective targeting and imaging. Developing new strategies can have remarkable effect on the effort of the perfect fluorescent marker design. By this way, scientists can focus on specific success of the targeting cell imaging. Accordingly, the newly proposed fluorescence probe behaves as a multifunctional scaffold for the cellular imaging system. Such scaffold would exhibit multicolor properties when combined with a targeting moiety.

The ideal design has to satisfy several requirements;

- (1) It should emit at two different wavelengths in order to achieve multicolor cell images.
- (2) These emission wavelengths should be significantly different to avoid quenching in their fluorescence property.
- (3) The composition can be tuned according to desired functionality.
- (4) The fluorescent probe, for sure, should mimic some of essential properties like photostability and biocompatibility.

Thus, it is possible to detect cellular internalization in live cells precisely without any necessity of overcoming all the drawbacks. In other words, such scaffold system provides self-checking. By this way, scientists can make up their mind in the design of perfect fluorescent markers for targeting cell imaging purpose. However, the major challenge in this type of system is to combine all these requirements in one scaffold. Hence, achieving this goal requires the incorporation

of multiple materials such as an organic fluorophore, a dye or a nanomaterial on the targeted probe which exhibit their own benefits on the same platform.

Wang et al [201] described such a multicolor system which was prepared using a conjugated polymer nanoparticle (CPN) together with four different polymers having different emissions. They used carboxyl functionalized CPNs prepared by a co-precipitation method based on hydrophobic interactions between the conjugated polymers and poly(styrene-co-maleic anhydride) (PSMA). The resulting properties were influenced by changing the choice, amount and ratio of CPN. However, in this design, polymers were in co-precipitated form and their conjugation backbones were present in the same solution. In other words, emission characteristics of the polymers can affect each other since they exist in the same conjugation path length. In the present design such an effect is minimized. The presence of anti-CD44, due to its structural nature, behaves as a non-conjugated spacer. Thus, the target bioconjugate consisting of different structures will exhibit independent emission characteristics in one scaffold.

4.1.6. Scope of the Study

Herein, we report a fluorescent probe which satisfies all the requirements mentioned above in order to examine cell specific binding ability of the bioconjugate. We selected a functional and fluorescent monomer; 3-(1H-phenanthro[9,10-d]imidazol-2-yl)phenol (PIP) and a commercial organic dye (CF555). Biomolecule conjugation was performed with anti-CD44 and specific cellular labeling was determined by fluorescence imaging and flow cytometry experiments.

CD44 is an attractive receptor for tumor targeting [202]. It is a cell surface glycoprotein expressed on many tumor cells. Also, CD44 is a marker for cancer stem cells which are a subpopulation of cancer cells with self-renewing properties [203].

The monomer PIP was synthesized and used as the part of the proposed scaffold. Pendant alcohol groups in the structure of the monomer enable covalent attachment to targeting moiety, anti-CD44. Such modification enhances the biological activity and specificity towards the target [204]. Moreover, it can be excited at 350 nm exhibiting blue fluorescence. Also, CF555 is an antibody labeling kit which labels the antibody. The dye, excited at 555 nm, was covalently linked to the antibody to exhibit red fluorescence. After labeling the anti-CD44 biomolecule, the monomer was linked to the labeled antibody through covalent binding using well-known carbonyldiimidazole (CDI) chemistry [205]. The resulting bioconjugate was used as the fluorescent probe, which can emit at two different wavelengths for targeted imaging of CD44 positive U87-MG cancer cells. Furthermore, the covalent attachment of the monomer PIP to the labeled anti-CD44 preserves its fluorescence character after bioconjugation. Hence targeting of cancer cells was achieved with no significant quenching in fluorescence. The bioconjugate was tested for in vitro studies, and the cellular internalization was monitored in live cells via fluorescence microscope technique. Expression of the CD44 receptor in U87-MG cells and HaCaT control cells was confirmed by flow cytometry. The results present that this strategy enables the bioconjugate to specifically bind U87-MG cells with high efficiency. To our best knowledge, this work represents the first demonstration of this type of fluorescent probe design. The key advances of this system are ability to synthesize the scaffold according to desired functions and use as an efficient fluorescent probe for cell targeting and imaging. Hence, such a probe design can shed new light into the biomedical sensing and diagnosis technologies.

4.2. RESULTS and DISCUSSION

4.2.1. Characterizations of PIP/CF555/anti-CD44 Bioconjugate

Our strategy for design and synthesis of fluorescence probe is to combine different requirements in one scaffold. While the blue fluorescent monomer PIP serves as the strong candidate for covalent attachment to the anti-CD44 using well-known CDI chemistry, CF555 dye has a strong emission in the red region of visible spectrum which can be linked covalently to the protein. The target bioconjugate

was tested for in vitro studies, and the cellular internalization was monitored in CD44 positive U87-MG cancer cells via fluorescence microscope technique. The designed bioconjugate were prepared using PIP and CF555 linked anti-CD44 in different ratios to overcome nonspecific binding of the protein and to get maximum solubility in water. From a synthetic point of view, the strategy describes a new approach for design and synthesis of fluorescent probes. Also, this model scaffold has the ability to further adapt itself in order to acquire different biological and photophysical properties according to desired aims.

Moreover, spectroscopic characterization of the intermediates at each stage and the bioconjugate was evaluated. All fluorescence spectra were obtained for corresponding aqueous solutions. Fluorescence properties of the proposed bioconjugate are representative since the model compound bears the same structure responsible for the photophysical properties. As seen from the fluorescence spectra demonstrated in Figure 4.1, the bioconjugate exhibits two maxima at 386 nm and 613 nm upon excitation at 350 nm and 555 nm. Compare to the fluorescence characteristics of PIP/anti-CD44 and CF555/anti-CD44, the target bioconjugate revealed a change in fluorescence intensity. Yet but no significant shift in emission wavelength was observed. The results mean that structures keep their functions when they join the proposed bioconjugate indicating that anti-CD44 was actually incorporated into the conjugates through the covalent attachment.

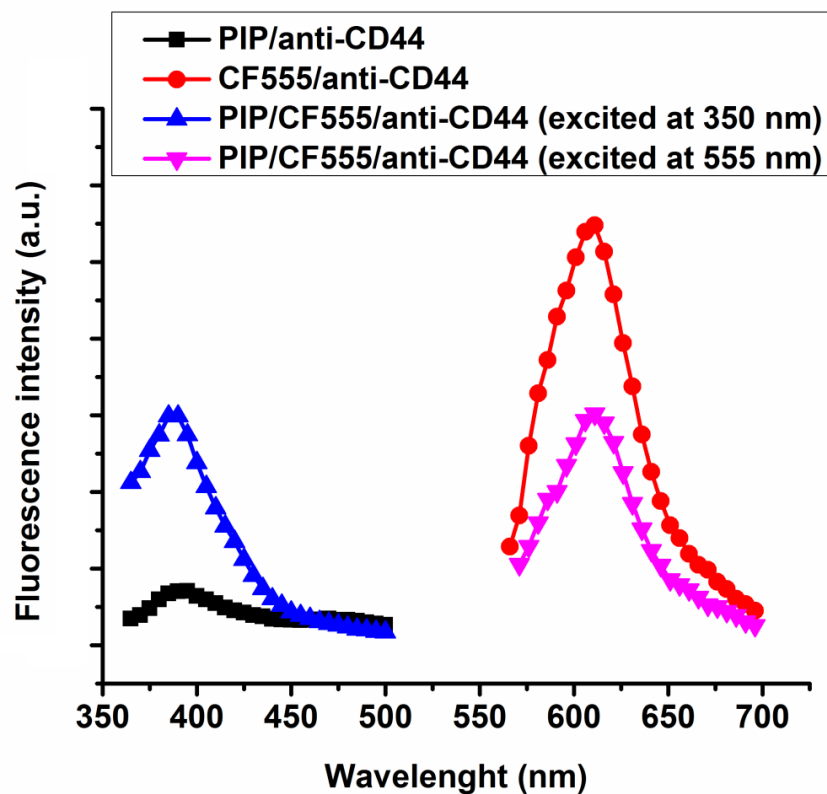


Figure 4.1. Fluorescence spectra of PIP/anti-CD44, CF555/anti-CD44, and PIP/CF555/anti-CD44 conjugates (excited at 350 and 555 nm)

Atomic force microscopy (AFM) is a powerful tool to observe microscopic surface morphology changes after each successive conjugation. Figure 4.2 illustrates 3-D and height images (scan area of 2 μm x 2 μm) of the surface of PIP, PIP/anti-CD44 and PIP/CF555/anti-CD44 in tapping mode, respectively.

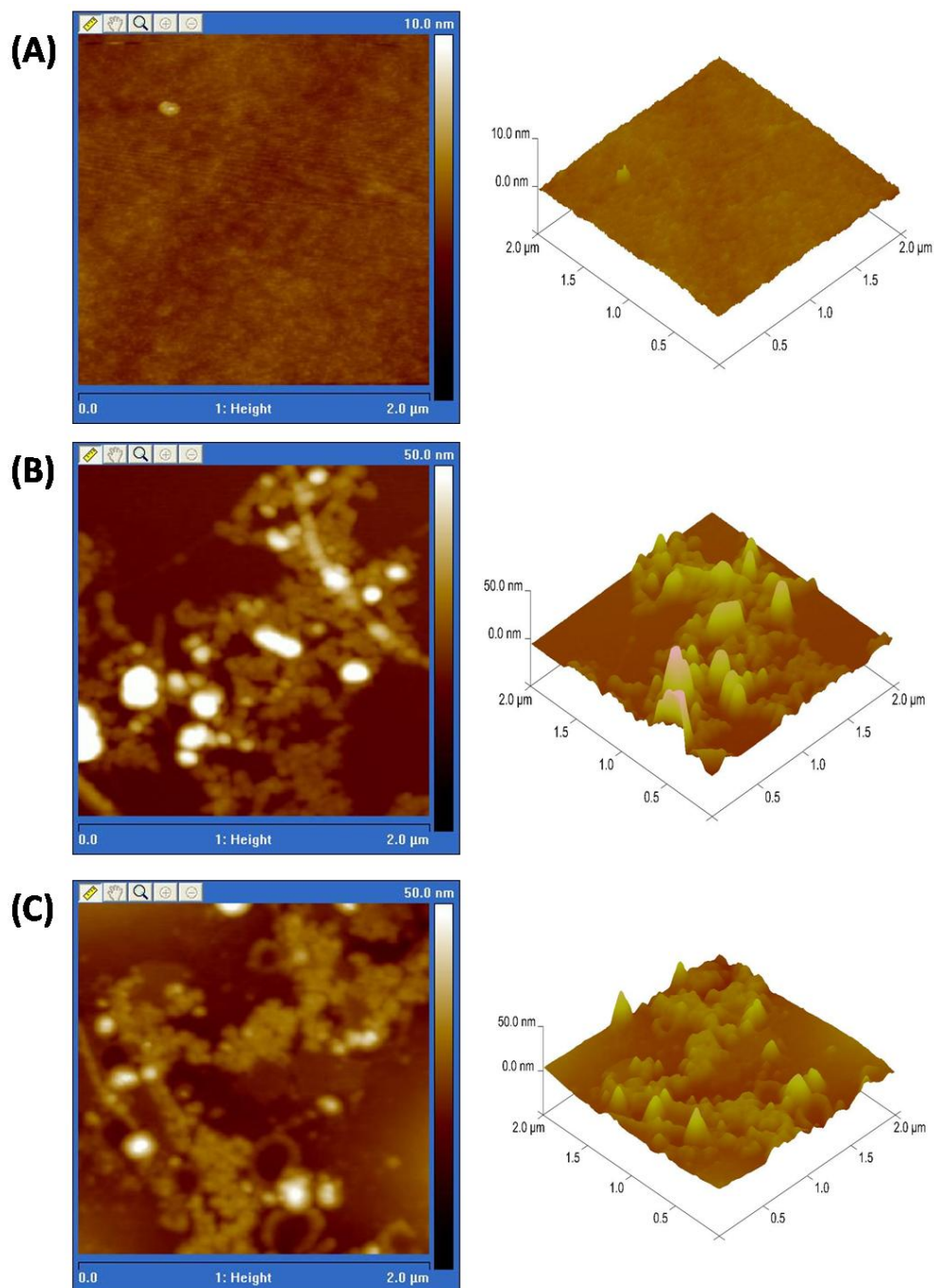


Figure 4.2. AFM images of PIP (A), PIP/anti-CD44 (B), PIP/CF555/anti-CD44 (C).

To observe microscopy images, plasma oxygen-treated silicon wafer were used as the substrate prior to surface imaging. PIP revealed a homogenous and flat surface (Figure 4.2A) whereas conjugation of anti-CD44 leads a characteristic hill-valley structure [206] (Figure 4.2B). The surface undergoes a significant change as a result of bioconjugation process. The dimension was increased by the covalent

incorporation of the protein structure with the monomer on the surface. After the proposed probe (PIP/CF555/anti-CD44) was satisfied there was no notable change in the surface morphology as expected. Since the size of the protein is huge with respect to both PIP and CF555, effect of anti-CD44 was dominant on the surface morphology as seen in Figure 4.2C. The observed change in the dimensions was successfully proven after each stage.

4.2.2. Cytotoxicity

Simple, rapid and sensitive detection of malignant tumors are crucial for the post-treatment of cancer. In this way, many reports and successful diagnosis applications have been demonstrated in the literature [207-209]. One of the tumor detection strategies is developing cell imaging agents with functional structures. Moreover, it is important to illuminate and detect cancer cells with a certain and noninvasive way. In the last decade, fluorescent techniques for targeted imaging strategies have gained attraction via using strong fluorescent materials.

CD44 has been characterized as the most common biomolecule and its overexpression was proven for many cancer types such as colon, breast, pancreatic, head and neck cancers [210-213]. Herein, the synthesized bioconjugate bears necessary functional structures and reveals several properties like multicolor fluorescence. It was firstly applied to a CD44 overexpressed U87-MG cells (which was supported by flow analysis) and CD44 negative HaCaT cell line. To create a noninvasive conjugate, it is important to adjust its dose prior to imaging studies. Figure 4.3A and B demonstrate the effect of PIP monomer, PIP/anti-CD44 and PIP/CF555/anti-CD44 conjugates upon U87-MG and HaCaT keratinocytes in a dose-dependent manner. According to this, the cell survival was decreased to approximately 50 % cell viability after 20 $\mu\text{g/mL}$. As seen in Figures 3A and B, PIP monomer affected the cytotoxicity of cells. In addition, HaCaT cells have shown no viability at the highest concentration of monomer. Since the highest non-toxic dose of monomer and conjugates is 20 $\mu\text{g/mL}$, further studies were carried out with this concentration.

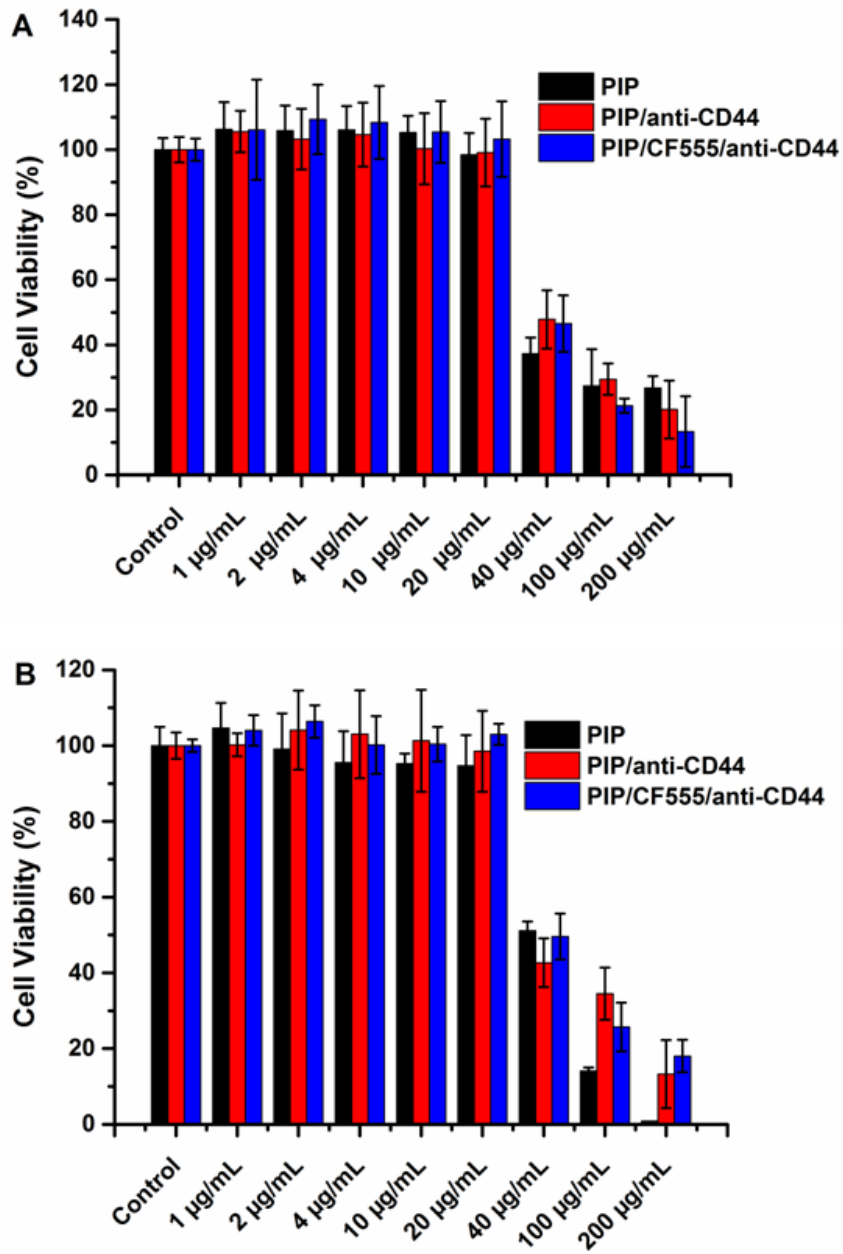


Figure 4.3. The dose-dependent toxicity of PIP, PIP/anti-CD44 and PIP/anti-CD44 for (A) U87-MG and (B) HaCaT cells. Values are the mean \pm standard deviation of the data (n = 4).

4.2.3. Flow Cytometry

CD44 expression levels of the cell lines were assessed via flow cytometry before targeting studies. Negative control staining with secondary antibody produced similar median fluorescence intensity (MFI); 427 and 359 for HaCaT and U87-MG, respectively (Figure 4.4A). On the other hand, more than 3-fold increase were seen for U87-MG MFI values after anti-CD44 antibody staining; 2665 and 8794 for HaCaT and U87-MG, respectively (Figure 4.4B). According to Eq. 8, nMFI was calculated as 3.9, which indicates 4-fold CD44 over expression in U87-MG cells compared to HaCaT cells. These results are in accordance with The Human Protein Atlas [214], where 5-fold CD44 over expression was observed in U87-MG cells. As a consequence, U87-MG was used CD44 positive cell line whereas HaCaT was used as control cell line to verify non-specific cell-surface interactions.

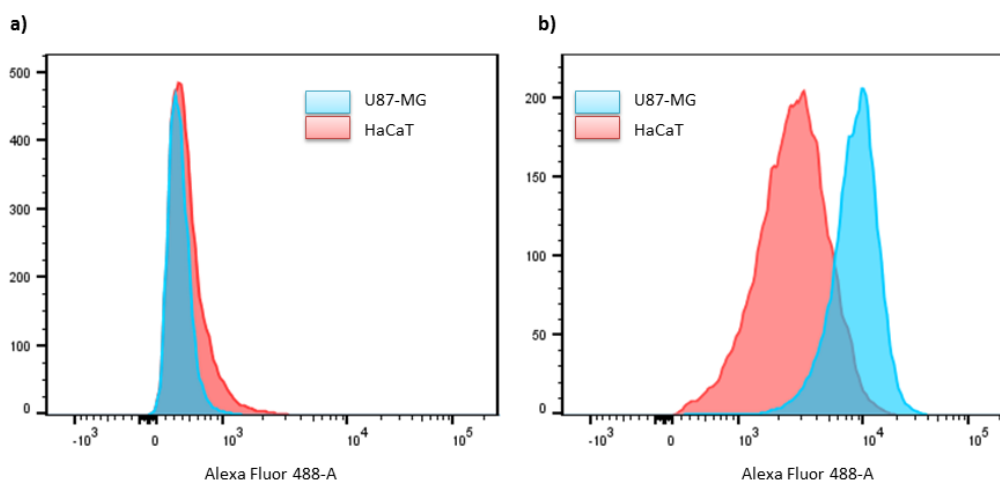


Figure 4.4. CD44 expressions of U87-MG and HaCaT cell lines. Negative control staining showed no non-specific binding of secondary antibody (A); U87-MG showed higher fluorescence than HaCaT after CD44 staining (B).

4.2.4. Photostability

After the successful synthesis of multicolored PIP/CF555/anti-CD44 bioconjugate, both this conjugate and unstained form of conjugate (PIP/anti-CD44) were tested

for the photostability. The resultant bioconjugates were diluted as 1:1 with PBS and subsequently portioned. The fluorescence intensities of both unstained conjugate and CF555 dye stained conjugates were recorded in certain time intervals for 30 days by storing the samples at 4°C and dark. All data were only obtained from the emission of the monomer PIP, since the main structure of both conjugates was PIP which excited at 350 nm. The fluorescent measurements demonstrated that no dramatic fluorescent change was observed for PIP/CF555/anti-CD44 for 20 days. However, the fluorescent intensity of unstained PIP/anti-CD44 conjugate increased by 30%.

4.2.5. Cellular Targeting

Fluorescent probes, which are capable of recognizing cancer-associated bioprobes such as receptor proteins and small nucleic acid residues, have great potential for monitoring cancer therapy. In this manner, water-soluble optical probes have been intensely investigated in order to handle non-invasive structures for the relevant cell line [215].

Herein, a newly synthesized PIP monomer which has high hydrophobicity was conjugated with anti-CD44 which was stained with commercial CF555 dye to monitor the CD44 overexpressed cancerous cell lines. In the general concept for the use of CD44 structure, hyaluronic acid (HA) and/or hyaluronan based targeted drug delivery systems, imaging agents have been improved [216,217]. On the other hand there may be different mechanisms towards the use of HA based targeting strategies since different molecular weight HAs can affect the cell uptake of developed particles in different ways [203,217]. Beside this, the usage of a monoclonal antibody which has greater specificity to CD44 receptors may open a certain investigation in such studies. Thereby, the developed PIP/CF555/anti-CD44 bioconjugate with multi-colored optical properties was applied to U87-MG (CD44 positive) and HaCaT keratinocyte (CD44 negative) cells for 2 h. The obtained images from the fluorescence microscopy enabled the most crucial data for this study. Concomitantly, it can be seen that the images belong to CD44 positive cell line U87-MG (Figure 4.5B, C1 and C2) were brighter than the images of HaCaT

cells. Expectedly, the monomer PIP did not play an effective role alone for both cell lines (Figure 4.5A). Anti-CD44 conjugates seemed to be more internalized into the U87-MG cells compared to HaCaT cells. Furthermore, Figures 4.5C1 and C2 illustrate the fluorescence of the PIP and CF555 dye, respectively. Hence, it can be claimed that both red and blue fluorescence characters of the bioconjugate showed their properties at the same area in the cells. As seen from the fluorescence images, probe treated U87-MG cells which has overexpressed CD44 receptors, are brighter than the control cell line (HaCaT). There may be an interference of background fluorescence from antibody targeted PIP monomer probe which could not internalize to the cells, effectively. However, there are bright spots in nuclei of U87-MG cells (CD44 positive) which originated from CD44 targeted probe with no background fluorescence. To conclude, it can be understood that the developed multi-colored probe could be used successfully as an outstanding imaging agent in diagnosis.

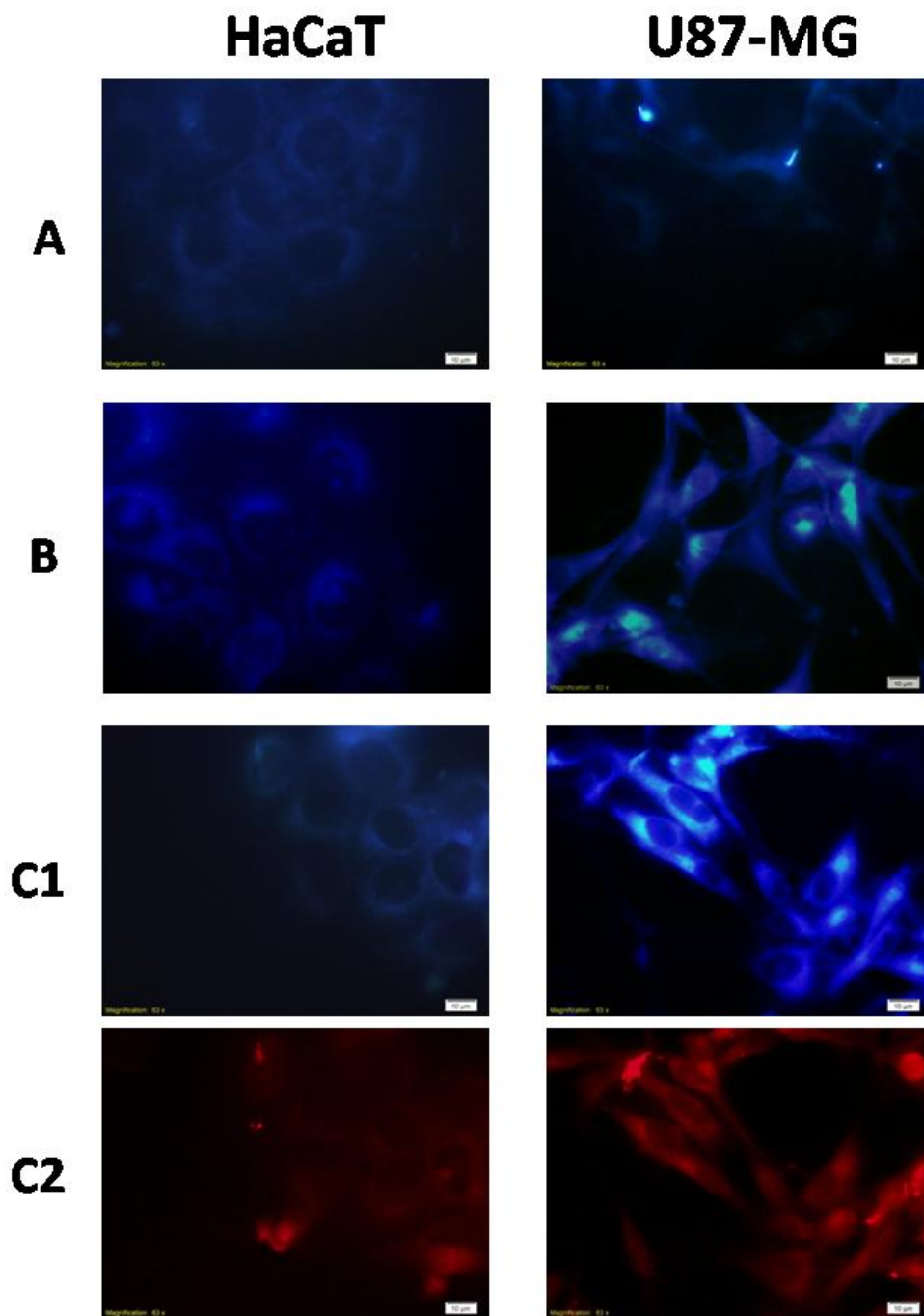


Figure 4.5. Imaging of HaCaT and U87-MG cells via fluorescence microscopy. Images were obtained after treatment of the cell with PIP monomer (A), PIP/anti-CD44 (B) and PIP/CF555/anti-CD44 (C1 and C2) for 2 h at 37°C and 5.0% CO₂ atmosphere, under humidity. Photos of A, B and C1 were taken with UV filter of fluorescence set up. Photos of C2 were taken with red filter of fluorescence set up with 100X magnification. All scale bars are 10 μm.

4.3. EXPERIMENTAL DETAILS

4.3.1. Reagents and Materials

9,10-Phenanthrenequinone, 3-hydroxybenzaldehyde, ammonium acetate (NH_4OAc), Mix-n-Stain CF555 antibody labeling kit and carbonyldiimidazole (CDI) were purchased from Sigma Aldrich (St. Louis, USA; www.sigmaaldrich.com) and acetic acid was purchased from Merck (Darmstadt, Germany; www.merck.com). Anti-CD44 antibody (ab41478) was purchased from Abcam. Reactions were performed under ambient atmospheric conditions. All solvents were analytical grade. Other inorganic and organic materials were commercially available and used as received.

Dulbecco's modified Eagle Medium (DMEM), Eagle's Minimum Essential Medium (EMEM), Fetal bovine serum (FBS), penicillin/streptomycin (P/S) (10000/10000 units) and 200 mM L-glutamine were purchased from Lonza. U87-MG (neuroglioma cells, ATCC) and HaCaT (Human keratinocytes, CLS) cell lines were maintained in EMEM and DMEM, respectively. Both of them supplemented with 10.0% FBS, and 1.0% P/S at 37°C in a humidified incubator with 5.0% CO_2 in air. All cells were subcultured at 80% confluency by trypsinization every two or three days.

4.3.2. Measurements and Characterizations

Atomic force microscopy (AFM) to study modified surfaces were carried out on Veeco Multimode V AS-130 ("J"). The tapping mode was used to take topographic images. Plasma oxygen-treated silicon wafer as the substrate was used for measurements. Samples were prepared via drop-coating.

4.3.3. Synthesis of 3-(1H-phenanthro[9,10-d]imidazol-2-yl)phenol (PIP)

Cirpan et al. [219] performed the synthesis of 3-(1H-phenanthro[9,10-d]imidazol-2-yl) phenol (PIP) (Figure 4.6).

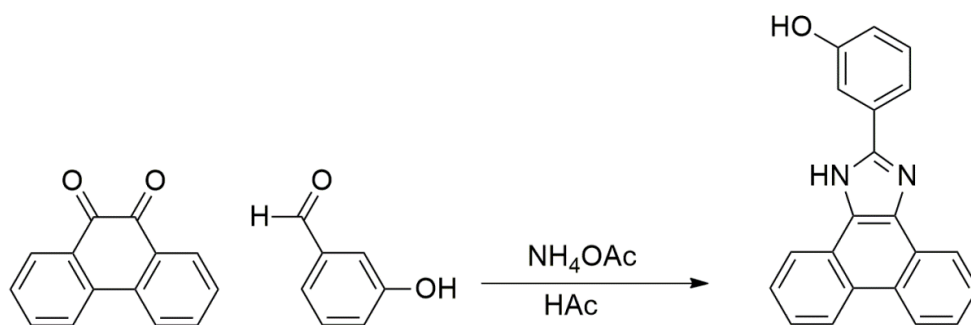


Figure 4.6. Synthesis of 3-(1H-phenanthro[9,10-d]imidazol-2-yl) phenol (PIP) [219].

4.3.4. Synthesis of the Bioconjugate

1.0 mg PIP and 10 mg CDI were dissolved in 200 μL DMSO. The solution was incubated for 2 h at 37°C with 1000 rpm to activate pendant alcohol groups of PIP for further coupling with antibody. The solution was diluted with 400 μL DMSO and 900 μL borate buffer solution (50 mM, pH 8.5). At the same time, CF555 dye was attached covalently to the anti-CD44 antibody via following the protocol. Then, 8.0 μL of labeled antibody solution and 200 μL of activated PIP with CDI solution were mixed in 42 μL borate buffer solution (50 mM, pH 8.5) to obtain target concentration of 20 $\mu\text{g}/\text{mL}$ labeled antibody and 400 $\mu\text{g}/\text{mL}$ activated PIP with CDI solution. It was shaken for 4 h at room temperature with 1000 rpm. Unconjugated biomolecules, excess reagents were separated via centrifugation with distilled water using 10 kDa membrane filters. For the all-cell culture experiments and characterizations, only freshly prepared conjugates were used. Figure 4.7 depicts the construction procedure of the proposed bioconjugate for PIP/CF555/anti-CD44.

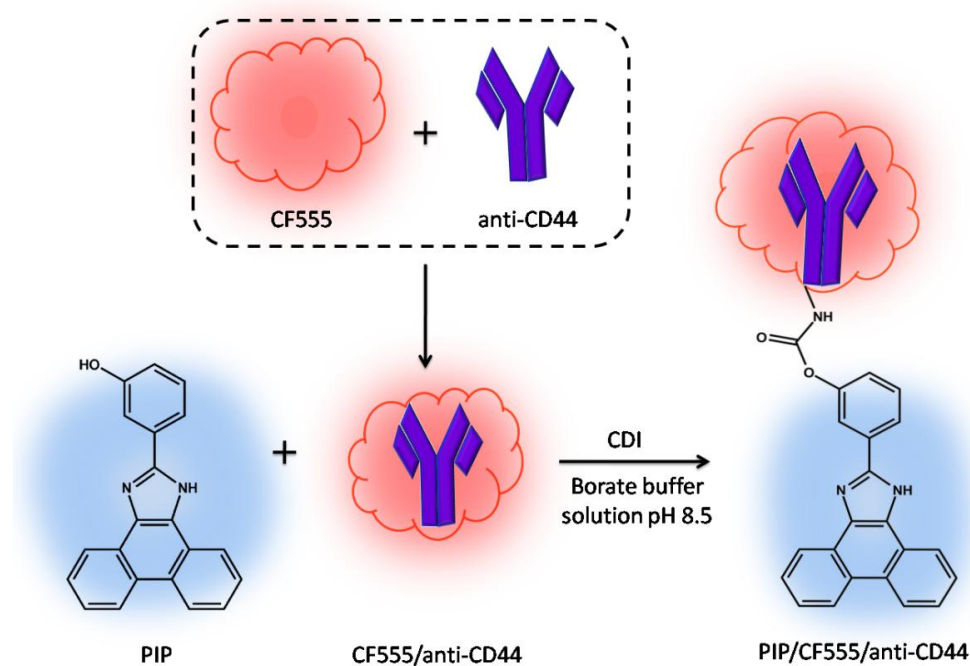


Figure 4.7. Preparation of the bioconjugate for PIP/CF555/anti-CD44.

4.3.5. Cell Viability

A cell proliferation assay kit (MTT reagent) was used to determine the changes in cell viability of cells treated with samples. To perform the MTT assay, both U87-MG cells and HaCaT cells were seeded into 96 well plates and incubated until reaching confluency with normal morphology. The samples of PIP monomer, PIP/anti-CD44 and PIP/CF555/anti-CD44 with concentrations of 1.0, 2.0, 4.0, 10, 20, 40, 100 and 200 $\mu\text{g}/\text{mL}$ were added to wells and then the cell culture plates were placed into CO_2 incubator for incubation at 37°C for 2 h. After incubation the cells were washed to remove culture medium. MTT assay on the cell lines was carried out according to standard procedure [220]. The dose-dependent cytotoxicity of bioconjugates was reported as cell viabilities relative to the control (untreated) cells.

4.3.6. Flow Cytometry Analysis

To compare CD44 expression levels, U87-MG and HaCaT cells were stained with anti-CD44 antibody (Sigma) and anti-rabbit IgG (H+L) Alexa Fluor® 488 (Invitrogen). For cell staining, cells were harvested and washed with cold PBS. Additional washing step was performed with incubation buffer (2.0% FBS in PBS). Pellet was treated with incubation buffer and maintained to obtain 1.0×10^6 cells per assay. After centrifugation, cell pellet was incubated with 2.0 μg anti-CD44 antibody in 500 μL incubation buffer for 1 h at room temperature. Negative control staining was performed without primary antibody (e.g. 500 μL incubation buffer). Unbound antibodies were removed by washing the cells three times in incubation buffer before adding secondary antibody. Samples were incubated with Anti-rabbit IgG (H+L) Alexa Fluor® 488 (1:2000 in incubation buffer) for 45 min at ambient conditions. Unbound antibodies were removed by washing the cells three times with incubation buffer. 10,000 cells were analyzed in BD FACS flow cytometer for Alexa Fluor® 488 signals. Data were plotted as fluorescence intensity/count histograms using FlowJo software (Tree Star, San Carlos, CA). Normalized median fluorescence intensity (nMFI) was calculated from median fluorescence intensity (MFI) values of histograms using the following equation (7):

$$nMFI = \frac{(MFICD44/MFIControl)_{U87MG}}{(MFICD44/MFIControl)_{HaCaT}} \quad (7)$$

4.3.7. Fluorescence Microscopy - Cell Culture Experiments

In order to observe the interactions of the prepared conjugates with both U87-MG and HaCaT cells, 100 μL of samples (20 $\mu\text{g}/\text{mL}$) were introduced into the cells grown in a chamber slide for two days. The cell images were taken via fluorescence microscope (Olympus BX53F) equipped with a CCD camera (Olympus DP72). After treatment for 2 h at 37 °C in CO₂ incubator, the cells were washed twice with PBS. Cell photographs were given separately according to the structure of bioconjugates and excitation fields.

4.4. CONCLUSION

The bioconjugated PIP/CF555/anti-CD44 was successfully used as a novel fluorescent bioprobe for targeted imaging of CD44 positive U87-MG cancer cells. The fluorescent bioprobe was designed according to newly proposed approach based on combination of all requirements in one scaffold. The target bioconjugate exhibit both red and blue fluorescence. Also, the generated scaffold facilitated covalent conjugation of the targeting protein anti-CD44 without affecting their photophysical properties. The proposed conjugate was characterized by fluorescence spectroscopy and atomic force microscopy and then tested for *in vitro* studies. Fluorescence images illustrate the cellular internalization of the target bioconjugate in live cells. Flow cytometry studies showed that U87-MG was used as CD44 positive cell line whereas HaCaT was used as the control cell line. The results present that this strategy to develop such bioconjugate can specifically bind to U87-MG cells with high efficiency. Taking all findings into account, this newly proposed strategy is promising for developing multifunctional probes. Also, such tailor made probes for cellular imaging opens a new viewpoint for further improvement in fluorescence toward *in vitro* and *in vivo* imaging.

This work was described in the following publication [219]:

M. Kesik, B. Demir, F. B. Barlas, C. Geyik, S. C. Cevher, D. Odaci Demirkol, S. Timur, A. Cirpan and L. Toppare, RSC Adv., 2015, 5, 83361.

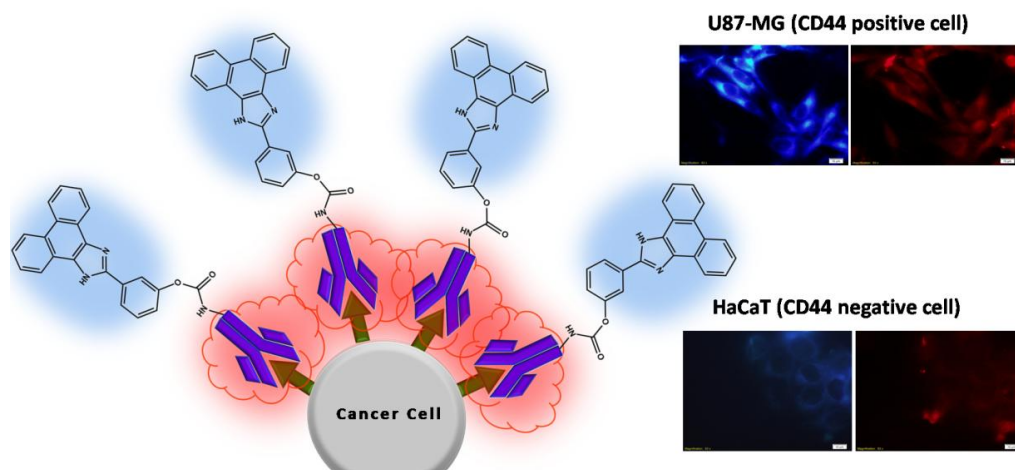


Figure 4.8. A multi-functional fluorescent scaffold as a multicolor probe [219].

REFERENCES

- [1] H. Shirakawa, F. J. Louis, A. G. MacDiarmid, C. K. Chiang, A.J. Heeger, J. Chem. Soc., Chem. Commun., 1977, 578, 578.
- [2] (a) H. Shirakawa, Angew. Chem. Int. Ed., 2001, 40, 2574; (b) A.J. Heeger, Angew. Chem. Int. Ed., 2001,40, 2591; (c) H. Shirakawa, Synth. Met., 2002, 125, 3; (d) A. G. MacDiarmid, Synth.Met., 2002, 125, 11; (e) A. J. Heeger, Synth. Met., 2002, 125, 23.
- [3] H. Letheby, J. Chem. Soc., 1862, 15, 161.
- [4] G. Natta, G. Mazzanti, P. Corradini, Atti Accad. Lincei Cl. Sci. Fis. Mat. Nat. Rend., 1958, 25, 3.
- [5] (a) A. G. MacDiarmid, J. Am. Chem. Soc., 1976, 98, 388; (b) F. B. Burt, Journal of Chemical Society, 1910, 68, 105.
- [6] A. Heeger, A. G. MacDiarmid, H. Shirakawa, The Nobel Prize in Chemistry 2000 - Advanced Information". Nobelprize.org. Nobel Media AB 2013. Web. 12 Jan 2014.
http://www.nobelprize.org/nobel_prizes/chemistry/laureates/2000/advanced.html.
- [7] G. Blasse, B.C. Grabmaier, Luminescent Materials, 1994, Springer-Verlag.
- [8] M. E. G. Lyons, Electroactive Polymer Electrochemistry, 1994, New York, p48.
- [9] A. G. MacDiarmid, A. J. Heeger, Synth. Met., 1979, 1, 101.
- [10] A. G. MacDiarmid, Angew. Chem. Int. Ed., 2001, 40, 2581.
- [11] J. A. Rogers, Z. Bao, V. R. Raju, Appl. Phys. Lett., 72 (1998) 2716
- [12] (a) N. Toshima, O. Ihata, Synth. Met., 1996, 79, 165; (b) Z.C. Sun, Y. H. Geng, J. Li, X. H. Wang, X. B. Jing, F. S. Wang, J. Appl. Polym. Sci., 1999, 72, 1077; (c) K. Yoshino, R. Hayashi, R. Sugimoto, Jpn. J. Appl. Phys., 1984, 23, L899.
- [13] A. Malinauskas, Polymer, 2001, 42, 3957.

- [14] R. H. Baughman, J. L. Bredas, R.R. Chance, R. L. Elsenbaumer, L. W. Shacklette, *Chem. Rev.*, 1982, 82, 209.
- [15] (a) L. Toppare, *Encyclopedia of Engineering Materials Part A, Polymer Science and Technology*, New York: Marcel Dekker, 1988, Vol. 1, Chapter 8; (b) K. Doblhofer, Rajeshwar in *Handbook of Conducting Polymers*, 2nd Edn., ed.; T.A. SSKotheid, R.L.Elsenbaumer, (c) J.R. Reynolds, Marcel Dekker, New York, 1998, 531.
- [16] (a) A. F. Diaz, A. Martinez, K. K. Kanazawa, M. M. Salmon, *J. Electroanal. Chem.*, 1981, 130, 181; (b) J. Roncali, *Chem. Rev.*, 1992, 92, 711.
- [17] (a) U. Bulut, A. Cirpan, *Synth. Met.*, 2005, 148, 68; (b) A. Balan, G. Gunbas, A. Durmus, L. Toppare, *Chem. Mater.*, 2008, 20, 7510; (c) A. Kumar, S. Jang, J. Padilla, T. F. Otero, G. A. Sotzing, *Polymer*, 2008, 49, 3686; (d) H. Li, K. Xie, Y. Pan, H. Wang, H. Wang, *Synth. Met.*, 2012, 162, 22.
- [18] (a) E. J. W. List, L. Holzer, S. Tasch, G. Leising, U. Scherf, K. Mullen, M. Catellani, S. Luzzati, *Solid State Commun.*, 1999, 109, 455, (b) H. Kang, G. Kim, I. Hwang, Y. Kim, K. Cheol Lee, S.H. Park, K. Lee, *Sol. Energ. Mat. Sol. C.*, 2012, 107, 148; (c) F. Xu, W.Q. Zhu, L. Yan, H. Xu, L.H. Xiong, J.H. Li, *Org. Electron.*, 2012, 13, 302; (d) P. Zacharias, M. C. Gather, A. Köhnen, N. Rehmman, K. Meerholz, *Angew. Chem. Int. Ed.*, 2009, 48, 4038.
- [19] (a) F. Li, W.J. Albery, *J. Electroanal. Chem. Interfacial Electrochem.*, 1991, 302, 279. (b) P. Novak, K. Muller, K. Santhanam, O. Haas, *Chem. Rev.*, 1997, 97, 207; (c) A. Guerfi, J. Trottier, I. Boyano, I. De Meatza, J.A. Blazquez, S. Brewer, K.S. Ryder, A. Vijh, K. Zaghbi, *J. Power Sources*, 2014, 248, 1099; (d) K. Gurunathan, D.P. Amalnerkar, D.C. Trivedi, *Mater. Lett.*, 2003, 57, 1642.
- [20] (a) D. S. H. Charrier, T. Vries, S. G. J. Mathijssen, E. J. Geluk, E. C. P. Smits, M. Kemerink, R. A. J. Janssen, *Org. Electron.*, 2009, 10, 994; (b) P. Jha, S.P. Koiry, Vibha Saxena, P. Veerender, Abhay Gusain, A.K. Chauhan, A.K. Debnath, D.K. Aswal, S.K. Gupta, *Org. Electron.*, 2013, 14, 2635; (c) J. Lee, W. Kim, H. Lim, *Microelectron. Eng.*, 2012, 98, 382; (d) F. Garnier, G. Horowitz, X. Peng, D. Fichou, *Adv. Mater.*, 1990, 2, 592.

- [21] (a) C. J. Brabec, N. S. Sariciftci, J. C. Hummelen., *Adv. Funct. Mater.*, 2001, 11, 15, (b) E. Kaya, A. Balan, D. Baran, A. Cirpan, L. Toppare, *Org. Electron.*, 2011, 12, 202. (c) C.O. Too, G.G. Wallace, A.K. Burrell, G.E. Collis, D.L. Officer, E.W. Boge, S.G. Brodie, E.J. Evans, *Synth. Met.*, 2001, 123, 53; (d) J. Wang, Y. Wang, D. He, Z. Liu, H. Wu, H. Wang, P. Zhou, M. Fu, *Sol. Energ. Mat. Sol. C.*, 2012, 96, 58.
- [22] (a) Kıralp S., Toppare L., Yagcı Y., *Int. J. Biol. Macromol.*, 2003, 33, 37; (b) Ö. Türkarlan, A.E. Büyükbayram, L. Toppare, *Synth. Met.*, 2010, 160, 808; (c) A. Mulchandani, N.V. Myung, *Curr. Opin. Biotech.*, 2011, 22, 502; (d) V. Mazeiko, A. Kausaite-Minkstiniene, A. Ramanaviciene, Z. Balevicius, A. Ramanavicius, *Sensor Actuat. B-Chem.*, 2013, 189, 187; (e) S. Soylemez, F. Ekiz Kanik, A.G. Nurioglu, H.Akpınar, L. Toppare, *Sensor Actuat. B-Chem.*, 2013, 182, 322.
- [23] (a) A. Katchalsky, H. Eisenberg, *Nature* 1950, 166, 267; (b) R. Kiefer, S.Y. Chu, P.A. Kilmartin, G.A. Bowmaker, R.P. Cooney, J. Travas-Sejdic, *Electrochim. Acta*, 2007, 52, 2386; (c) Y. A. Ismail, J. G. Martínez, A. S. Al Harrasi, S.J. Kim, Toribio F. Otero, *Sensor Actuat. B-Chem.*, 2011, 160, 1180.
- [24] (a) G. Valdés-Ramírez, J. R. Windmiller, J.C. Claussen, A.G. Martinez, F.Kuralay, M. Zhou, N. Zhou, R. Polsky, P.R. Miller, R. Narayan, J. Wang, *Sensor Actuat. B-Chem.*, 2012, 161, 1018; (b) M. Sharma, G.I.N. Waterhouse, S.W.C. Loader, S. Garg, D. Svirskis, *Int. J. Pharm.*, 2013, 443, 163.
- [25] (a) F. Ozturk Kirbay, R. Ayranci, M. Ak, D. Odaci Demirkol, Suna Timur, *J. Mater. Chem. B*, 2017, 5, 7118; (b) J. Pecher, J. Huber, M. Winterhalder, A. Zumbusch, S. Mecking, *Biomacromolecules*, 2010, 11, 2776.
- [26] (a) T. F. Otero, J. G. Martinez, J. Arias-Pardilla, *Electrochim. Acta*, 2012, 84,112. (b) V. Serafin, L. Agui, P. Yanez-Sedeno, J. M. Pingarron, *J. Electroanal. Chem.*, 2011, 656, 152, (c) Parham, H., Rahbar, N., 2010. *J. Hazard. Mater.*, 177, 1077–1084.
- [27] M.Gerard, A. Chaubey, B.D. Malhotra, *Biosens. Bioelectron.*, 2002, 17, 345.
- [28] S. Cosnier, *Appl. Biochem. Biotech.*, 2000, 89, 127.

- [29] T. Ahuja, I.A. Mir, D. Kumar, Rajesh, *Biomaterials*, 2007, 28, 791.
- [30] J.C. Vidal, E.G. Ruiz, J.R. Castillo, *Microchim. Acta*, 2003, 143, 93.
- [31] (a) K.V. Santhanam, *Pure Appl. Chem.*, 1998, 70, 1259, (b) Y.Xian, Y.Hu, F. Liu, Y. Xian, H. Wang, L. Jin, *Biosens. Bioelectron*, 2006, 21, 1996.
- [32] W. Schuhmann, *Microchim. Acta*, 1995, 21, 1.
- [33] B.D. Malhotra, A. Chaubey, S.P.Singh, *Anal. Chim. Acta*, 2006, 578, 59.
- [34] (a) P. Kumar, R. Meena, R. Paulraj, A. Chanchal, A.K. Verma, H.B. Bohidar, *Colloid. Surface. B*, 2012, 91, 34 ; (b) Y. Gao, X. Zou, J.X. Zhao, Y. Li, X. Su, *Colloid. Surface. B*, 2013, 112, 128; (c) Y. Zhang, A. Haage, E. M. Whitley, I. C. Schneider, A. R. Clapp, *Colloid. Surface B*, 2012, 94, 27.
- [35] G. Liu, M. Swierczewska, G. Niu, X. Zhang, X. Chen, *Mol. BioSyst.*, 2011, 7, 993.
- [36] D. G. Colak, I. Cianga, D. Odaci Demirkol, O. Kozgus, E.I. Medine, S. Sakarya, P. Unak, S.Timur, Yusuf Yagci, *J. Mater. Chem.*, 2012, 22, 9293.
- [37] S.W. Thomas, G.D. Joly, T.M. Swager, *Chem. Rev.* 2007, 107, 1339.
- [38] W.S. May, S.R. Padgett, *Nature Biotechnology*, October 1983, pp 677-683.
- [39] S.W. May, *Enzymatic epoxidation reactions, Enzyme and Microbial Technology*, January 1979, 1(1), pp 15-22.
- [40] M. Sono, M.P. Roach, E.D. Coulter, J.H. Dawson, *Chem. Rev.*, 1996, 96, 2841.
- [41] J.B. van Beilen, W.A. Duetz, A. Schmid, B. Witholt, *Trends Biotechnol.*, 2003, 21, 170.
- [42] W.P. Dijkman, G. de Gonzalo, A. Mattevi, M.W. Fraaije, *Appl. Microbiol. Biotechnol.*, 2013, 97, 5177.
- [43] B Kuswandi, M Ahmad, *OA Alcohol*, 2014, 18, 1.
- [44] A.M. Azevedo, D.M.F. Prazeres, J.M.S. Cabral, L.P. Fonseca, *Biosens. Bioelectron.*, 2005, 21, 235.

- [45] J. Vonck, E.F van Bruggen, *Biochim. Biophys. Acta*, 1990, 1038, 74.
- [46] P. Goswami, S.S.R. Chinnadayala, M. Chakraborty, A.K. Kumar, A. Kakoti, *Appl. Microbiol. Biotechnol.*, 2013, 97, 4259.
- [47] J.R. Woodward, (1990) *Biochemistry and applications of alcohol oxidase from methylotrophic yeasts*. In: Codd GA, Dijkhuizen L, Tabita FR, Hoff DMN (eds) *Advances in autotrophic microbiology and one-carbon metabolism*. Springer, Leeds, pp 205–238.
- [48] (a) S. Suye, *Curr. Microbiol.*, 1997, 34, 374; (b) K. Isobe, A. Kato, J. Ogawa, M. Kataoka, A. Iwasaki, J. Hasegawa, S. Shimizu, *J. Gen. Appl. Microbiol.*, 2007, 53, 177.
- [49] A.K. Kumar, P. Goswami, *Appl. Microbiol. Biotechnol.*, 2006, 72, 906.
- [50] D.V. Banthorpe, E. Cardemil, C. Del, M. Contraras, *Phytochem.*, 1976, 15, 391.
- [51] A. Hernández-Ortega, P. Ferreira, A.T. Martínez, *Appl. Microbiol. Biotechnol.* 2012, 93, 1395.
- [52] P. Ozimek, M. Veenhuis, I. J. van der Klei, *FEMS Yeast Res.*, 2005, 5, 975.
- [53] (a) M.I. Prodromidis, I. Karayannis, *M. Electroanal.*, 2002, 14, 241; (b) X, Luo, J. Xu, J. Wang, H. Chen, *Chem. Commun.*, 2005, 2169–2171; (c) G.G.Guilbault, G.J.Lubrano, *Anal. Chim. Acta.*, 1974, 69, 189.
- [54] L. Wu, M. McIntosh, X. Zhang, H. Ju, *Talanta*, 2007, 74, 387.
- [55] L. Clark, C. Lyons, *Ann. N.Y. (1962). Acad. Sci.* 102. 29
- [56] S. F. Peteu, D. Emerson, R. M. Worden, *Biosens. Bioelectron.*, 1996, 11, 1059
- [57] L. Gorton, A. Lindgren, T. Larsson, F.D. Munteanu, T. Ruzgas, I. Gazaryan, *Anal. Chim. Acta*, 1999, 400, 91.
- [58] J.H.T. Luong, A. Mulchandani, G.G. Guilbault, *Trends Biotechnol.*, 1988, 6, 310.
- [59] S. K. Sharma, N. Sehgal, A.Kumar, *Curr. Appl. Phys.*, 2003, 3, 307.
- [60] A.K. Sarma, P. Vatsyayan, P. Goswami, S. D. Minteer, *Biosens. Bioelectron.*, 2009, 24, 2313.
- [61] L.C. Clark Jr., *Trans. Am. Artif. Intern. Organs*, 1956, 2, 41.

- [62] S.J. Updike, G.P. Hicks, *Nature*, 1967, 214, 986.
- [63] L. D. Mello, L.T. Kubota, *Food Chem.*, 2002, 77, 237.
- [64] A. Chaubey, B.D. Malhotra, *Biosens. Bioelectron.* 2002, 17, 441.
- [65] J. Wang, *Chem. Rev.*, 2008, 108, 814.
- [66] S. Borgmann, G. Hartwich, A. Schulte, W. Schuhmann, *Perspectives in Bioanalysis*, 2005.
- [67] B.D. Malhotra, A. Chaubey, *Sensor Actuat. B-Chem.*, 2003, 91, 117.
- [68] J. Castillo, S. Gáspár, S. Leth, M. Niculescu, A. Mortari, I. Bontidean, V. Soukharev, S.A. Dorneanu, A.D. Ryabov, E. Csöregi, *Sensor Actuat. B-Chem.*, 2004, 102, 179.
- [69] S.R. Chinnadayala, A. Kakoti, M. Santhosh, P. Goswami, *Biosens. Bioelectron.*, 2014, 55, 120.
- [70] (a) B. Brunetti, P. Ugo, L.M. Moretto, C.R. Martin, *J. Electroanal. Chem.*, 2000, 491, 166; (b) J.H.T. Luong, C. Masson, R.S. Brown, K.B. Male, A.L. Nguyen, *Biosens. Bioelectron.*, 1994, 9, 577; (c) C.R. Molina; M. Boujtita, N.E. Murr, *Anal. Chim. Acta*, 1999, 401, 155.
- [71] (a) Y. Xu, H. Kraatz, *Tetrahedron Lett.*, 2001, 42, 2601; M. Karadag, C. Geyik, D. Odaci Demirkol, F. N. Ertas, S. Timur, *Mater. Sci. Eng. C*, 2013, 33, 634.
- [72] J. Qiu, W. Zhou, J. Guo, R. Wang, R. Liang, *Anal. Biochem.*, 2009, 385, 264.
- [73] (a) J. Chen, A. K. Burrell, G. E. Collis, D. L. Officer, G. F. Swiegers, C. O. Too, G. G. Wallace, *Electrochim. Acta*, 2002, 47, 2715; (b) M. Senel, E. Cevik, M. F. Abasıyanık, *Sensor Actuat. B-Chem.*, 2010, 145, 444; (c) N. C. Foulds, R. C. Lowe, *Anal. Chem.*, 1988, 60, 2473.
- [74] (a) Y. Dai, M. Xu, J. Wei, H. Zhang, Y. Chen, *Appl. Surf. Sci.*, 2012, 258, 2850; (b) T. Tsuruta, *Adv. Polym. Sci.*, 1996, 126, 1; (c) J. Jagur-Grodzinski, *React. Funct. Polym.*, 1999, 39, 99; (d) O. Pillai, R. Panchagnula, *Curr. Opin. Chem. Biol.*, 2001, 5, 447.
- [75] (a) K. Ishikawa, T. Endo, *J. Am. Chem. Soc.*, 1988, 110, 2016; (b) M. T. Krejchi, E. D. Atkins, A. J. Waddon, M. J. Fournier, T. L. Mason, D. A. Tirrell, *Science*, 1994, 265, 1427; (c) T. Koga, M. Matsuoka, N. Higashi, *J. Am. Chem. Soc.*, 2005, 127, 17596.

- [76] (a) J. Ling, H. Peng, Z. Shen, *J. Polym. Sci., Part A: Polym. Chem.*, 2012, 50, 3743; (b) R. Obeid, C. Scholz, *Biomacromolecules*, 2011, 12, 3797.
- [77] F. E. Appoh, D. S. Thomas, H. B. Kraatz, *Macromolecules*, 2006, 39, 5629.
- [78] N. C. Kekec, F. Ekiz Kanik, Y. Arslan Udum, C. G. Hizliates, Y. Ergun, L. Toppare, *Sens. Actuat. B-Chem.*, **2014**, 193, 306.
- [79] M. Boujtita, J. P. Hart, R. Pittson, *Biosens. Bioelectron.*, 2000, 15, 257.
- [80] S.A. Wring, J.P. Hart, *Anal. Chim. Acta*, 1990, 231, 203.
- [81] M. Das, P. Goswami, *Bioelectrochem.*, 2013, 89, 19.
- [82] O. Smutok, B. Ngounou, H. Pavlishko, G. Gayda, M. Gonchar, W. Schuhmann, *Sens. Actuat. B-Chem.*, 2006, 113, 590.
- [83] M. Kesik, H. Akbulut, S. Söylemez, Ş.C. Cevher, G. Hızalan, Y. Arslan Udum, T. Endo, S. Yamada, A. Çırpan, Y. Yagci, L. Toppare, *Polym. Chem.*, 2014, 5, 6295.
- [84] L. Guan, Z. Shi, M. Li, Z. Gu, *Carbon*, 2005, 43, 2780.
- [85] M. Rutnakornpituk, N. Puangsin, P. Theamdee, B. Rutnakornpituk, U. Wichai, *Polymer*, 2011, 52, 987.
- [86] E. Yildiz, P. Camurlu, C. Tanyeli, I. Akhmedov, L. Toppare, *J. Electroanal. Chem.*, 2008, 612, 247.
- [87] S. Tuncagil, D. Odaci, E. Yildiz, S. Timur, L. Toppare, *Sens. Actuat. B-Chem.*, 2009, 137, 42.
- [88] (a) F. Lisdat, D. Schäfer, *Anal. Bioanal. Chem.*, 2008, 391, 1555; (b) E. P. Randviir, C. E. Banks, *Anal. Methods*, 2013, 5, 1098.
- [89] L. Lineweaver, D. Burk, *J. Am. Chem. Soc.*, 1934, 56, 658.
- [90] D. Carelli, D. Centonze, A. De Giglio, M. Quinto, P. G. Zambonin, *Anal. Chim. Acta*, 2006, 565, 27.
- [91] H. B. Yildiz, L. Toppare, *Biosens. Bioelectron.*, 2006, 21, 2306.
- [92] S. Soylemez, F. Ekiz Kanik, S. Demirci Uzun, S. O. Hacıoglu, L. Toppare, *J. Mater. Chem. B*, 2014, 2, 511.
- [93] M. M. Barsan, C. M. A. Brett, *Talanta*, 2008, 74, 1505.
- [94] I. S. Alpeeva, A. Vilkanaukyte, B. Ngounou, E. Csoregi, I. Yu. Sakharov, M. Gonchar, W. Schuhmann, *Microchim. Acta*, 2005, 152, 21.

- [95] F. W. Janssen, H. W. Ruelius, *Biochim. Biophys. Acta*, 1968, 151, 330.
- [96] A. R. Vijayakumar, E. Csöregi, A. Heller, L. Gorton, *Anal. Chim. Acta*, 1996, 327, 223.
- [97] M. Kesik, O. Kocer, F. Ekiz Kanik, N. Akbasoglu Unlu, E. Rende, E. Aslan-Gurel, R. M. Rossi, Y. Arslan Udum, L. Toppare, *Electroanalysis*, 2013, 25, 1995.
- [98] B. A. DaSilveira Neto, A. Santana Lopes, G. Ebeling, R. S. Gonçalves, V. E. U. Costa, F. H. Quina, J. Dupont, *Tetrahedron*, 2005, 61, 10975.
- [99] Y. Tsubata, T. Suzuki, T. Miyashi, Y. Yamashita, *J. Org. Chem.*, 1992, 57, 6749.
- [100] X. Guo, D. M. Watson, *Org. Lett.*, 2008, 10, 533.
- [101] H. Akpınar, A. Balan, D. Baran, E. K. Ünver, L. Toppare, *Polymer*, 2010, 51, 6123.
- [102] H. Ju, V.B. Kandimalla, *Biosensors for pesticides, Electrochemical Sensors, Biosensors and Their Biomedical Applications*, 2008 by Academic Press, Inc., pp 31-36.
- [103] M. Aránzazu Goicolea, Alberto Gómez-Caballero and Ramón J. Barrio, *New Materials in Electrochemical Sensors for Pesticides Monitoring, Pesticides - Strategies for Pesticides Analysis*, University of the Basque Country (UPV/EHU), Spain, pp 333.
- [104] D. Di Tuoro, M. Portaccio, M. Lepore, F. Arduini, D. Moscone, U. Bencivenga, D.G. Mita, *New Biotechnology*, 2011, 29, 132.
- [105] H. Kidd, D. Hartley, *UK pesticides for farmers and growers*, in *The Royal Society of Chemistry, Nottingham* (1987).
- [106] (a) A.P. Periasamy, Y. Umasankar, S.-M. Chen, *Sensors*, 2009, 9, 4034; (b) T. Elersek, M. Filipic, in: M. Stoytcheva (Ed.), *Organophosphorous Pesticides –Mechanisms of Their Toxicity, Pesticides – The Impacts of Pesticides Exposure*, 2011, ISBN: 978-953-307-531-0; R. Fukuta, *Environ. Health Perspect.* 87 (1990) 245–254; NCBI, National Center for Biotechnology Information, Donepezil, Pubmed, U.S. National Library of Medicine, Rockville Pike, Bethesda, MD, USA, 2014,

<http://www.ncbi.nlm.nih.gov/pccompound?term=pesticide> (accessed June 2014).

- [107] T.R. Fukuto, *Environ. Health Perspect.*, 1990, 87, 245.
- [108] T.S. Ribeiro, A. Prates, S.R. Alves, J.J. Oliveira-Silva, C.A.S. Riehl, J.D.Figueroa-Villar, *J. Braz. Chem. Soc.*, 2012, 23, 1216.
- [109] H. Schulze, S. Vorlova, F. Villatte, T.T. Bachmann, R.D. Schmid, *Biosens. Bioelectron.*, 2003, 18, 201.
- [110] (a) S. Chapalamadugu, G.R. Chaudhry, *Crit. Rev. Biotechnol.*, 1992, 12, 357; (b) T.S.S. Dikshith, *Pesticides*, in: T.S.S. Dikshith (Ed.), *Toxicology of Pesticides in Animals*, CRC Press, Boston, 1991, pp. 1–39.
- [111] A. Cagnini, I. Palchetti, I. Lioni, M. Mascini, A.P.F. Turner, *Sens. Actuat. B-Chem.*, 1995, 24–25, 85.
- [112] R. Solna, S. Sapelnikova, P. Skladal, M. Winther-Nielsen, C. Carlsson, J. Emmenus, T. Ruzgas, *Talanta*, 2005, 65, 349.
- [113] H.Z. Wu, Y.C. Lee, T.K. Lin, H.C. Shih, F.L. Chang, H.P.P. Lin, *J. Taiwan Inst. Chem. Eng.*, 2009, 40, 113.
- [114] A. Chatonnet, O. Lockridge, *Biochem. J.*, 1989, 260, 625.
- [115] M. Pohanka, *Anal. Lett.*, 2013, 46, 1849.
- [116] N.A. Hosea, H.A. Berman, P. Taylor, *Biochemistry*, 1995, 34, 11528.
- [117] M. Ahmed, J. B. Rocha, M. Correa, C. M. Mazzanti, R. F. Zanin, A. L. Morsch, V. M. Morsch, M. R. Schetinger. *Chem. Biol. Interact.*, 2006, 162, 165.
- [118] S. Andreescu, Jean-Louis Marty, *Biomolecular Engineering*, 2006, 23 1.
- [119] M. Pohanka, *Biomed. Pap. Med. Fac. Univ. Palacky Olomouc Czech Repub.*, 2011, 155, 219.
- [120] T. Montensinos, S.P. Mungnia, F. Valdez, J.L. Marty, *Anal. Chim. Acta*, 2001, 431, 231.
- [121] I. Palchetti, A. Cagnini, M.D. Carlo, C. Coppi, M. Mascini, A.P.T. Turner, *Anal. Chim. Acta*, 1997, 337, 315.
- [122] Y. Zhao, W. Zhang, Y. Lin, D. Du, *Nanoscale*, 2013, 5, 1121.
- [123] R. Solna, E. Dock, A. Christenson, M. Winther-Nielsen, C. Carlsson, J. Emneus, T. Ruzgas, P. Skladal, *Anal. Chim. Acta*, 2005, 528, 9.

- [124] A. Curruli, S. Drugulescu, C. Cremisini, G. Palleschi, *Electroanalysis*, 2001, 13, 236.
- [125] O.R. Zaborsky, *Immobilized Enzymes*, 1973, CRC Press, Cleveland.
- [126] Ö. Yılmaz, D.Odacı Demirkol, S. Gülcemal, A. Kılınç, S. Timur, B. Çetinkaya, *Colloid Surface B.*, 2012, 100, 62.
- [127] E. Başkurt, F. Ekiz, D. Odacı Demirkol, S. Timur, L. Toppare, *Colloid Surface B.*, 2012, 97, 13.
- [128] S. Cosnier, M. Holzinger., *Chem. Soc. Rev.*, 2011, 40, 2146.
- [129] W.H. Scouten, J.H.T. Luong, R.S. Brown, *Trends in Biotechnology*, 1995, 13, 178.
- [130] M. Aizawa, S. Yabuki. In: *Proceedings of the 51st annual meeting Japan chemical society*. 1985, p. 6.
- [131] R.E. Gyurcsanyi, Z. Vagföldi, G. Nagy, *Electroanalysis*, 1999, 11, 712.
- [132] R. Xue, T.-F. Kang, L.-P. Lu, S.-Y. Cheng, *Appl. Surf. Sci.*, 2012, 258, 6040.
- [133] C. Gao, Z. Guo, J.-H. Liu, X.-J. Huang, *Nanoscale*, 2012, 4, 1948.
- [134] J. Wang, R.P. Deo, P. Poulin, M. Mangey, *J. Am. Chem. Soc.*, 2003, 125, 14706.
- [135] J. Wang, *Electroanalysis*, 2005, 17, 7.
- [136] Y. Yan, M. Zhang, K. Gong, L. Su, Z. Guo, L. Mao, *Chem. Mater.*, 2005, 17, 3457.
- [137] (a) M.A. Hamon, H. Hu, P. Bhowmik, S. Niyogi, B. Zhao, M.E. Itkis, R.C. Haddon, *Chem. Phys. Lett.*, 2001, 347, 8; (b) D.B. Mawhinney, V. Naumenko, A. Kuznetsova, J.T. Yates, J. Liu, R.E. Smalley, *Chem. Phys. Lett.* 2000, 324, 213; (c) J. Chen, M.A. Hamon, H. Hu, Y. Chen, A.M. Rao, P.C. Eklund, R.C. Haddon, *Science*, 1998, 282, 95; (d) M.A. Hamon, J. Chen, H. Hu, Y. Chen, M.E. Itkis, A.M. Rao, P.C. Eklund, R.C. Haddon, *Adv. Mater.*, 1999, 11, 834; (e) M. Monthieux, B.W. Smith, B. Bouteaux, A. Claye, J.E. Fischer, D.E. Luzzi, *Carbon*, 2001, 39, 1251.
- [138] J. Chen, A.M. Rao, S. Lyuksyutov, M.E. Itkis, M.A. Hamon, H. Hu, R.W. Cohn, P.C. Eklund, D.T. Colbert, R.E. Smalley, R.C. Haddon, *J. Phys. Chem. B*, 2001, 105, 2525.

- [139] B. F. Lu, G. Lingrong, J. M. Mohammed, W. Xin, G. L. Pengju, M. V. Lucia, C. Li, P. S. Ya, *J. Mater. Chem. B*, 2009, 21, 139.
- [140] (a) R.L. McCreery, in: A.J. Bard (Ed.), *Electroanalytical Chemistry*, Marcel Dekker, New York, 1991, pp. 221–374 (Chapter 17); (b) J. Li, H.T. Ng, A. Cassell, W. Fan, H. Chen, Q. Ye, J. Koehne, J. Han, M. Meyyappan, *Nano Lett.*, 2003, 3, 597; (c) G. Liu, Y. Lin, Y. Tu, Z. Ren, *Analyst*, 2005, 130, 1098.
- [141] A.L. Goff, M. Holzinger, S. Cosnier, *Analyst*, 2011, 136, 1279.
- [142] D. Du, J. Ding, J. Cai, A. Zhang, *J. Electroanal. Chem.*, 2007, 605, 53.
- [143] H. Yin, S. Ai, J. Xu, W. Shi, L. Zhu, *J. Electroanal. Chem.*, 2009, 637, 21.
- [144] T. Liu, H. Su, X. Qu, P. Ju, L. Cui, S. Ai, *Sens. Actuat. B-Chem.*, 2011, 160, 1255.
- [145] X. Sun, X. Wang, *Biosens. Bioelectron.*, 2010, 25, 2611.
- [146] F. Arduini, F. Ricci, C.S. Tuta, D. Moscone, A. Amine, G. Palleschi, *Anal. Chim. Acta*, 2006, 580, 155.
- [147] B. Bucur, D. Fournier, A. Danet, J.-L. Marty, *Anal. Chim. Acta*, 2006, 562, 115.
- [148] Y.-G. Li, Y.-X. Zhou, J.-L. Feng, Z.-H. Jiang, L.-R. Ma, *Anal. Chim. Acta*, 1999, 382, 277.
- [149] H. Schulze, E. Scherbaum, M. Anastassiades, S. Vorlová, R.D. Schmid, T.T. Bachmann, *Biosens. Bioelectron.*, 2002, 17, 1095.
- [150] G. Valdés-Ramírez, D. Fournier, M.T. Ramírez-Silva, J.-L. Marty, *Talanta*, 2008, 74, 741.
- [151] I.C. Hartley, J.P. Hart, *Anal. Proc.*, 1994, 31, 333.
- [152] F. Arduini, A. Amine, D. Moscone, G. Palleschi, *Mikrochim. Acta*, 2010, 170, 193.
- [153] L. Wu, X. Zhang, H. Ju, *Anal. Chem.*, 2007, 79, 453.
- [154] T. Ramanathan, F.T. Fisher, R.S. Fisher, R.S. Ruoff, L.C. Brinson, *Chem. Mater.*, 2005, 17, 1290.
- [155] F. Ekiz, F. Oguzkaya, M. Akin, S. Timur, C. Tanyeli, L. Toppare, *J. Mater. Chem.*, 2011, 21, 12337.

- [156] F.E. Kanik, M. Kolb, S. Timur, M. Bahadir, L. Toppare, *Int. J. Biol. Macromol.*, 2013, 59, 111.
- [157] (a) T. Nakajima, M. Koh, *Carbon*, 1997, 35, 203; (b) E. Pamula, P.G. Rouxhet, *Carbon*, 2003, 41, 1905; (c) N. Li, X. Wei, Z. Mei, X. Xiong, S. Chen, M. Ye, S. Ding, *Carbohydr. Res.*, 2011, 346, 1721; (d) S. Hubert, M.C. Pham, L.H. Dao, B. Piro, Q.A. Nguyen, M. Hedayatullah, *Synth. Met.*, 2002, 128, 67.
- [158] (a) M. Lin, M.S. Cho, W.S. Choe, Y. Lee, *Biosens. Bioelectron.*, 2009, 25, 28; (b) E. Chow, E.L.S. Wong, T. Bocking, Q.T. Nguyen, D.B. Hibbert, J.J. Gooding, *Sens. Actuators B: Chem.*, 2005, 111–112, 540.
- [159] A.J. Bard, L.R.L.R. Faulker, *Electrochemical Methods: Fundamentals and Applications*, John Wiley, New York, 2000.
- [160] A. Vakurov, C.E. Simpson, C.L. Daly, T.D. Gibson, P.A. Millner, *Biosens. Bioelectron.*, 2004, 20, 1118.
- [161] Y. Wei, Y. Li, Y. Qu, F. Xiao, G. Shi, L. Jin, *Anal. Chim. Acta*, 2009, 643, 13.
- [162] F.N. Kok, F. Bozoglu, V. Hasirci, *Biosens. Bioelectron.*, 2002, 17, 531.
- [163] D. Du, S. Chen, J. Cai, A. Zhang, *Biosens. Bioelectron.*, 2007, 23, 130.
- [164] N. Jha, S. Ramaprabhu, *Nanoscale*, 2010, 2, 806.
- [165] M. Pohanka, D. Jun, K. Kuca, *Sensors*, 2008, 8, 5303.
- [166] V.A. Pedrosa, J. Caetona, A.S. Sergio, S.A.S. Machado, R.S. Freire, M. Bertotti, *Electroanalysis*, 2007, 19, 1415.
- [167] G. Istamboulie, S. Andreescu, J.-L. Marty, T. Noguier, *Biosens. Bioelectron.*, 2007, 23, 506.
- [168] K.C. Gulla, M.D. Gouda, M.S. Thakur, N.G. Karanth, *Biochim. Biophys. Acta*, 2002, 1597, 133.
- [169] M. Bernabei, S. Chiavarini, C. Cremisini, G. Palleschi, *Biosens. Bioelectron.*, 1993, 8, 265.
- [170] G. Palleschi, M. Bernabei, C. Cremisini, M. Mascini, *Sens. Actuators B: Chem.*, 1992, 7, 513.
- [171] M. Kesik, F. Ekiz Kanik, J. Turan, M. Kolb, S. Timur, M. Bahadir, L. Toppare, *Sens. Actuators B: Chem.*, 2014, 205, 39.

- [172] J.M. Nugent, D. Du, X. Huang, J. Cai, A. Zhang, *Biosens. Bioelectron.*, 2007, 23, 285.
- [173] American Cancer Society. *Cancer Facts and Figures*; American Cancer Society: Atlanta, Georgia, 2010
- [174] R. Weissleder, *Science*, 2006, 312 1168.
- [175] R. Etzioni, N. Urban, S. Ramsey, M. McIntosh, S. Schwartz, B. Reid, J. Radich, G. Anderson, L. Hartwell, *Nat. Rev. Cancer*, 2003, 3, 243.
- [176] R. Weissleder, U. Mahmood, *Radiology*, 2001, 219, 316.
- [177] M. Thakur, B.C. Lentle, *Radiology*, 2005, 236, 753.
- [178] H. Kobayashi, M. Ogawa, R. Alford, P.L. Choyke, Y. Urano, *Chem. Rev.*, 2010, 110, 2620.
- [179] T. Schaeffter, *Prog. Drug Res.*, 2005, 62, 15.
- [180] C.A. Boswell, M.W. Brechbiel, *Nucl. Med. Biol.*, 2007, 34, 757.
- [181] Y. Tsai, C. Hu, C. Chu, T. Imae, *Biomacromolecules*, 2011, 12, 4283.
- [182] J. Yao, M. Yang, Y. Duan, *Chem. Rev.*, 2014, 114, 6130.
- [183] S. Yu, R. Dong, J. Chen, F. Chen, W. Jiang, Y. Zhou, X. Zhu, D. Yan, *Biomacromolecules*, 2014, 15, 1828.
- [184] A. Duarte, K. Y. Pu, B. Liu, G. C. Bazan, *Chem. Mater.*, 2011, 23, 501.
- [185] X. Michalet, F.F. Pinaud, L.A. Bentolila, J.M. Tsay, S. Doose, J.J. Li, G. Sundaresan, A.M. Wu, S.S. Gambhir, S. Weiss, *Science*, 2005, 307, 538.
- [186] S. Md. Sharker, S. M. Kim, S. H. Kim, I. In, H. Lee, S. Y. Park, *J. Mater. Chem. B*, 2015, 3, 5833.
- [187] G. Unak, F. Ozkaya, E. I. Medine, O. Kozgus, S. Sakarya, R. Bekis, P. Unak, S. Timur, *Colloids Surf., B*, 2012, 90, 217.
- [188] R. Bongartz, D. Ag, M. Selecı, J. Walter, E. E. Yalcinkaya, D. O. Demirkol, F. Stahl, S. Timur, T. Scheper, *J. Mater. Chem. B*, 2013, 1, 522.
- [189] D. Ag, M. Selecı, R. Bongartz, M. Can, S. Yurteri, I. Cianga, F. Stahl, S. Timur, T. Scheper, Y. Yagci, *Biomacromolecules*, 2013, 14, 3532.
- [190] O.S. Wolfbeis, *Chem Soc Rev.*, 2015, 44, 4743.
- [191] M. Peters, N. Zaquen, L. D'Olieslaeger, H. Bove, D. Vanderzande, N. Hellings, T. Junkers, A. Ethirajan, *Biomacromolecules*, 2016, 17, 2562.

- [192] S. Biswas, X. Wang, A. R. Morales, H. Ahn, K. D. Belfield, *Biomacromolecules*, 2011, 12, 441.
- [193] W. Cao, J. Zhou, Y. Wang, L. Zhu, *Biomacromolecules* 2010, 11, 3680.
- [194] B. C. Lagerholm, M. Wang, L. A. Ernst, D. H. Ly, H. Liu, M. I. P. Bruchez, A. S. Waggoner, *Nano Lett.*, 2004, 4, 2019.
- [195] E. L. Bakota, L. Aulisa, D. A. Tsyboulski, R. B. Weisman, J. D. Hartgerink, *Biomacromolecules* 2009, 10, 2201.
- [196] G. Yilmaz, B. Demir, S. Timur, C. R. Becer, *Biomacromolecules*, 2016, 17, 2901.
- [197] A. S. Wadajkar, T. Kadapure, Y. Zhang, W. Cui, K. T. Nguyen, J. Yang, *Adv Healthc Mater.*, 2012, 1, 450.
- [198] J. Shen, K. Li, L. Cheng, Z. Liu, S. Lee, J. Liu, *ACS Appl. Mater. Interfaces*, 2014, 6, 6443.
- [199] S. Bera, M. Ghosh, M. Pal, N. Das, S. Saha, S. K. Dutta, S. Jana, *RSC Adv.*, 2014, 4, 37479.
- [200] E. I. Medine, D. Odaci, B. N. Gacal, S. Sakarya, P. Unak, S. Timur, Y. Yagci, *Macromol. Biosci.*, 2010, 10, 657.
- [201] L. Feng, L. Liu, F. Lv, G. C. Bazan, S. Wang, *Adv. Mater.*, 2014, 26, 3926.
- [202] M. Zöller, *Nat. Rev. Cancer*, 2011, 11, 254.
- [203] M. H. El-Dakdouki, D. C. Zhu, K. El-Boubbou, M. Kamat, J. Chen, W. Li, X. Huang, *Biomacromolecules*, 2012, 13, 1144.
- [204] M. Akin, R. Bongartz, J. G. Walter, D. O. Demirkol, F. Stahl, S. Timur, T. Scheper, *J. Mater. Chem.*, 2012, 22, 11529.
- [205] G. T. Hermanson, *Bioconjugate Techniques*, Elsevier Academic Press, San Diego, CA, 2nd edn, 2004, p. 196.
- [206] H. S. Seo, Y. M. Ko, J. W. Shim, Y. K. Lim, J. Kook, D. Cho, B. H. Kim, *Appl. Surf. Sci.*, 2010, 257, 596.
- [207] M. Yuksel, D. G. Colak, M. Akin, I. Cianga, M. Kukut, E. I. Medine, M. Can, S. Sakarya, P. Unak, S. Timur, Y. Yagci, *Biomacromolecules*, 2012, 13, 2680.
- [208] F. Ekiz Kanik, D. Ag, M. Selecici, M. Kesik, H. Akpınar, G. Hizalan, F. B. Barlas, S. Timur, L. Toppare, *Biotechnol. Prog.*, 2014, 30, 952.

- [209] M. Liu, J. Ji, X. Zhang, X. Zhang, B. Yang, F. Deng, Z. Li, K. Wang, Y. Yang, Y. Wei, *J. Mater. Chem. B*, 2015, 3, 3476.
- [210] M. Al-Hajj, M. S. Wicha, A. Benito-Hernandez, S. J. Morrison, M. F. Clarke, *Proc. Natl. Acad. Sci. U. S. A.*, 2003, 100, 3983.
- [211] A. T. Collins, P. A. Berry, C. Hyde, M. J. Stower, N. J. Maitland, *Cancer Res.*, 2005, 65, 10946.
- [212] P. Dalerba, S. J. Dylla, I. K. Park, R. Liu, X. Wang, R. W. Cho, T. Hoey, A. Gurney, E. H. Huang, D. M. Simeone, A. A. Shelton, G. Parmiani, C. Castelli, M. F. Clarke, *Proc. Natl. Acad. Sci. U. S. A.*, 2007, 104, 10158.
- [213] C. Li, D. G. Heidt, P. Dalerba, C. F. Burant, L. Zhang, V. Adsay, M. Wicha, M. F. Clarke, D. M. Simeone, *Cancer Res.*, 2007, 67, 1030.
- [214] M. Uhlen, L. Fagerberg, B. M. Hallstrom, C. Lindskog, P. Oksvold, A. Mardinoglu, A. Sivertsson, C. Kampf, E. Sjostedt, A. Asplund, I. Olsson, K. Edlund, E. Lundberg, S. Navani, C. A. Szigartyo, J. Odeberg, D. Djureinovic, J. O. Takanen, S. Hober, T. Alm, P. H. Edqvist, H. Berling, H. Tegel, J. Mulder, J. Rockberg, P. Nilsson, J. M. Schwenk, M. Hamsten, K. von Feilitzen, M. Forsberg, L. Persson, F. Johansson, M. Zwahlen, G. von Heijne, J. Nielsen, F. Ponten, *Science*, 2015, 347, 1260419.
- [215] X. Xu, H. Cheng, W. Chen, S. Cheng, R. Zhuo, X. Zhang, *Sci. Rep.*, 2013, 3, 2679.
- [216] S. R. Hamilton, S. F. Fard, F. F. Paiwand, C. Tolg, M. Veiseh, C. Wang, J. B. McCarthy, M. J. Bissell, J. Koropatnick, E. A. Turley, *J. Biol. Chem.*, 2007, 282, 16667.
- [217] H. S. ShaQhattal, X. Liu, *Mol. Pharmacol.*, 2011, 8, 1233.
- [218] M. H. El-Dakdouki, D. C. Zhu, K. El-Boubbou, M. Kamat, J. Chen, W. Li, X. Huang, *Biomacromolecules*, 2012, 13, 1144.
- [219] M. Kesik, B. Demir, F. B. Barlas, C. Geyik, S. C. Cevher, D. Odaci Demirkol, S. Timur, A. Cirpan, L. Toppare, *RSC Adv.*, 2015, 5, 83361-83367.
- [220] D. Ag, R. Bongartz, L. E. Dogan, M. Seleci, J. Walter, D. O. Demirkol, F. Stahl, S. Ozcelik, S. Timur, T. Scheper, *Colloids Surf., B*, 2014, 114, 96.

CURRICULUM VITAE

PERSONAL INFORMATION

Surname, Name: Kesik Mancar, Melis

Nationality: Turkish (TC)

Date and Place of Birth: 15 September 1989, Erzurum

E-mail: kesik.melis@gmail.com

EDUCATION

Degree	Institution	Year of Graduation
PhD	METU Chemistry Department	2017
MSc	METU Chemistry Department	2014
BSc	METU Chemistry Department	2012
High School	Çankaya Milli Piyango Anatolia High School	2003

WORK EXPERIENCE

Year	Place	Enrollment
2016-Present	ROKETSAN AŞ., Ankara	R&D Engineer
2012-2016	METU Chemistry Department	Teaching Assistant

PUBLICATIONS

1. Sorption and diffusion of carbon dioxide and nitrogen in poly(methyl methacrylate),

The Journal of Chemical Physics, 139, 124902 (2013)

Hossein Eslami, Melis Kesik, Hossein Ali Karimi-Varzaneh, and Florian Müller-Plathe

2. Effective and functional surface design for biosensing applications based on a novel conducting polymer and PMMA/clay nanocomposite

Electroanalysis, 25, 1995 (2013)

Melis Kesik, Ozgecan Kocer, Fulya Ekiz Kanik, Naime Akbasoglu Unlu, Eda Rende, Evren Aslan-Gurel, Rene M. Rossi, Yasemin Arslan Udum, Levent Toppare

3. A functional immobilization matrix based on a conducting polymer and functionalized gold nanoparticles: Synthesis and its application as an amperometric glucose biosensor.

Polymer, 54, 4463 (2013)

Melis Kesik, Fulya Ekiz Kanik, Gönül Hızalan, Duygu Kozanoglu, Emren Nalbant Esenturk, Suna Timur, Levent Toppare

4. A novel DAD type and folic acid conjugated fluorescent monomer as a targeting probe for imaging of folate receptor overexpressed cells

Biotechnology Progress, 4, 952 (2014)

Fulya Ekiz Kanik, Didem Ag, Muharrem Selecı, Melis Kesik, Hava Akpınar, Gonul Hizalan, Firat B Barlas, Suna Timur, Levent Toppare

5. An acetylcholinesterase biosensor based on a conducting polymer using multiwalled carbon nanotubes for amperometric detection of organophosphorous pesticides.

Sensors and Actuators B-Chemical, 205, 39 (2014)

Melis Kesik, Fulya Ekiz Kanik, Janset Turan, Marit Kolb, Suna Timur, Müfit Bahadır, Levent Toppare

6. Synthesis and characterization of conducting polymers containing polypeptide and ferrocene side chains as ethanol biosensors

Polymer Chemistry, 5, 6395 (2014)

Melis Kesik, Huseyin Akbulut, Saniye Söylemez, Şevki Can Cevher, Gönül Hızalan, Yasemin Arslan Udum, Takeshi Endo, Shuhei Yamada, Ali Çırpan, Yusuf Yağcı, Levent Toppare

7. Development of an amperometric biosensor based on a novel conducting copolymer for detection of anti-dementia drugs

Journal of Electroanalytical Chemistry, 735, 43 (2014)

Janset Turan, Melis Kesik, Saniye Soylemez, Seza Goker, Marit Kolb, Müfit Bahadır, Levent Toppare

8. A novel and effective surface design: Conducting polymer/ β -Cyclodextrin host-guest system for cholesterol biosensor

ACS Applied Materials & Interfaces, 6, 18290 (2014)

Saniye Soylemez, Serife O. Hacioglu, Melis Kesik, Hande Unay, Ali Cirpan, Levent Toppare

9. Selenium containing conducting polymer based pyranose oxidase biosensor for glucose detection

Food Chemistry, 172, 219 (2015)

Tugba Ceren Gokoglan, Saniye Soylemez, Melis Kesik, Sinem Toksabay, Levent Toppare

10. Electrochemical and optical properties of a conducting polymer and its use in a novel biosensor for the detection of cholesterol

Sensors and Actuators B-Chemical, 212, 425 (2015)

Saniye Soylemez, Yasemin A. Udum, Melis Kesik, Cevher Gündođdu Hızlıates, Yavuz Ergun, Levent Toppare

11. A novel architecture based on a conducting polymer and calixarene derivative: its synthesis and biosensor construction

RSC Advances, 5, 35940 (2015)

Tugba Ceren Gokoglan, Saniye Soylemez, Melis Kesik, Hande Unay, Serkan Sayin, Huseyin Bekir Yildiz, Ali Cirpan and Levent Toppare

12. A benzimidazole-based conducting polymer and a PMMA-clay nanocomposite containing biosensor platform for glucose sensing

Synthetic Metals, 207, 102 (2015)

Fatma Bilge Emre, Melis Kesik, Fulya Ekiz Kanik, Hava Zekiye Akpınar, Evren Aslan-Gurel, Rene M. Rossi, Levent Toppare

13. Multi-functional fluorescent scaffold as a multicolor probe: design and application in targeted cell imaging

RSC Advances, 5, 83361 (2015)

M. Kesik, B. Demir, F. B. Barlas, C. Geyik, S. C. Cevher, D. Odaci Demirkol, S. Timur, A. Çırpan, L. Toppare

- 14.** An effective surface design based on a conjugated polymer and silver nanowires for the detection of paraoxon in tap water and milk
Sensors and Actuators B, 228, 278 (2016)
Janset Turan, Melis Kesik, Saniye Soylemez, Seza Goker, Sahin Coskun, Husnu Emrah Unalan and Levent Toppare
- 15.** A novel acetylcholinesterase biosensor: core-shell magnetic nanoparticles incorporating conjugated polymer for the detection of organophosphorus pesticides
ACS Applied Materials and Interfaces, 8, 8058 (2016)
Cancar Huriya Dzudzevic, Saniye Soylemez, Yeliz Akpınar, Melis Kesik, Seza Goker, Gorkem Gunbas, Murvet Volkan and Levent Toppare
- 16.** Conjugated polymer based scaffolds for amperometric biosensing devices: an overview of progress and recent advances (Review)
Encyclopedia of Polymer Applications (submitted)
Saniye Soylemez, Melis Kesik, Levent Toppare
- 17.** A novel approach for the fabrication of a flexible glucose biosensor: the combination of vertically aligned CNTs and a conjugated polymer
Food Chemistry 220, 299 (2017)
Tugba Ceren Gokoglan, Saniye Soylemez, Melis Kesik, Itir Bakis Dogru, Onur Turel, Recep Yuksel, Husnu Emrah Unalan, Levent Toppare
- 18.** Construction and amperometric biosensing performance of a novel platform containing carbon nanotubes-zinc phthalocyanine and a conducting polymer
International Journal of Biological Macromolecules, 96, 61 (2017)
Ece Buber, Abdulcelil Yuzer, Saniye Soylemez, Melis Kesik, Mine Ince, Levent Toppare
- 19.** Paper based glucose biosensor using graphene modified with a conducting polymer and gold nanoparticles
Journal of The Electrochemical Society, 164, G59 (2017)
Tugba Ceren Gokoglan, Melis Kesik, Saniye Soylemez, Recep Yuksel, Husnu Emrah Unalan, Levent Toppare
- 20.** A bio-sensing platform utilizing a conjugated polymer, carbon nanotubes and PAMAM combination
Journal of Electroanalytical Chemistry, 799, 370 (2017)
Ece Buber, Melis Kesik, Saniye Soylemez, Levent Toppare